# Surface Conductivity on Hydrogenated Diamond

Oliver Aneurin Williams

This thesis is submitted for the degree of Doctor of Philosophy

Department of

Electronic and Electrical

Engineering

University College

London
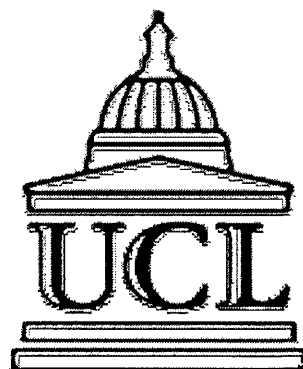
ProQuest Number: U644306

ProQuest U644306

Acknowledgements

I would like to thank my family for all their support, sorry its probably incomprehensible but relax I don't understand that much more than you. Now I can actually phone you without being asked when I'm going to submit. Bliss.

A substantial amount of the work detailed in this thesis was performed at the Walter Schottky Institute in Munich, and I would like to thank them for putting up with me to the point where upon seeing Martin Stutzmann at a conference he says "Oh hi, I haven't seen you in at least a week...". Maybe the WSI logo should be on my thesis... I would specifically like to thank Christoph Nebel for his patience and reminding me that liquid helium is really expensive, as well as Jose Garrido and all the other people who helped me when I got stuck and couldn't speak German. In all seriousness, I learned a lot from these people, and continue to do so. I'll try not to break anything next time I visit......

I would like to thank Philippe GA "Silicon is quite good actually" Bergonzo and Roy "So when do you think you may buy a new Astex?" Gat for all the emails telling me how to actually switch the Astex growth reactor on. Actually, I still have your IIa diamonds you know... Tim Mollart has also helped a lot here, especially in leaning on Richard to buy us a $10,000 pyrometer – it is useful to know the real temperature you know! Thanks for the secret diamond loan – oops. Lakeshore cryotronics have been very patient in dealing with my tedious requirements for the hall apparatus, especially my whining "well otherwise I can't measure my diamonds", particularly Jeff Lindemuth.

Abstract

Diamond has many extreme properties that make it an ideal candidate for high performance electronics devices. Unfortunately, due to the high density of the diamond lattice it is difficult to dope, and to date very little success has been achieved in this field with the exception of boron. However, even boron has a very deep activation energy (0.37 eV), which corresponds to less that 1% of acceptors being activated at room temperature.

Hydrogen surface conductivity is a method of rendering an undoped diamond surface highly conductive. A brief hydrogen plasma exposure can generate a high density of holes in the near surface, with extremely low activation energy. This layer has been used to fabricate devices such as Schottky diodes, MESFETs and Single Hole Transistors.

The work in this thesis concentrates on the electrical characterisation of this layer, techniques include the hall effect over a wide range of temperatures (10-500K), conductivity and I/V device testing. This data is compared with the literature and the various proposed models are addressed.

Contents

Chapter 1

Introduction

Diamond has inspired the human race for thousands of years. Natural diamond has a perhaps undeserved mystic about it, which has made it a source of both passion and warfare. The synthesis of diamond in a laboratory has been attempted for over a hundred years, but it is widely agreed that it was first achieved at General Electric in the 1950's. This breakthrough had a profound effect on the diamond industry, leading to an industrial diamond market that is now valued at over $500 million. This amount is but a small fraction of the lucrative gem industry (over $1 billion), which is protected by a worldwide cartel.

These techniques are viewed by some as a kind of modern day alchemy, and this material is often referred to by the uninformed as "fake" diamond. However, fake it is not, and this material can match or even surpass natural diamond in many applications, including the gem industry. These early techniques relied on high pressures and high temperatures, which are both expensive and dangerous. The resulting material is also "gem shaped" which is inappropriate for electronic devices where thin films are required.

The growth of diamond at low pressures by Chemical Vapour Deposition opened up totally new possibilities for this extreme material. Now diamond could be synthesised at extremely low cost, over large areas and with the purity required by electronic applications. However, this technique also had flaws, principally the growth of diamond on any other material other than diamond lead to polycrystalline material. This material yields poorer electronic performance and is difficult to process with standard clean room techniques. Thus, to date, the size of synthetic single crystal diamond has been limited to the maximum producible by the earlier High Pressure High Temperature (HPHT) process. This is perhaps the most serious limitation of

diamond growth to date, and has hindered the progress of almost all of the applications of diamond.

Doping diamond has been a major problem since idea of diamond electronics was first suggested. The extremely tight lattice responsible for many of the extreme properties of diamond also limits the solubility of other materials in diamond, To date, success has only really been achieved with boron (p – type) and phosphorus (n – type). However, this success has come at a price, with the shallowest activation energy of boron being reported at 0.37 eV, leading to around only 1% of acceptors being ionised at room temperature. The case for donors is worse with phosphorus at 0.6 eV, nitrogen at 1.7 eV. These high activation energy levels are comparable with the bandgaps of other semiconductors, and doping continues to be a major problem in diamond for the device engineer.

In 1989, a curious discovery that the diamond surface was highly conductive after growth, lead to an entirely new method for charge carrier generation. This conductivity was specific to diamond grown within a hydrogen containing plasma, and was subsequently linked to the hydrogen termination of the surface. The confirmation of the p – type character of the surface, with a very low activation energy, lead to much excitement about this new "dopant". Indeed, high performance devices were fabricated, exceeding all those previously fabricated on conventionally doped material.

However, the mechanism by which holes are generated in the near surface was far from clear. Several conflicting models were proposed and to date there has been no all encompassing model. This is the motivation of the work in this thesis.

The introductory chapters in this thesis (chapters 2-5) review the literature and methods used in this thesis. Chapter 2 introduces the properties of diamond and overviews the main synthesis methods. Chapter 3 discuses doping diamond, in particular, the specific problems with such an extreme material. Chapter 4 sumarises the progress that has been made in device fabrication on diamond using the available dopants. Chapter 5 reviews the techniques used to grow and characterise diamond in

this thesis. The experimental work starts at chapter 6 with low temperature characterisation. Chapter 7 details the effects the ambient environment has on surface conductivity. Chapter 8 illustrates the particular case of black diamond, whereas Chapter 9 focuses on polished diamond. Chapter 10 discuses homoepitaxy as a means to produce high performance, stable, surface conductive diamond.

Chapter 2

The Properties and Growth of Diamond

Contents

Section 2.1 Introduction

Diamond has a multitude of extreme properties that make it very attractive for a number of applications. The more successful areas of diamond include heat spreading, wear resistant coatings, optical window and tribological applications. However, diamond also has very impressive theoretical electronic characteristics that have lead to speculation that it could replace silicon. However, numerous problems such as the polycrystalline nature of heteroepitxial growth, doping issues and the lack of reproducibility within synthesis have held back widespread use of the material within electronics.

The growth of diamond has been performed by many very different techniques all with their respective merits and flaws. High Pressure High Temperature (HPHT) synthesis is popular within the gem trade due to the single crystal nature of the result and the ability to manipulate optical centres in diamond to colour stones. The resulting material however is a randomly shaped diamond stone and is hence not ideal for electronic applications. Combustion flame synthesis is favoured for its extremely high growth rate and low equipment cost, but due to safety concerns is rarely performed in research environments as the gas flow rate is also extremely high. Hot filament Chemical Vapour Deposition (HFCVD) is both simple and easily scaled up but the resulting films are contaminated with filament elements and hence it is not ideal for electronic grade material. Microwave Plasma Enhanced Chemical Vapour Deposition (MWPECVD) produces high quality large area films with a reasonable growth rate and is hence ideal for electronic applications. However, the cost of these systems is relatively high and the engineering requirements rather demanding.

Section 2.2 Structure of Diamond

Diamond is an allotrope of carbon, the most common allotrope being graphite which is energetically more favourable under atmospheric conditions. The different structure of diamond and graphite yield vastly different properties; i.e. diamond is the hardest material known to man, brittle and electrically resistive, whereas graphite is soft and conductive. Carbon is a group IV element and as such has four electrons in its outer shell, in the configuration $1s^2 \, 2s^2 \, 2p^2$. The $1s^2$ represents two electrons in the k (1st) shell, which only allows two electrons of opposite spin and hence is full and at the lowest possible energy. This shell is completely stable and does not take part in any bonding. The next shell (L – shell) contains four electrons in two different sub - shells, the s and p. The 2s electrons have opposite spin and the 2p electrons parallel spin. This is summarised in figure 2.1 and is refered to as the ground state as all the electrons are in their minimum orbits, with the lowest possible energy closest to the nucleus.

Nucleus
6 Protons
6 Neutrons
(Carbon-12)

K Shell
L Shell

K Shell Electrons	L Shell Electrons			
1s	2s	$2p_x$	$2p_y$	$2p_z$
↑↓	↑↓	↓	↓	

Two half-filled 2p orbitals

Note: Arrow indicates direction of electron spin
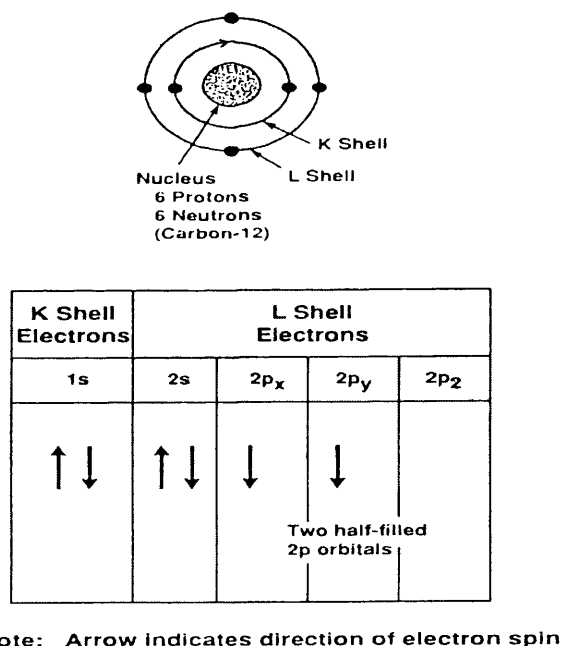
Figure 2.1 Electronic Structure of Carbon in the Ground State [Pierson 1993]

However, when a carbon atoms bonds, hybrid atomic orbitals are formed where four electrons instead of two are in separate orbitals with their spin uncoupled. In this arrangement the electrons the L shell is modified so that one of the 2s orbitals is promoted to a higher 2p orbital. These new hybrid orbitals are labelled sp^3 as they are formed from one s orbital and three p orbitals. The energy required for this hybridisation is 230 kJ mol^{-1} [Pierson 1993] and is only possible as it substantially reduces the energy required to form bonds.

The four sp^3 valence electrons result in strong covalent bonds (called sigma or σ bonds) and are amplified by the small size of the atom. Figure 2.2 (A) shows the result of an entirely covalent tetrahedral carbon lattice and the structure is known as diamond.
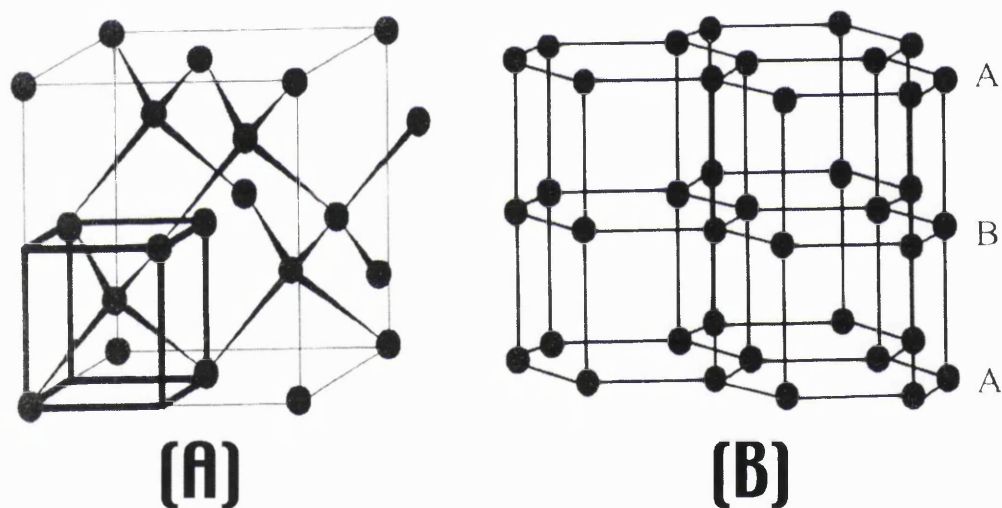
Figure 2.2 Structure of Graphite and Diamond
[Prelas 1998]

An alternative hybridisation can also occur where the electrons of the L shell are modified by one of the 2s electrons being promoted to and combined with two of the 2p orbitals to from three sp^2 orbitals and an unhybridised free p orbital electron. When bonded the three sp^2 orbitals are in the same plane and form strong sigma bonds. However, the fourth orbital is directed perpendicular to this plane and forms a weaker pi (π) bond. This is the structure of Graphite (figure 2.2 (B)).

Section 2.3 Properties of Diamond

Diamond is best known for its extreme hardness, but it has numerous other properties listed in the following tables:

Property	Diamond	Notes
Knoop's Hardness (kg mm^{-2}	7000	Hardest material known (SiC 2480, Si 850, stainless steel 660)
Coefficient of friction	0.1	Very low in air
Young's Modulus (10^{11} M m^{-2})	10.35	Highest mechanical strength (SiC 7, Si 1.9, stainless steel 2)
Sound propagation velocity (km s^{-1})	18.2	1.6 x aluimina
Chemical inertness		Inert to all acids, bases and solvent at 300K
Range of high transmittance (μm)	0.22 – 2.5 & 6	Orders of magnitude lower than other materials in infra - red
Refractive index	2.41	1.6 x silica
Thermal conductivity @ 300K (W cm^{-1} K^{-1})	20	Highest @ 300K (Si 2.3, SiC 3.2, Cu 5)
Thermal expansion (10^{-6} K^{-1})	1	(Si 2.33, SiC 3.3, Stainless steel 17.3)

Table 2.1 Selected Properties of Diamond [Bachmann 1991]

Table 2.1 summarises the mechanical / general properties of diamond whereas table 2.2 compares the electronic properties of diamond with other common semiconductors.

Property	Diamond	Si	GaAs	3C-SiC	GaN
Bandgap (eV)	5.45	1.1	1.43	2.2	3.39
Electron Mobility $(cm^2 \, V^{-1} \, s^{-1})$	2000	1500	8500	1000	900
Hole Mobility $(cm^2 \, V^{-1} \, s^{-1})$	1800	600	400	40	150
Breakdown Field Strength $(10^6 \, V \, cm^{-1})$	10	0.3	0.4	4	5
Intinsic Resistivity $(\Omega \, cm)$	10^{16}	10^3	10^9	$>10^9$	$>10^9$
Saturation electron velocity $(10^7 \, cm \, s^{-1})$	2.7	1	2	2	2.7
Dielectric constant	5.7	11.9	12.8	9.7	9

Table 2.2 Electronic Properties Compared with other Semiconductors [Yoder 1993, Morkoc 1994]

A number of these properties are of particular interest for electronic devices, such as the wide bandgap and high mobilities. However, care must be taken when evaluating a material based on these "best case" values as they are rarely obtained in practice and certainly not all at the same time. This is the same for all materials, for example, mobility is always detrimentally affected by doping which is essential to generate free carriers.

Section 2.4 Natural Diamond

Naturally occurring diamond was first reported in India 2700 years ago however the true beauty was not unveiled until faceting and polishing techniques were developed in the 14th and 15th centuries [Pierson 1993], diamond is produced in nature under high pressure and temperature conditions in volcanic shafts. In order to maintain its structure diamond must be cooled under high pressure or it will be transformed into graphite. The majority of natural diamonds are mined in Africa (Botswana, Zaire, Republic of South Africa), Australia and Russia [Bakon 1993] and the distribution is tightly controlled by a worldwide cartel dominated by the De Beers Organisation [Herbert 1972].

The use of natural diamond in characterisation is essential as a means of a standard control. However, there are various classes of natural diamond and their purity varies widely. Table 2.3 lists the varies types and their abundance.

Type	Abundance	Nitrogen Content	Notes
Ia	~ 98%	500 – 5000 ppm	Aggregated
Ib	~ 0.1%	5 – 500 ppm	Single - substitutional
IIa	~ 2%	< 100 ppm	Single – substitutional
IIb	Very rare	< 100 ppm	~ 0.25 ppm Boron

Table 2.3 Natural Diamond Types [Wilks 1991]

Type I diamonds are the most commom accounting for almost all mined stones. Type IIa are the purest and Type IIb are extremely rare and have p – type semiconductor properties [Collins 1971]. It should be noted that even type IIa diamonds are not really of device grade as up to 100ppm is equivalent to nearly 1×10^{19} cm^{-3} carriers if all the nitrogen atoms are in substitutional sites. Clearly the "high purity" label is adequate for the gem trade only.

Section 2.5 HPHT Synthesis

High Pressure High Temperature (HPHT) Synthesis was first achieved in 1955 by General Electric, AESA Sweden and the Institute for High Pressure Physics USSR as a reproducible method for the synthesis of diamond [see for example Davidson 1994]. HPHT synthesis essentially duplicates the natural process in a laboratory, however, as this process is extremely slow in nature, a catalyst is used to make the transformation between graphite and diamond faster. Figure 2.3 shows these conditions:
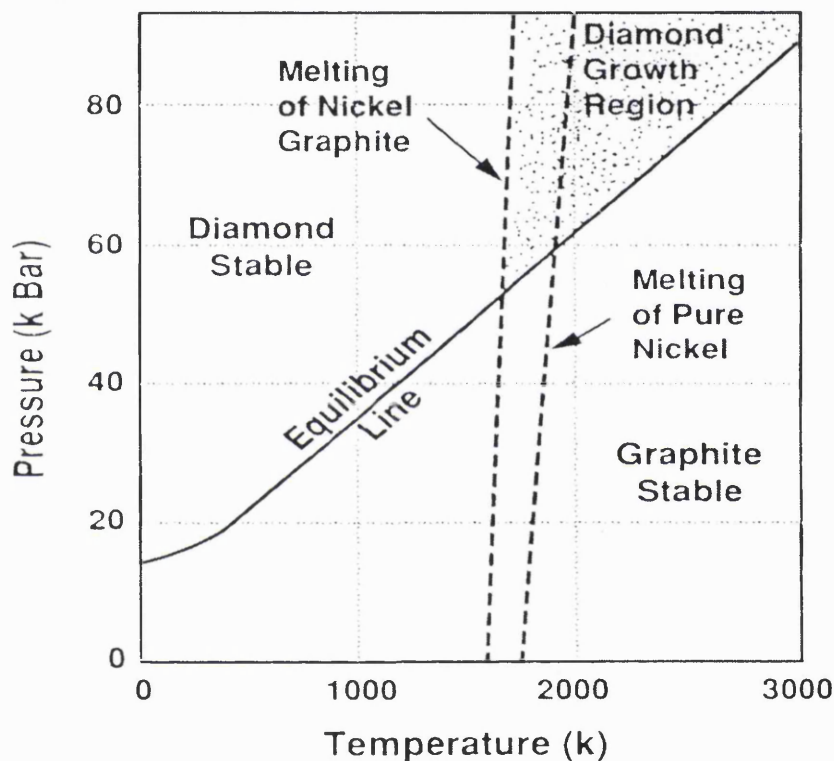
Figure 2.3 Pressure / Temperature Diagram of Diamond / Graphite [Bundy 1973]

The equilibrium line is the so called Berman – Simon curve which is the boundary between the stable states of carbon, and divides the preferred allotropes in terms of which has the lowest thermodynamic energy However, there is a problem with just applying a high pressure at room temperature to produce graphite, namely the strong carbon – carbon bonds within graphite. At atmospheric pressure, temperatures as high as 1800 K are required to convert diamond to graphite and hence the reverse process

requires similar temperatures. The problem with these temperatures is now the pressure required to grow diamond is increased dramatically ($>6 \times 10^4$ Bar!) and is not feasible in a laboratory or even commercial environment. To proceed at an observable rate, conditions as high as $> 13 \times 10^4$ Bar at > 3300 K were required [Bundy 1973, Adams 1981]. However it possible to circumvent this problem by using a catalyst and this technique is the foundation of modern HPHT methods.

Transition metals are used as the catalyst and these metal solvents dissolve carbon, breaking the bonds between carbon – carbon atoms and individual bonds. The solvent catalyst process establishes a reaction path with lower activation energy than the direct transformation. It allows a faster transformation under far less demanding conditions and is used by many commercial companies such as General Electric and Sumitomo to produce cheap diamond material for many applications.

Table 2.4 gives an idea of the relative amounts / value of these diamonds with natural material:

	Gemstone	Industrial Diamond
Production (tons)	~ 1 (all natural)	90 (70 synthetic, 20 natural)
Market value	$7 billion	$500 million

Table 2.4 Estimated Annual Diamond Business 1992 [Pierson 1993]

Synthetic diamonds are a large cause of concern to the De Beers corporation, as the highest quality synthetics are almost indistinguishable to even a highly trained gemmologist. The detection of transition metals by cathodoluminescence is often used as a means of fingerprinting synthetic diamond as metal inclusions are almost always left within the diamond. However, recent advances in HPHT have used getters such as nitrogen to remove these metals and have even managed to mask the effect of the nitrogen getter on the colour of the diamond.

Section 2.6 Chemical Vapour Deposition

Diamond Chemical Vapour Deposition (CVD) has been researched since the early 1950's. Eversole first reported the growth of diamond by CVD in 1954 and patented in 1962 [Eversole 1962]. Angus et al repeated the work of Eversole and confirmed that the mass increase of diamond grit was due to the growth of diamond [Angus 1968]. However, this technique was generally considered to be not practical and more progress was made in the former soviet union where it was discovered that atomic hydrogen plays a crucial role in removing unwanted graphite and leaving the diamond relatively untouched. In earlier growth experiments it was necessary to stop the growth and etch away graphite to continue diamond growth and this lead to highly polycrystalline material.

CVD growth of diamond is a metastable process and as such there is a competing rate of nucleation with the growth of graphite and other undesirable amorphous carbon phases. The CVD process is shown schematically in figure 2.4:
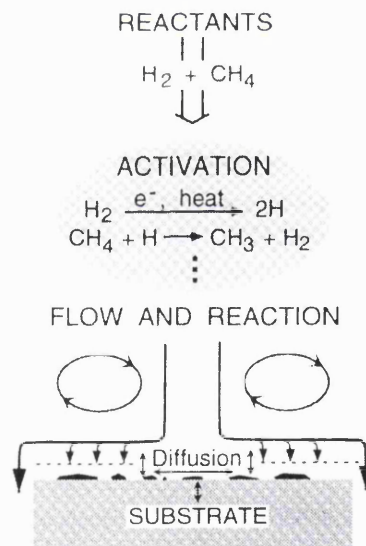
Figure 2.4 CVD Process [Butler 1993]

First the carbon containing gas phase must be activated, then the activated species must be transported to the substrate surface. The precursors must be adsorbed and

diffused to the growth sites. Then atomic hydrogen suppresses the formation of graphite as it etches it some 50 times as fast as diamond [Bachmann 1991].

Hydrogen is a diatomic molecule (H_2) which requires high temperatures for dissociation (> 2000° C) and the rate of dissociation is a function of temperature which increases rapidly above this temperature and with decreasing pressure. The half life of atomic hydrogen is also very short. Atomic hydrogen has many other roles in CVD apart from the etching of graphite, such as the termination of the surface which stabilises the sp^3 structure and thus prevents it from collapsing into the graphite structure.

The growth of diamond for electronics requires large thin films and so heteroepitaxy is required. This was first shown by Spitsyn et al [Spitsyn 1981], and growth is now possible on various substrates such as molybdenum, glass, tungsten, silicon being the most convenient. CVD growth on materials other than diamond to date has been polycrystalline, and this is one of the major stumbling blocks for diamond as a semiconductor device material.

Another problem with heteroepitxay is the requirement for the substrate to be seeded – that is there need to be adequate nucleation sites. Nucleation sites are generally created by scratching the diamond surface with diamond powder, this improves the density on silicon from almost nothing to 10^8 per cm^2. During homoepitaxy however this is not necessary as the methyl radicals already have carbon sites to attach to. The general process of nucleation is the adsorption of the carbon containing species, followed by desorption, etching of atomic hydrogen or the formation of a stable nucleation site.

The various techniques of CVD are reviewed extensively in the literature [e.g. Bachmann 1993] and are summarised in the following sections.

Section 2.7 Combustion Flame Synthesis

Combustion flame synthesis utilises an oxy – acetylene torch to deposit diamond around the tip of the acetylene feather. It was discovered in 1988 by Hirose [Hirose 1988] who realised that acetylene flames produce large amounts of atomic hydrogen. This technique allows extremely high growth rates (30 – 200 μm h^{-1}) [Snail 1991] with good quality at the lower deposition rates. The flame temperature can be as high as 3700K [Hirose 1989], and hence it is essential to cool the substrate to prevent graphitisation of the grown diamond. Figure 2.5 shows the basic setup:
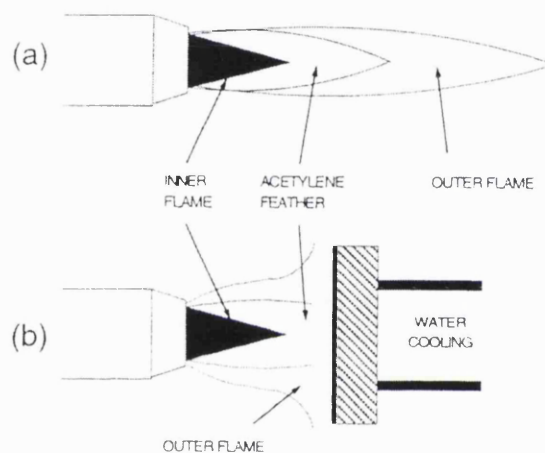
Figure 2.5 Combustion Flame [Dischler 1998]

The most important variable in combustion synthesis is the volumetric ratio of oxygen to acetylene. For diamond growth to occur an acetylene rich flame is required or the diamond will be etched rather than grown. The growth rate increases exponentially with temperature [Snail 1992] and also effects the morphology. Higher growth rates produce lower quality diamond and the morphology switches from 111 to 100 [Schermer 1993]. The high growth rates of combustion flame synthesis can lead to graphitic inclusions and the resulting material is generally not suitable for electronic applications.

Section 2.8 Hot Filament Synthesis

Hot Filament Chemical Vapour Deposition (HFCVD) is one of the simplest methods of diamond growth. Hot tungsten filaments were first used to generate atomic hydrogen for etching non – diamond carbon from diamond [Chauhan 1976], and much later demonstrated as a growth technique [Matsumoto 1982[a+b]]. A Diagram of a typical HFCVD reactor is shown in figure 2.6:
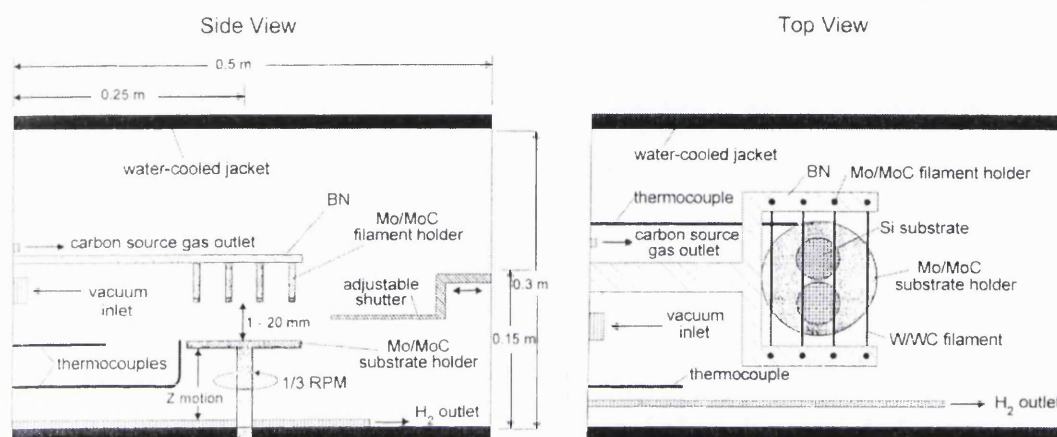
Figure 2.6 HFCVD Reactor [Cassidy 1995]

The HFCVD technique is fundamentally different from plasma based techniques in that it operates at a much lower gas activation temperature and consequently produces much less atomic hydrogen. The constraints placed on the filament temperature also limit the concentration of atomic hydrogen and so low pressures are used to enhance the production and transport of atomic hydrogen. Unfortunately these low pressures result in low growth rates, and the filament material is usually incorporated into the resulting film.

However, this technique is directly scalable and is used commercially by many companies including Diamonex inc. The resulting material is generally considered not suitable for electronics due to the filament contamination and graphitic phases resulting form the low atomic hydrogen concentration.

Section 2.9 MWPECVD Synthesis

Microwave Plasma Enhanced Chemical Vapour Deposition is by far the most successful technique for the deposition of electronic grade diamond. Microwave Plasmas revolutionised the growth of diamond by decoupling the substrate and gas phase temperatures even further than previous methods. It has been shown that the growth rate of diamond is directly correlated with the temperature of the CVD gas phase [Bachmann 1990], and this is due to the higher efficiency of generation of atomic hydrogen as well as the enhanced formation of growth species at these elevated temperatures. This demonstrates the reason for the decoupling of the substrate and gas phase temperatures, as the temperature for graphitisation of diamond is around 1500 °C.

Decoupling is also achieved by the hot filament process but is limited to < 2400 °C due to filament burn out [Matsumoto 1982[2], Sommer 1991]. DC plasmas were suggested as a means to circumvent this problem [Spitsyn 1981,1991], but the first plasma discharge by 2.45 Ghz microwaves became the defining moment in high speed CVD synthesis [Kamo 1983]. The choice of very specific frequencies is mainly due to the availability of components that comply with national regulations [Prelas 1998].

The igniting of the plasma is carried out at low pressures and powers and then the power is scale up with the pressure to growth conditions. At low pressures such plasmas are non - isothermal [Janzen 1992], meaning thst the free electrons are accelerated to very high energies (several thousand degrees) whereas the neutral species and heavy ions are not influenced by the alternating field or cannot follow the field changes fast enough. This means that the electron temperature is much higher than the gas temperature. Most reactors are started under these conditions and then they are operated in "local thermal equilibrium" where the neutrals and ions also heat up. This is summarised in figure 2.7:
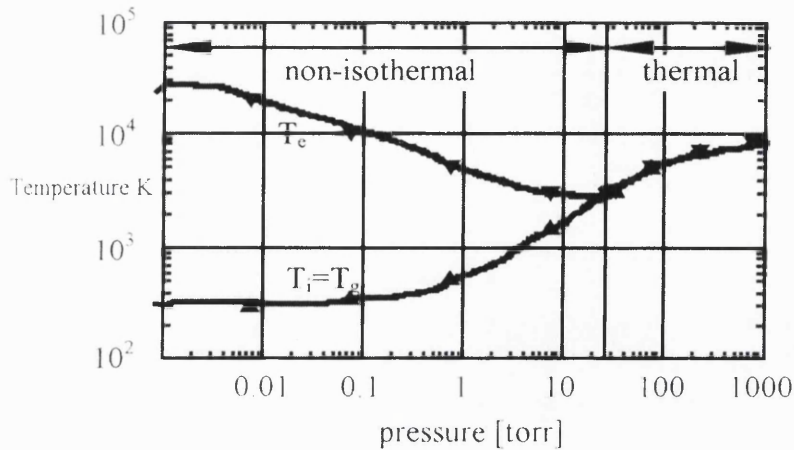
Figure 2.7 Gas Temperatures In Plasmas

The first MWPECVD reactors were based around silica tubular of quartz bell jar chambers, due to ease of application of microwaves. However, this design can lead to contamination of the diamond with quartz and the maximum power / temperature is limited by the bell jar. Astex improved the design by replacing the bell jar with a double skinned water cooled vacuum chamber, using a quartz glass window at the top as a vacuum seal and microwave entry port (see figure 2.8).
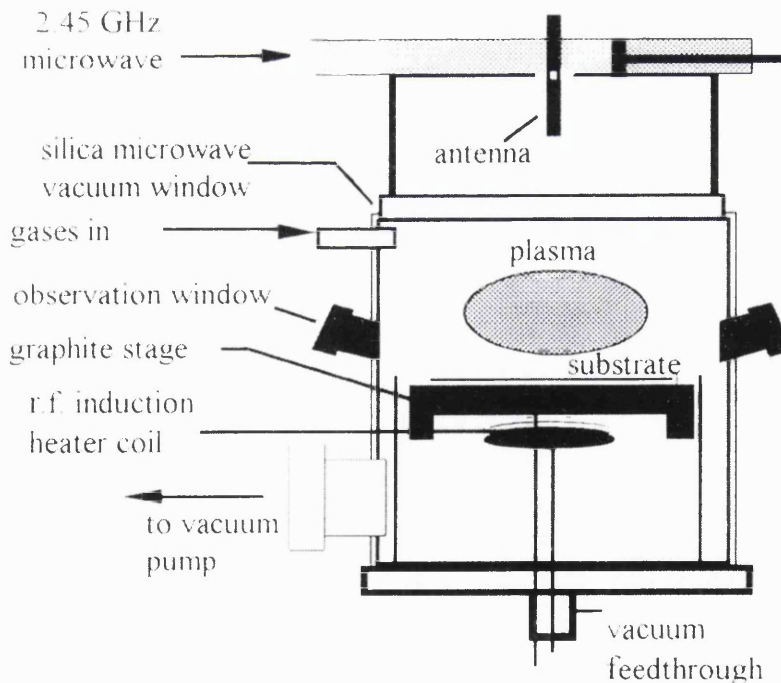
Figure 2.8 Astex MWPECVD Reactor [Prelas 1998]

This design is by far the most commercially successful reactor and Astex systems are the most common within the laboratory environment also. Further improvements were made by the application of a 5 kW generator, previous bell jar reactors were limited to 1 – 1.5 kW. These modern systems can grow 2 inch diamond wafers at linear rates of 4 – 14 μm / hour depending on the gas concentration. These systems are extremely reliable and can be run for weeks unattended. This stability is absolutely essential for the growth of high quality films.

References

Adams D.M.,

Inorganic Solids, 1981 John Wiley & Sons, New York, USA

Angus J.C., Will H.A. and Stanko W.S.,

Journal of Applied Physics, **39** (1968) 2915

Bachman P., Edited by Lettington A. and Steeds J.W.,

Thin Film Diamond, 1993 Chapman & Hall, London, UK

Bachman P.,

Physics World, **April** (1991), 32

Bachmann P.K., Lydtin H. edited by Lukovsky G., Ibbotson D.E. and Hess D.W.,

Materials Research Society Symposium Proceedings, **118** (1990) 165

Bakon A. and Szymanski A.,

Practical Uses of Diamond, 1993 Ellis Harwood, West Sussex, UK

Bundy F.P., Strong H.M. and Wentorf R.H.,

Chemistry and Physics of Carbon, Vol 10, 1974 Marcel Dekker Inc., New York USA.

Butler J.E. and Woodin R.L.,

Philosophical Transactions of the Royal Society, London, **342** (1993) 209

Cassidy W.D., Morrison P.W. and Angus J.C.,

Proceedings of the 4th International Symposium on Diamond Materials, **95** (1995) 85

Chauhan S.P., Angus J.C. and Gardner N.C.,

Journal of Applied Physics, **47** (1976) 4746

Collins A.T. and Williams A.W.S.,

Journal of Physics C, **4** (1971) 1789

Davidson J.L., ed Spear K.E. and Dismukes J.P.,

Synthetic Diamond: Emerging Science and Technology, 1994 John Wiley, New York, USA

Dischler B. and Wild C.,

Low – Pressure Synthetic Diamond, Springer 1998, Heidleberg, Germany

Eversole W.G.,

Synthesis of Diamond, U.S. Patent No. 3,030,188 (17th April 1962

Herbert I.,

The Diamond Diggers, 1972 Tom Spacey Publications, London

Hirose Y. and Kondo N.,

Japan Applied Physics 1988 Spring Meeting, Japanese Physical Society, 434

Hirose Y., Amanuma S., Okada N. and Komaki K.,

1st International Symposium on Diamond and Diamond Like Films, The Electrochemical Society Inc, Pennington, New Jersey, 80

Kamo M., Sato Y., Matsumoto S. and Setaka N.,

Journal of Crystal Growth, **62** (1983) 642

Matsumoto S., Sato S.Y., Kamo M. and Setaka N.,

Journal of Applied Physics, **21** (1982[a]) L183

Matsumoto S., Sato Y., Tsutsumi M. and Setaka N.,

Journal of Materials Science, **17** (1982[b]) 3106

Morkoc H., Strite W.S., Gao G.B., Lin M.E., Sverdlov B. and Burns M.,

Journal of Applied Physics, **76** (1994) 1363

Pierson H.O.,

Handbook of carbon, graphite, diamond and fullerenes, 1993 Noyes Publications,

New Jersey, USA

Prelas M.A., Popovici G. and Bigelow L.K.,

Handbook of Industrial Diamonds and Diamond Films, 1998 Marcel Dekker Inc, New

York, USA

Schermer J.,Hogenkamp J.E.M., Otter G.C.J., Janssen G., van Enckevort W.J.P. and

Giling L.J.,

Diamond and Related Materials, **2** (1993) 1149

Snail K.A. and Hanssen L.M,

Journal of Crystal Growth **112** (1991) 651

Snail K.A. and Marks C.M.,

Applied Physics Letters, **60** (1991) 3135

Sommer M., Smith F.W., edited by Messier R.F., Glass J.T., Butler J.E. and Roy R.,

New Diamond Science and Technology, Materials Research Society 1991,

Pittsburgh, PA

Spitsyn B.V., Bouilov L.L. and Derjaguin B.V.,

Journal of Crystal Growth, **52** (1981) 219

Spitsyn B.V., Bouilov L.L. and Deryagin B.V.,

Journal of Crystal Growth, **52** (1981) 219

Spitsyn B.V., edited by Tzeng Y., Yoshikawa M., Muranaka M. and Feldman A.,

Applications of Diamond Films and Related Materials,Elsevier Science Publishers 1991,, Amsterdam, 475

Wilks J. and Wilks E.,

Properties and Applications of Diamond, 1991 Butterworth – Heinemann, Oxford, UK

Yoder M.N.,

Diamond Films and Coatings, 1993 Noyes Publications, New Jersey, USA

Chapter 3

Diamond Doping

Contents

Section 3.1 Introduction

The majority of electronic devices require some form of doping. The large bandgap of diamond (5.45 eV) makes it a good insulator at room temperature. In the previous chapter the superlative properties of diamond were discussed and compared with other semiconductors. Many of these extreme properties are a direct result of the tight lattice of diamond, and this also has negative effects on doping. The diamond structure has a lattice parameter of 3.567 Å with a small tetrahedral radius of carbon (0.77 Å) [Gildenblat 1991]. This is a serious problem for doping as any impurity other than boron will deform the lattice.

Boron is relatively easy to incorporate into diamond and this has been accomplished by HPHT, CVD and also occurs naturally. There are reports claiming the reduction of vacancies and planar defects with incorporation of boron and that it reduces the graphitic content of diamond. The high probability of incorporation of boron into the diamond lattice can also cause serious contamination problems when trying to dope films n – type or simply grow high purity intrinsic diamond.

Nitrogen is also a common impurity but has deep donor like behaviour [Davies 1977]. Many potential n –type dopants have been tested with little success, the most useful being phosphorous. The doping of phosphorous has only been achieved reproducibly by two independent laboratories but much progress is being made very recently. Sulfur is perhaps the most recent candidate for an n type dopant but is very controversial.

This chapter reviews the current status of both conventional dopants and the more radical hydrogen surface conductive layer. Progress with diamond doping to date is disappointing and perhaps the main restraint on the materials success in modern electronics.

Section 3.2 Naturally Occurring Dopants

As mentioned in chapter two, natural diamonds are classed with regards to their impurity concentrations. A dopant is just an intentional impurity and thus these natural occurring impurities have effects on the free carrier concentrations of the diamonds in which they situated. At least 62 elements have been reported to occur in diamond, but most are at the ppb or ppt level [Prelas 1998]. Nitrogen is an exception and is present in most natural diamonds in concentrations up to 5000 ppm (0.5 wt %) [Prelas 1998]. It is generally considered that most impurities other than nitrogen and boron exist in non – substitutional sites.

Type IIb diamonds contain boron (< 0.25 ppm) and have been studied extensively. These diamonds have a blue colour and display p – type semiconducting properties. The boron atoms are present in substitutional sites with an activation energy of 0.37 eV and doping concentrations of 8 x 10^{16} cm^{-3} [Collins 1971]. This leads to the problem that at room temperature less than 1 % of the dopants are ionised [Geis 1992]. Figure 3.1 displays hall data from a natural type IIb diamond.
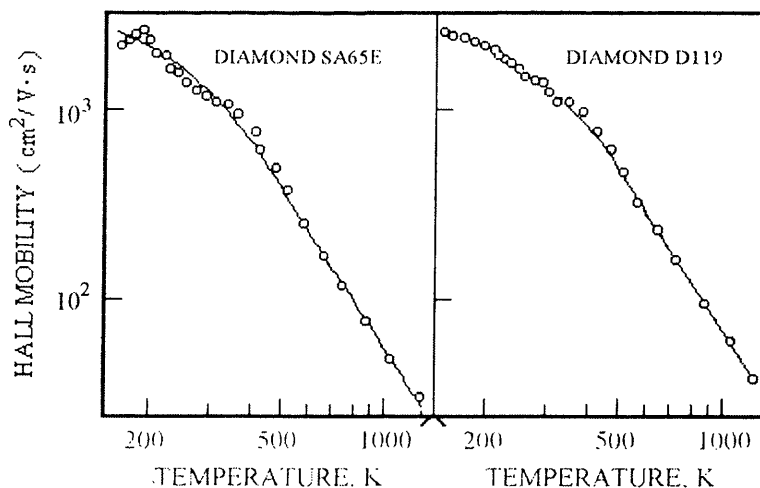
Figure 3.1 Type IIb Diamond

Type Ib natural diamonds contain nitrogen in isolated substitutional sites. This seems an ideal candidate for n – type doping but unfortunately it is a very deep donor at around 2 eV below the conduction band [Collins 1989]. This energy barrier is greater

than the bandgap of silicon and as such has little effect on the electron concentrations at room temperature. Type Ib diamonds are also rather rare and generally type I diamonds contain nitrogen in aggregates as at the elevated pressures and temperatures in the mantle nitrogen diffuses and aggregates.

Section 3.3 Doping During HPHT Synthesis

As the HPHT process is very similar to natural diamond growth in stands to reason that similar types of diamond can be grown. Adding boron to the mixture of carbon and catalysts during HPHT synthesis was first reported by Wentorf [Wentorf 1962]. The resulting resistivity was rather high however (10^5 Ω cm), most probably due to compensation effects from the nitrogen impurities in the diamond. Holes can be annihilated when electrons drop from the nitrogen level to the boron level and hence the dopants will be compensated.

As nitrogen is so readily incorporated into diamond it whould be an ideal candidate as mentioned in the previous section. However, even the theoretical value for nitrogen is 1,7 eV [Davies 1977] which is far to deep for room temperature or even moderately high temperature device applications.

The main problems with doping during HPHT are related to the technique by which the diamond is grown. As catalysts are required the material is far from device grade purities and metal inclusions make serious impurity concentrations. The situation is made worse by the use of a nitrogen getter as this contaminates the material even further and will compensate any p – type dopants. This process is also rather difficult to control, especially to the level required by device engineers.

HPHT diamond growth produces small random shaped diamonds which need to be cut for use in electronics. This is a wasteful process and requires skill and investment. The process is not really cost effective and the growth equipment cannot be easily scaled up. Ultimately the process is too crude as it is exceptionally difficult to control the uniformity of the doped material. Controlling the thickness of the doped layer or acheiving selective area doping as will ultimately be required are particular problems.

Section 3.4 Ion Implantation

Ion – implantation is the method of choice for doping conventional materials such as silicon. The reason for this is largely down to the amount of control the technique provides, for example, local areas of the surface can be doped with varying concentration of acceptors / donors with relative ease. The basic method is very simple, energetic ions are forced into solid targets by their high kinetic energy. Any high energy impact of ions on a materials surface will cause some kind of damage and this damage needs to be removed by annealing. The situation with diamond is complicated further by the tendency of diamond to graphitise under these high energies. This is serious problem as graphitic phases will make the diamond more conductive and this has lead to much controversy over apparent doping especially when claimed on resistivity measurements alone.

Covalently bonded materials are known to become amorphous under high dose ion implantation [Williams 1986], and in the case of diamond, broken bonds are likely to rearrange to from the more stable sp^2 structure, i.e. high doses lead to graphitisation [Vavilov 1974]. As the passage of energetic ions through a solid will result in extensive bond breakage there will be a threshold damage level beyond which the diamond structure will collapse into the graphite phase. This transformation is very noticeable as the diamond turns optically black [Connel 1988] and the Raman structure changes dramtically [Sato 1988]. It has also been shown that the diamond changes to an etchable material with a conductivity comparable to graphite [Prins 1983]. Figure 3.2 shows this critical dose D_c where the resistance falls rapidly. This figure also shows a remarkable similarity between these values with Xe and C implants. This proves that the change is due to damage as carbon cannot become a substitutional dopant in diamond! The slight difference between Xe and C is due to different nuclear energies deposited by these ions, as Xe will deposit about 20 times C and the curves are displaced by a factor of 20. Diamonds implanted with energies below this critical dose can be restored to a pristine state by thermal annealing [Braunstein 1980]. At higher doses the damaged diamond converts to graphite on annealing.
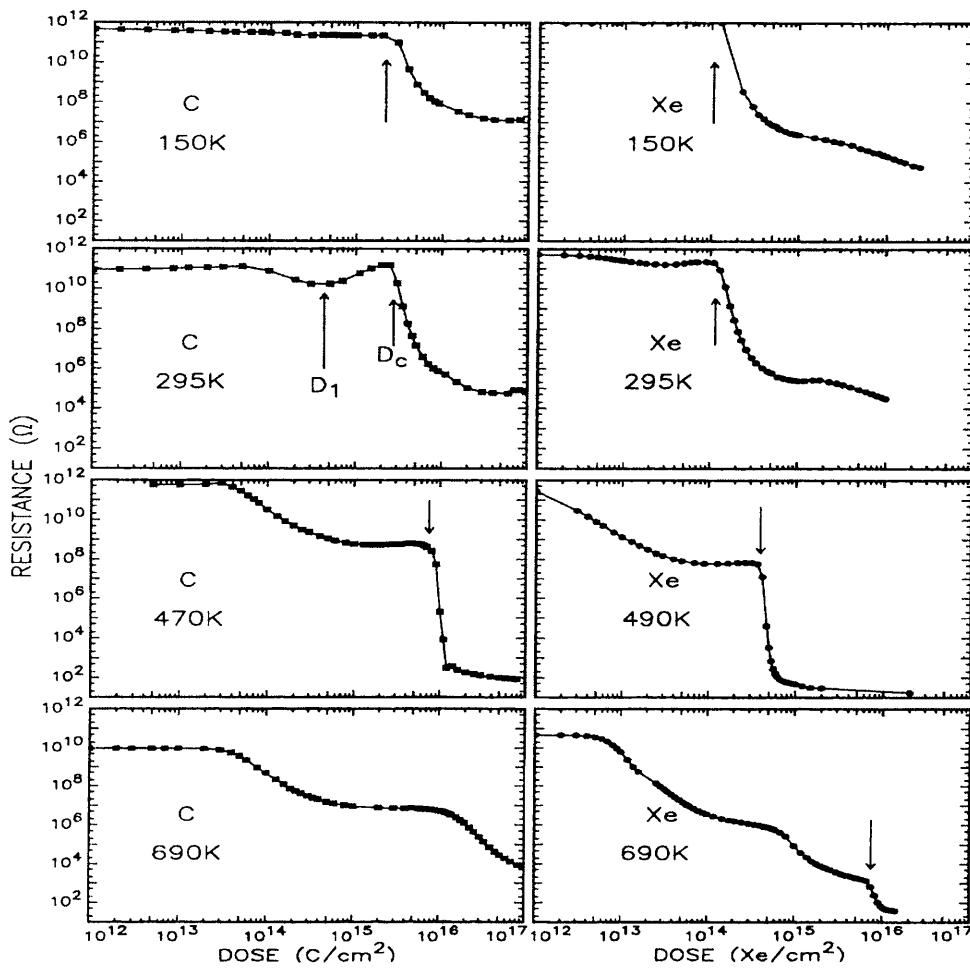
Figure 3.2 Critical Dose [Prawar 1995]

Implantation temperature is also crucial and can be divided into three regimes [Prins 1992]:

1. Low Temperatures ($T_i < 320$ K) where interstitials and vacancies are immobile and implantation damage is frozen in.

2. Intermediate Temperatures ($320 < T_i < 800$ K) where interstitials are mobile but vacancies are not.

3. High Temperatures ($T_i > 800$ K) where both interstitials and vacancies can diffuse.

These factors have influenced the methods by which ion implantation is carried out and explain the relative levels of success achieved. The three main techniques used

today are hot implantation, high dose implantation followed by chemical etching and cold implantation followed by rapid annealing (CIRA).

In hot implantation damage is instantaneously annealed by the high temperature ($T^i >$ 800 K). This technique has evolved from early work demonstrating the growth of diamond by implanting high dose C into hot diamond [Hartley 1973, 1982]. The implantation into heated diamond substrates diminishes the accumulation of point defects and drives the implanted species into lattice sites where they should be electrically active [Braunstein 1981]. However, the resulting mobilities are disappointing [Zeidler 1993], due to the formation of defect clusters. These clusters are almost impossible to remove by post implantation annealing and as such the technique is not suitable for high performance devices.

In an alternative approach the diamond is implanted with a very high dose (higher than the critical dose D_c), followed by a high temperature anneal (1400 °C), and then the graphitic surface layer is chemically etched. The surface on the intact diamond (that previously situated below the graphitic layer) contains the "tail" of the implant distribution with the majority of the implanted species located in electrically active substitutional sites. This method has been shown unambiguously to produce p – type activity due to B doping [Braunstein 1983], however there is little control over the dopant concentration due to the self limiting process determined by the critical dose. The carriers are unfortunately only located in a shallow region close to the surface and thus the carrier mobilties are very low. However, this technique is ideal for the formation of high quality ohmic contacts [Uzan – Saguy 1995, Prins 1989].

The CIRA process is by far the most successful ion implantation technique [Prins 1993]. This technique relies on freezing in the point defect damage by implanting at low temperatures, the diamond is kept cold until it is ready to be annealed. On annealing some of the implanted species can combine with vacancies to become activated and self – interstitials can recombine with vacancies to anneal residual damage. At higher temperatures C self – interstitials can diffuse and recombine with vacancies during the implantation and so there are fewer vacancies for the implanted species. This has lead to the further refinement that is co – implantation [Prins 1988]

where C is implanted with the desired species in order to generate more vacancies. However, more recent work has suggested that this is not really necessary and that the annealing temperature is more important as self – interstital – vacancy recombination rates increase with increasing temperature whereas boron – interstitial – vacancy recombination rates decrease with increasing temperature [Prins 1991]. The highest mobility on boron implanted diamond was achieved using this technique (600 cm^2 V^{-1} s^{-1}) and is shown in figure 3.3.
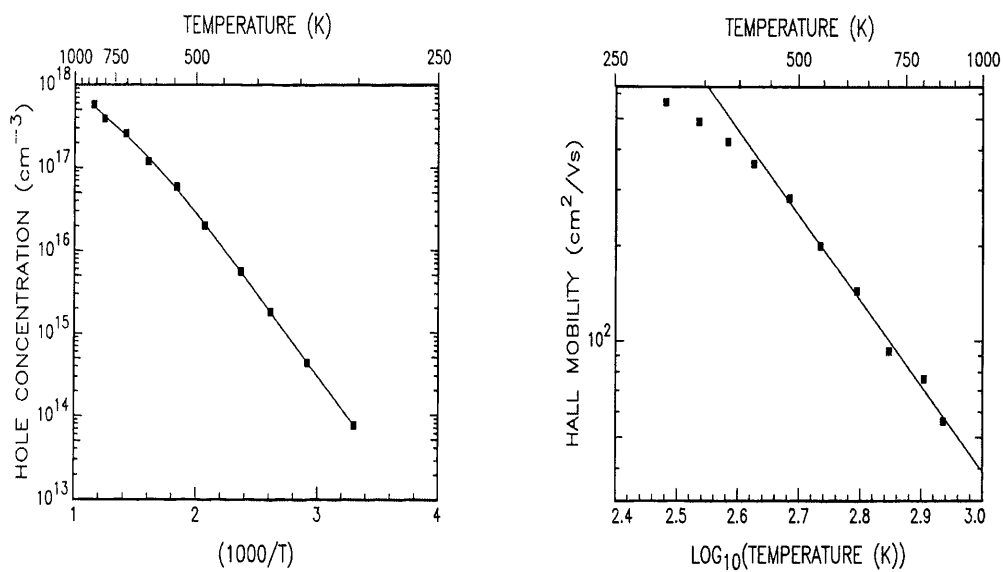
Figure 3.3 CIRA Implantation [Uzan – Saguy 1998]

Unfortunately, many ion implantation reports do not display hall characteristics and care must be taken when interpreting resistivity measurements due to the aforementioned damage issues.

Section 3.5 In – situ Doping During CVD

Doping diamond during chemical vapour deposition is a simple process where the dopant can be introduced as a solid, liquid or gas. The most common examples of CVD doping utilise the introduction of a gaseous form of the dopant such as diborane (B_2H_6) [Gildenbalt 1991]. Unfortunately diborane is highly toxic and this has lead the search for alternatives such as boron trioxide (B_2O_3) [Okano 1990] which are non – toxic.

Initial hall measurements on boron – doped epitaxial films deposited yielded mobilities of 470 $cm^2V^{-1}s^{-1}$ at 300K [Fujimori 1990] and are summarised are figure 3.4.
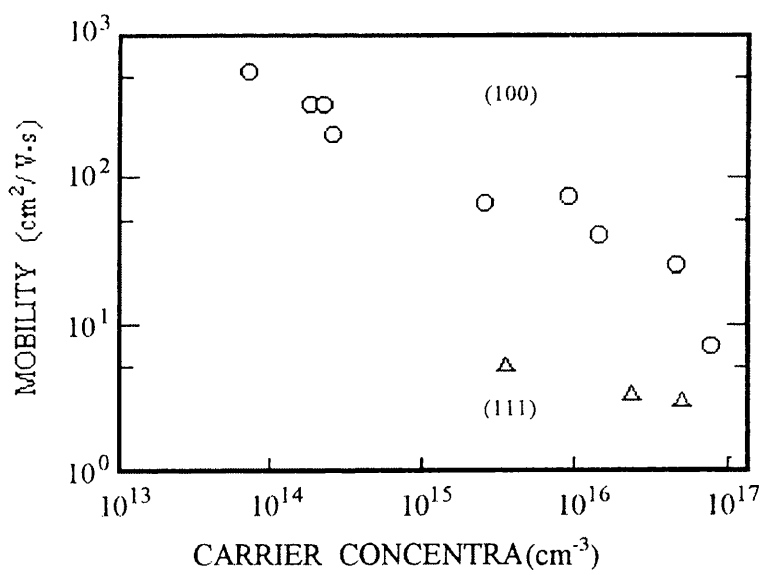
Figure 3.4 Early Boron Doping Data [Fujimori 1990]

The increase in carrier concentration produces a marked decrease in mobility from a respectable 590 $cm^2V^{-1}s^{-1}$ to a poor 7.8 $cm^2V^{-1}s^{-1}$. The hole mobility in homoepitaxial diamond films is much lower than that in the best quality type IIb natural diamonds as shown in figure 3.5. Homoepitxial intrinsic films have been grown with high carrier mobility (1635 $cm^2V^{-1}s^{-1}$) and it has been shown that the mobility reduces substantially to 500 $cm^2V^{-1}s^{-1}$ on introducing boron [Landstrass 1993].
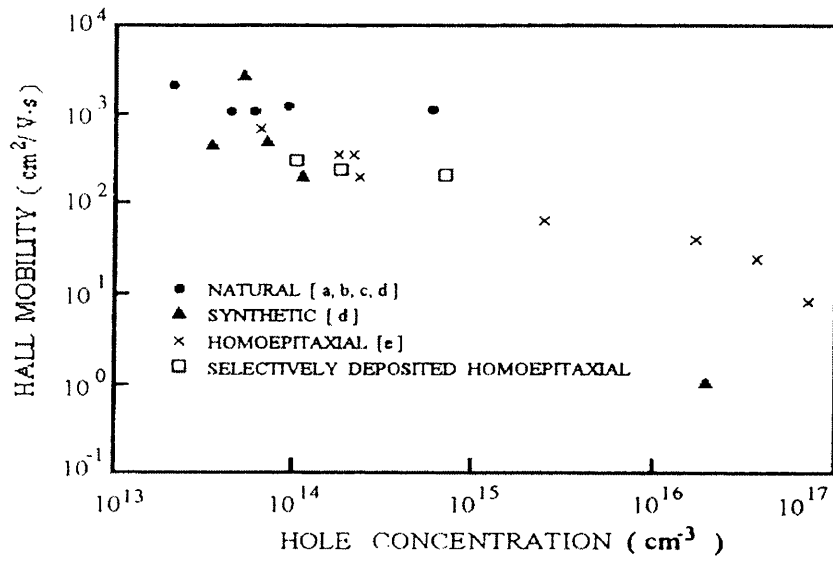
Figure 3.5 Comparison of Naturally and Synthetically Doped Films [Prelas 1998]
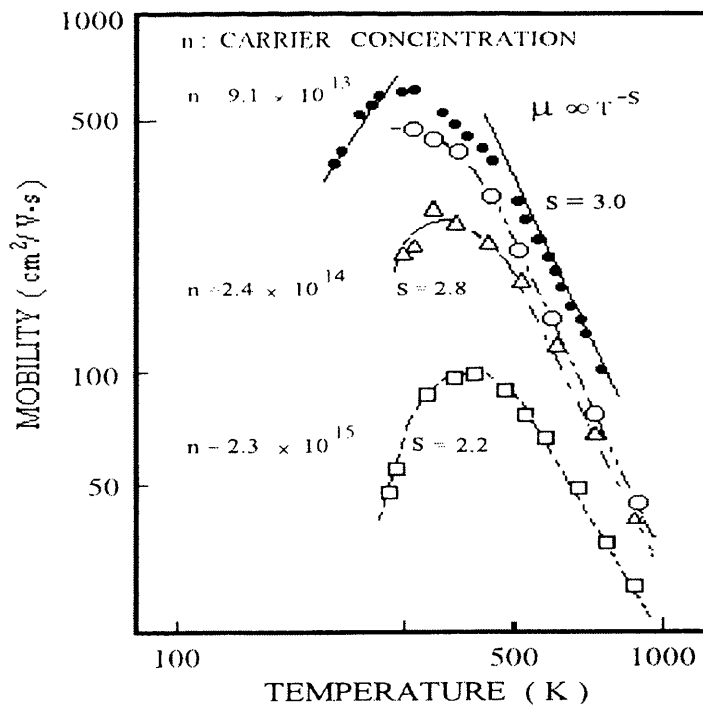
Figure 3.6 Mobility as a function of Temperature for Boron Doped Films [Visser 1992]

The main reason for the substantial reduction in mobility is the high concentration of boron atoms required to yield the desired carrier concentration. This is due to the high activation energy (0.37 eV) as previously mentioned, meaning that around 100 times the required carrier concentration of boron atoms is required [Geis 1992]. These high levels of boron atom can lead the scattering mechanisms to deviate from the theory as shown in figure 3.6. The mobility maxima lie around 300K, whereas in the low – temperature range the index for impurity scattering is around 2.2 [Visser 1992].

Heavily boron (3 x 10^{18} cm^{-3}) doped polycrystalline diamond films have yielded very low mobilities of around 0.6 cm^{2}V^{-1}s^{-1} [Nishimura 1991]. At lower concentrations (2.3 x 10^{15} cm^{-3}) the mobility increased to 32 cm^{2}V^{-1}s^{-1} [Aslam 1992]. The concentration of boron atoms was around 10^{17} cm^{-3} i.e. 100 times, the highest doping concentration achieved in this paper was 1.72 x 10^{17} cm^{-3} which required a boron concentration around 10^{21} cm^{-3} and so the situation only gets worse for high doping levels. In polycrystalline diamond the mobility also decreases with increasing carrier concentration but is much lower than in homoepitaxial films. Grain boundaries and intergranular defects are all detrimental to mobility. A comparison of homoepitaxial and polycrystalline films is available in [Fox 1993], and confirms the lower mobility in polycrystalline films. Film properties improve with grain size, growth temperature, purity and structural perfection [Prelas 1998].

High carrier concentrations therefore require very high levels of boron and high impurity concentrations dictate hopping or impurity band conduction with low mobility [Fox 1993]. Furthermore, the carrier scattering effects on neutral and ionised impurities plus the heavy effective mass in impurity bands will have a large impact on transport properties in heavily doped films [Nishimura 1991].

Section 3.6 Potential n – type dopants

Doping diamond n –type is even more difficult than boron doping and rather less successful. Although relatively shallow levels (~ 0.2 – 0.5 eV) have been predicted for many possible dopants [Li, Na interstitial and N, P substitutional) from ab initio calculations, the incorporation of these impurities into diamond under stable thermodynamic conditions is unlikely [Kajihara 1991]. As mentioned earlier, nitrogen is readily incorporated into diamond films but its high activation produces no real application except field emission from heavily doped layers [Okano 1996].

The most obvious candidate for an n – type dopant in diamond is phosphorus, but this element has a large positive formation energy (10.4 eV) leading to a very small equilibrium solubility [Kajihara 1991]. This is due to the large radius of phosphorus (1.10 Å) compared to carbon (0.77 Å), and the rigidity of the diamond lattice. There are many reports phosphorus doping in the literature [Shimomura 1999, Schauer 1994, Koizumi 1998, Hofsass 1997, Gheeraert 2002, Haenen 2001], but only a few with detailed hall measurements as a function of temperature [e.g. Koizumi 1998]. In fact, doping with phosphorus has proved especially difficult and to date it is widely regarded as only having been achieved in two separate laboratories, NIRIM and CNRS many years later. Figure 3.7 shows the hall results of the NIRIM group.
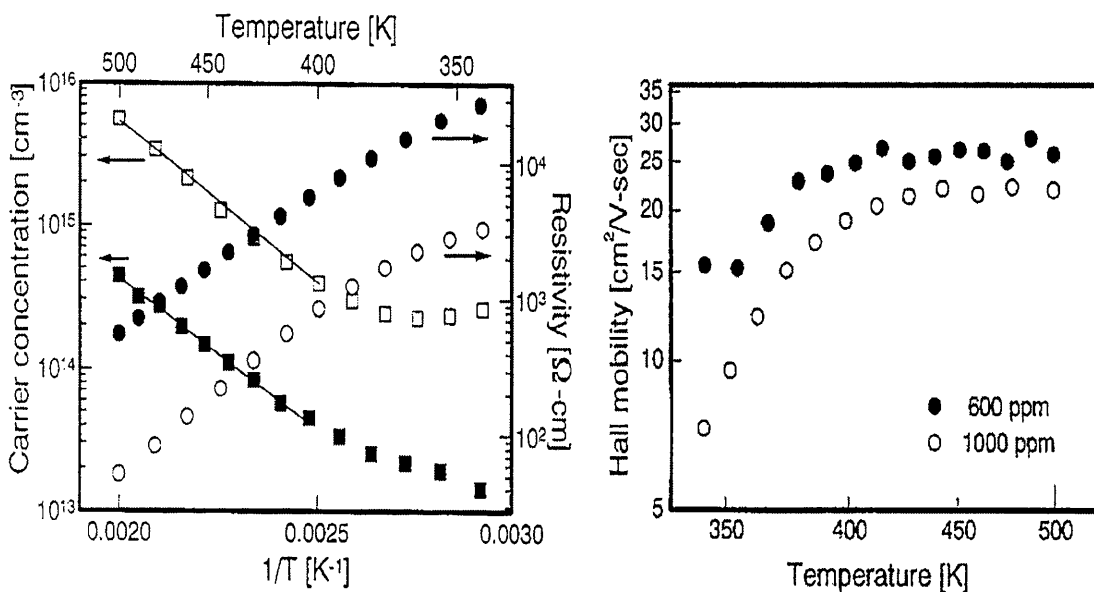
Figure 3.7 Phosphorus CVD Doping [Koizumi 1998]

This data shows the relatively low mobility at room temperature, but later reports show that higher values are achievable (250 $cm^2V^{-1}s^{-1}$ @ 300K) and can be produced routinely [Koizumi 2002]. Phosphorus doped diamond has also been grown epitaxially on boron doped diamond to form the first true p – n junction which even emits UV light [Koizumi 2002]. These results have satisfied even the most vehement sceptics, however no conclusive ion implantation data has been recorded to date [Kalish 2001].

Sulfur doping is still very controversial, and current opinion changes at almost each conference or publication. The possibility of doping with sulfur was first predicted by Saada [Saada 2000], and the first hall measurements were reported by Nishitani – Gamo [Nishitani – Gamo 2000] and reported a mobility of 600 $cm^2V^{-1}s^{-1}$ at 300K. However, the activation energy was 0.37 eV which is suspicially similar to that of boron. Later third party SIMS measurements showed that in fact these samples were contaminated with boron and the hall voltage had been misinterpreted [Kalish 2000]. This unfortunate event was even repeated by another group [Gheeraert 2002] and has led to the common disbelief in new sulfur data regardless of its origin. Ion implantation data is also inconclusive to date [Kalish 2001].

Doping diamond n – type has also been attempted by the use of an interstitial species such as Lithium and Sodium. Ion implantation of these species showed no effect on resistivity except using high doses and in these case hall effect measurements were not possible and thus carrier hopping cannot be ruled out [Prawar 1993]. Ion implantation of oxygen has also been reported as n – type but with no detailed hall measurements and as such is controversial [Prins 2000].

Section 3.7 Hydrogen Surface Conductivity

The discovery of a highly conductive surface layer on as deposited diamond resulted in much excitement in the late 80's [Landstrass 1989]. This conductivity layer was later characterised as p – type [Maki 1992]. Detailed hall measurements showed values of 30 $cm^2V^{-1}s^{-1}$ for a sheet carrier concentration of around 10^{13} cm^{-2} [Hayashi 1997]. As the depth of the layer is not really known, estimates of the depth are made from the SIMS profiles, and the accepted number is around 20nm. This value gives a carrier concentration around 10^{18} cm^{-3} at 297K. Figure 3.8 shows some more recent data on a hydrogenated polycrystalline diamond.
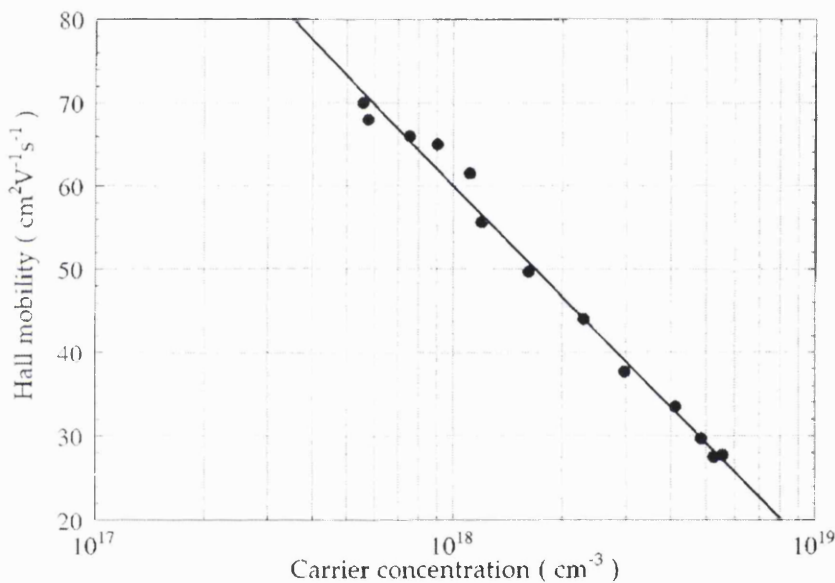
Figure 3.8 Hydrogenated Polycrystalline Diamond [Looi 1998]

These results show that reasonable mobility values are achievable at high carrier concentrations. These films have also been characterised down to liquid nitrogen temperature showing very little variation over the temperature range [Jiang 1999]. As this is the main topic of this thesis, the origin and behaviour of this phenomenon is detailed in the experimental chapters.

References

Aslam M.M., Tamor M.A. and Potter T.F.,

Applied Physics Letters, **61** (1992) 1832

Braunstein G. and Kalish R.,

Applied Physics Letters, **38** (1981) 416

Braunstein G. and Kalish R.,

Journal of Applied Physics, **54** (1983) 2106

Braunstein G., Talmi A., Kalish R., Bernstein T. and Besserman R.,

Radiation Effects, **48** (1980) 139

Collins A.T. and Williams A.W.S.,

Journal of Physics C, **4** (1971) 1789

Collins A.T.,

Semiconductor Science and Technology, **4** (1989) 605

Connell S., Comins J.D. and Sellschop J.P.F.,

Radiation Effects Express, **2** (1988) 57

Davies G.,

The Optical Properties of Diamond,Marcel Dekker Inc 1977, New York, USA

Fox B.A., Malta D.M., Wynands H.A. and van Windhein J.A.,

Proceedings of the third international symposium on diamond materials, Penington, NJ, **97** (1993) 759

Fujimori N., Nakahata H. and Imai T.,

Japanese Journal of Applied Physics, **29** (1990) 824

Geis M. and Angus J.C.,

Scientific American, **October** (1992) 64

Gheeraert E., Casanova N., Tajani A., Deneuville A., Bustarret E., Garrido J.A.,

Nebel C.E. and Stutzmann M.,

Diamond and Related Materials, **11** (2002) 289

Gheeraert E., Casanova N., Tajini A., Deneuville A., Bustarret E., Garrido J.A., Nebel

C.E. and Stutzmann M.,

Diamond and Related Materials, **11** (2002) 289

Gildenblat S. Sh., Grot S.A. and Badzian A.,

Proceeding of the IEEE, **79** (1991) 647

Gildenblat S. Sh., Grot S.A. and Badzian A.,

Proceedings of the IEEE, **79** (1991) 647

Haenen K., Meykens K., Nesladek M., Knuyt G., Stals L.M., Teraji T., Koizumi S.

and Gheeraert E.,

Diamond and Related Materials, **10** (2001) 439

Hartley N.E.W. and Poole M.J.,

Materials Science, **8** (1973) 900

Hartley N.E.W., edited by Picraux S.T. and Choyke W.J.,

Metastable Materials Formation by Ion Inplantation, North Holland 1982, Amsterdam

295

Hayashi K., Yamanaka S., Watanabe H., Sekiguchi T., Okushi H. and Kajimura K.,

Journal of Applied Physics, **81** (1997) 744

Hofsass H., Dalmer M., Restle M. and Ronning C.,

Journal of Applied Physics, **81** (1997) 2566

Jiang N. and Ito T.,
Journal of Applied Physics **85**(1999) 8267

Kajihara S.A., Antonelli A., Bernholc J. and Car R.,
Physical Review Letters, **66** (1991) 2010

Kalish R., Reznik A., Uzan – Saguy C. and Cytermann C.,
Applied Physics Letters, **76** (2000) 757

Kalish R.,
Diamond and Related Materials, **10** (2001) 1749

Koizumi S., Kamo M., Sato Y., Mita S., Sawabe A., Raznik A., Uzan – Saguy C. and
Kalish R.,
Diamond and Related Materials, **7** (1998) 540

Koizumi S., Watanabe K., Hasegawa M. and Kanda H.,
Diamond and Related Materials, **11** (2002) 307

Landstrass M.I. and Ravi K.V.,
Applied Physics Letters, **55** (1989) 975

Landstrass M.I., Plano M.A., Moreno M.A., Williams S.Mc., Pan L.S., Kania D.R.
and Han s.,
Diamond and Related Materials, **2** (1993) 1033

Looi H.J., Jackman R.B. and Foord J.S.,
Applied Physics Letters, **72** (1998) 353

Maki T., Shikama S., Komori M., Sakaguchi Y., Sakuta K. and Kobayashi T.,
Japanese Journal of Applied Physics, **31** (1992) L1446

Nishimura K., Das K. and Glass I.T.,

Journal of Applied Physics, **69** (1991) 3142

Nishitani – Gamo M., Yasu E., Xiao C., Kikuchi Y., Ushizawa K., Sakaguchi I.,

Suzuki T. and Ando T.,

Diamond and Related Materials, **9** (2000) 941

Okano K., Kiyota H., Iwasaki T., Nakamura Y., Akiba Y., Kurosu T., Iida M. and

Nakamura T.,

Applied Physics A, **51** (1990) 344

Okano K., Koizumi S., Silva S.R.P. and Amaratunga G.A.J.,

Nature, **381** (1996) 140

Prawar S. and Kalish R.,

Physical Review, **B51** (1995) 15711

Prelas M.A., Popovici G. and Bigelow L.K.,

Handbook of Industrial Diamonds and Diamond Films, 1998 Marcel Dekker Inc, New

York, USA

Prins J.F.,

Diamond and Related Materials, **9** (2000) 1275

Prins J.F.,

Journal of Physics D, **22** (1989) 1562

Prins J.F.,

Materials Science Reports, **7** (1992) 271

Prins J.F.,

Nuclear Instrument Methods Physics Research, **B59/60** (1991) 1387

Prins J.F.,

Physica B, **185** (1993) 132

Prins J.F.,

Physical Review, **B38** (1988) 5576

Prins J.F.,

Radiation Effects Letters, **76** (1983) 79

Saada D., Adler J. and Kalish R.,

Applied Physics Letters, **77** (2000) 878

Sato S. and Iwaki M.,

Nucleur Instrument Methods Physics Research, **B32** (1988) 145

Shimomura M., Nishimori T., Aukawa T., Takakuwa Y., Sakamoto H. and Kono S.,

Journal of Applied Physics, **85** (1999) 3931

Uzan – Sagay C., Cytermann C., Brener R., Shaanan M. and Kalish R.,

Applied Physics Letters, **67** (1995) 1194

Uzan – Saguy C.,Kalish R., Walker R., Jamieson D.N. and Prawer S.,

Diamond and Related Materials, **7** (1998) 1429

Vavilov V.S., Krasnopevtsev V.V., Milijutin Y.V., Gorodetsky A.E. and Zakharov A.P.,

Radiation Effects, **22** (1974) 141

Visser E.P., Bauhuis G.T., Jaussen G., Vollenberg W., van Enekevort W.J.P. and Giling L.J.

,Journal of Physics: Condensed Matter, **4** (1992) 7365

Williams J.S.,

Reports of Progressions in Physics, **49** (1986) 491

Zeidler J.R., Hewett C.A. and Wilson R.G.,

Physical Review, **B** (1993) 2065

Chapter 4

Diamond Electronic Devices

Contents

Section 4.1 Introduction

Diamond is a very attractive material for electronics for many of the reasons mentioned in earlier chapters. Conventional semiconductors are limited to low temperature operation due to their lower bandgap energy resulting in high intrinsic carrier concentrations at high temperatures. Diamond has a wide bandgap (5.45 eV), is chemically inert and due to its tight lattice has a low diffusion coefficient of impurities blocking in diffusion of metal contacts at high temperatures.

Figure of merit are often used to compare semiconductor performance. The Johnson Figure of Merits (JFM) [Johnson 1963] compares semiconductors in terms of their theoretical performance in microwave power applications:

$$JFM = \frac{E_c v_s}{2\pi}$$

where v_s = Saturated Electron Velocity

E_c = Breakdown Field Strength

$v_s = 2.8 \times 10^7$ cm s^{-1} [Ferry 1975]

$E_c = 10^7$ V cm^{-1} [Bogdanov 1982]

This yields a value of 4.45×10^{13} s^{-1} for diamond which is almost two orders of magnitude greater than silicon and better than any current semiconductor [Davis 1988]. However, this measure has little real meaning as it fails to account for the problems with the doping and growth of diamond as mentioned in earlier chapters. There are alternative figures of merit such as the Keyes Figure of Merit KFM [Keyes 1975] and those proposed by Shenai [Shenai 1987] and Collins [1992] but they all suffer from similar flaws. These calculations also fail to take into account other advantages of diamond for niche application such as the radiation hardness etc.

Section 4.2 Ohmic Contacts

Ohmic contacts are essential for almost all electronic devices. Figure 4.1 shows the most basic method of fabricating an ohmic contact on a p − type semiconductor:

(A)   **(B)**
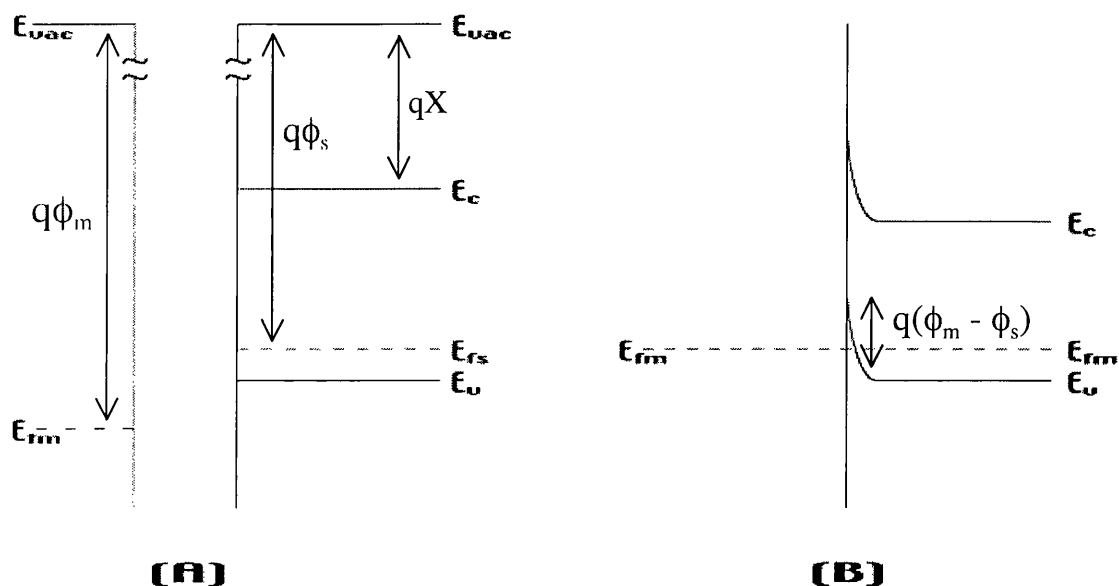
Figure 4.1 Ohmic Contacts

This procedure utilises a metal with a similar work function to the semiconductor, this results in a small barrier height and hence a near ohmic contact. Another approach is to dope the semiconductor very heavily in the contact region and hence reduce the depletion region width. These methods are not generally used on diamond as it has a very large bandgap and is also difficult to dope.

Diamond can be damaged in local areas to create graphitic regions which can be used to make ohmic contacts. Several methods can be used to locally damage the surface, such as particle bombardment [Hoffman 1990], laser irradiation [Geis 1989]. However, these techniques can lead to noisy contacts as the contact area is an undefined mixture of diamond and damaged carbon phases. These contacts are particularly poor for variable temperature measurements.

A far more controllable approach to locally damaging the surface can be achieved during the metal deposition. By using a carbide forming metal such as titanium

beneath the Au contact, carbide formation results and can be enhanced by heating to 400 °C [Moazed 1998, Shiomi 1989, Werner 1996]. A very thin layer can be used, but it needs to be protected from the atmosphere by the Au cap. However, a considerable amount of intermixing between the Ti and Au layers occurs after the high temperature anneal [Venkatesan 1993]. Ti has also been detected on the contact surface on this effect has resulted in an increase in contact resistance due to the formation of Titanium oxide [Naseem 1993]. Ti diffuses very slowly through Pt [Tisone 1972], which doesn't readily form an oxide and when used as an intermediate buffer layer can restrict diffusion up to temperatures of 900 °C [Waytena 1996]. An alternative approach is to used a Si layer to form SiC at the metal – diamond interface [Werner 1996]. In a study of contacts to IIa diamonds, carbide forming materials produced ohmics with a contact resistance as low as 10^{-3} Ω cm while non – carbide forming metals produced blocking contacts [Hewett 1993]. This method can produce strong adherence and low contact resistance, but requires a three layer evaporation utilising an e – beam for the Pt layer.

The formation of local heavily doped regions on diamond for ohmic contacts is highly problematic due to the problems doping diamond. As with conventional semiconductors there are two main approaches, growth or ion implantation in the relevant areas.

Selective growth of local areas of highly doped CVD diamond is made difficult by the problem of masking areas where deposition is not desired [Chen 1995]. Nishimura et al [Nishimura 1990] reduced the contact resistivity to 10^{-4} Ω cm^{-2} with a local carrier concentration of 3 x 10^{20} cm^{-3}. This approach does not result in the creation of a damaged region as in the case of ion implantation.

Ion implantation is a controversial topic, not least because it is difficult to de - convolute the resulting damage from the apparent doping. The advantage of ion implantation is the ease at which it is performed, as the masking process is greatly simplified. However, it is rather difficult to drive the dopants into substitutional sites. The first method was published by Prins [Prins 1989], and the resulting damaged was annealed as mentioned in previous chapters. This technique was refined to produce

contacts with specific contact resistance as low as 10^{-6} Ω cm^2 [Venkatesan 1992]. Unfortunately this technique requires a post implantation anneal which may not be appropriate for some devices.

Hydrogen terminated diamond has significant advantages over normal diamond for ohmic contacts as it has been shown to reduce Fermi Level pinning presumably by passivating interface states [Mori 1991]. This leads to a Schottky Barrier Height that depends on the metal work function / electronegativity and hence a suitable candidate can be chosen for an ohmic contact, as seen in figure 4.2 (A) [Mori 1991].
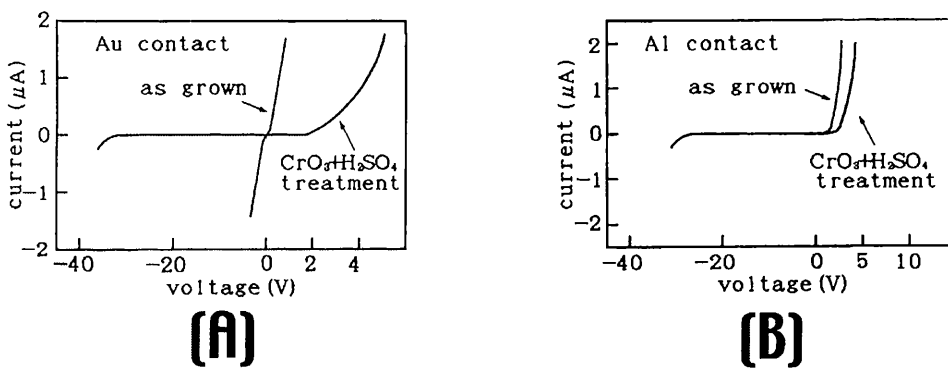
Figure 4.2 Ohmic / Schottky Contacts [Mori 1991]

This will result in a very shallow barrier height and as there are a high density of carriers in the hydrogen surface conductivity layer the depletion region will be negligible. Au is generally chosen as the ohmic but can lead to adhesion problems due to the inertness of both the metal and the substrate. In this case Ti can be used as the adhesion aid and as the gold will over cover the edges the contact will still be ohmic.

Thermal evaporation of any material onto the diamond surface will also remove adsorbates and their associated conductivity [Williams 2002]. This means that all structures fabricated on the hydrogen surface conductive layer must be planar.

Section 4.3 Schottky Contacts

Schottky barrier diodes are formed as a result of differing work functions between the semiconductor and the metal as shown in figure 4.2:

(A)   **(B)**
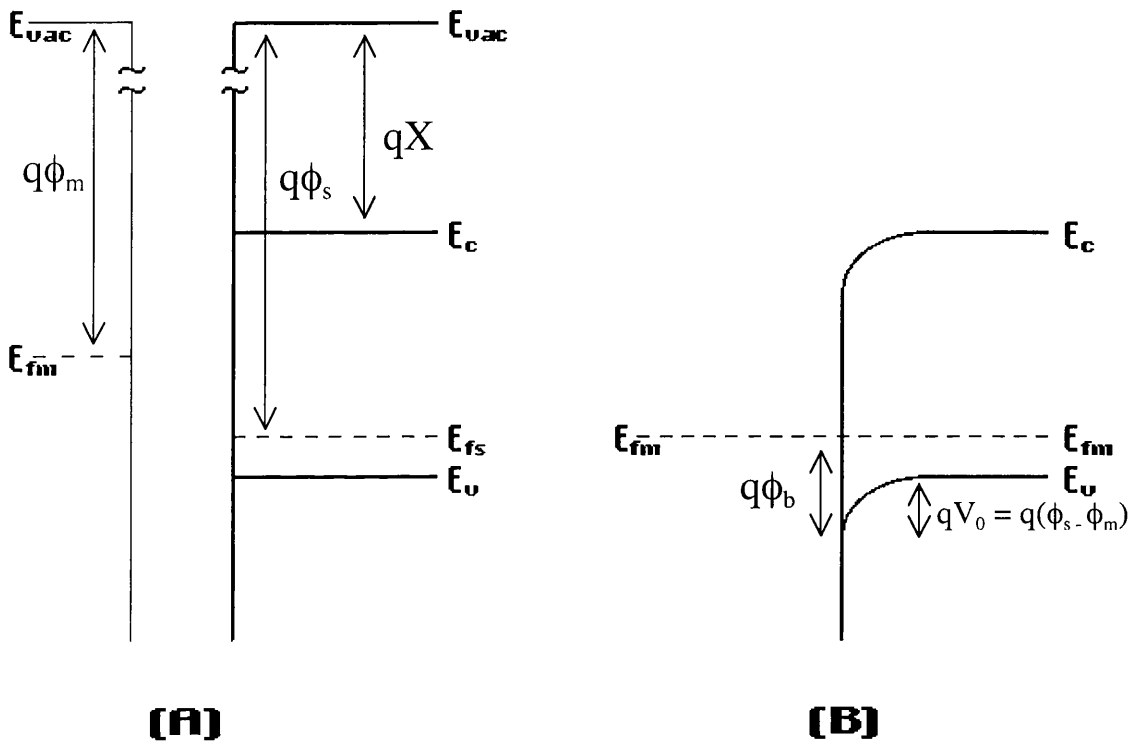
Figure 4.3 Schottky Contacts

As the metal and semiconductor come into contact there is a transfer of charge until the Fermi levels align at equilibrium. In the case of a p – type semiconductor (figure 4.3), electrons are injected from the metal causing a negative charge on the semiconductor side and a depletion region is formed due to the recombination with holes. This sets up a dipole as there is now an overall negative charge at the semiconductor interface due to the lack of compensating holes and a positive charge in the metal due to out diffusion of electrons. This also means that the valence band of the semiconductor must bend away from the Fermi Level at the interface. As the metal has an enormous electron density its Fermi Level is unaffected by the relatively small flow of electrons into the semiconductor and the depletion region is almost entirely within the semiconductor.

Most schottky diode fabrication on diamond is carried out on boron doped material due to the difficulty of doping diamond n – type. Schottky Barrier Heights in the region of 1.7 eV have been reported regardless of the metal used [Glover 1973, Mead 1976], this is a common phenomenon in semiconductors and is referred to as Fermi Level pinning. Several groups have demonstrated these devices operating at temperatures up to 700° C [Glover 1973, Lightowlers 1976, Geis 1987, Gildenblat 1991, Tachibana 1992].

The leakage current of these structures was lower on (100) diamond than (110) and (111). It has been suggested that this is due to the (100) surface being generally smoother and containing a lower structural defect density than the other orientations [Gildenblat 1990], this also explains the generally poorer performance on polycrystalline diamond.

Figure 4.4 shows a cutting edge device with over 11 orders of rectification and reverse bias leakage as low as 10^{13} A cm^{-2} i.e. below the detection limit [Geis 1993]. Near ideal schottky junctions have been fabricated on highly doped films of the order of 10^{17} cm^{-3} [Takeuchi 2001].
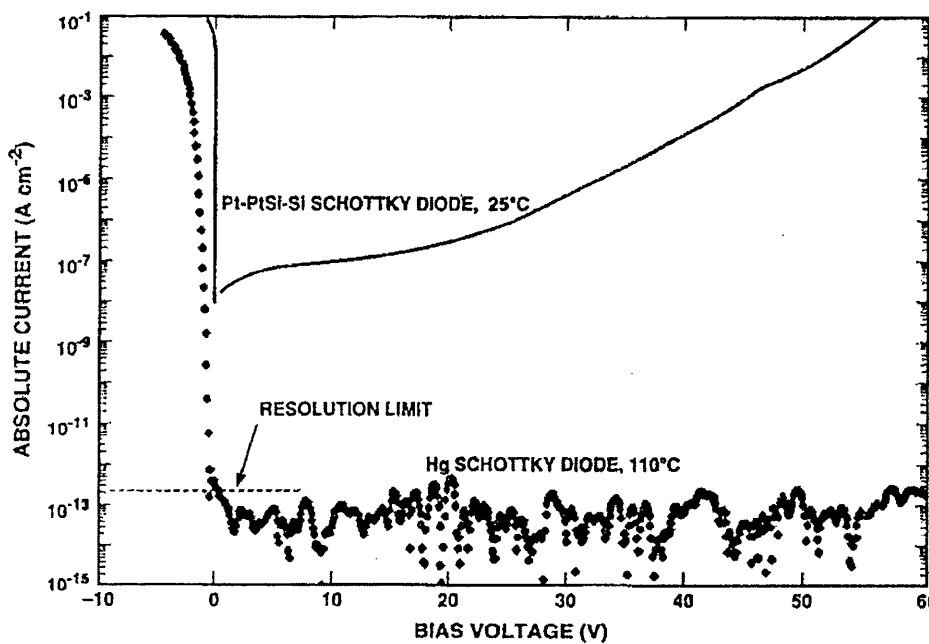
Figure 4.4 Boron Schottky Contact [Geis 1993]

At the beginning of the 1990's many papers on boron devices are complicated by the added effect of the hydrogen surface conductivity layer. This also explains to some extent why boron doped devices are improved by cleaning in $CrO_3 + H_2SO_4$ at 170° C, as this will totally remove the layer [Gildenblat 1990]. It also explains why some boron devices show a schottky barrier height dependence on the metal contact [Hayashi 1996].

Very high performance schottky contacts have been fabricated on intrinsic diamond utilising the hydrogen surface conductivity layer. These devices show very low ideality factor (1.1 [Kawarada 1994]) and exceptionally low leakage. Hydrogen surface conductivity removes Fermi Level pinning as mentioned earlier (see also figure 4.2), and the pinning returns on acid treatment [Mori 1991]. Figure 4.5 shows an exceptional schottky contact fabricated on the hydrogen surface conductivity layer:
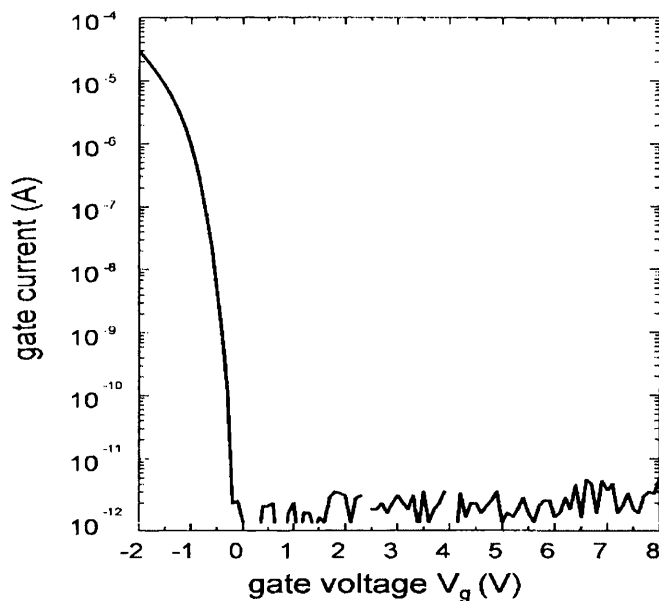
Figure 4.5 Hydrogen Surface Conductive Device
[Gluche 1997]

Comparable devices have been fabricated on polycrystalline diamond by simple shadow masking techniques [Looi 1998] and generally do not breakdown until very high voltages (> 100V).

Section 4.4 MISFET Structures

Unfortunately diamond does not have a native oxide like silicon and so MISFET Structures must be fabricated on diamond by using different materials as the insulating gate. Intrinsic diamond [Pang 1997], SiO_x [Tsugawa 1999] and CaF_2 [Umezawa 2000, Williams 2002] have all been studied as gate materials on diamond. Devices with low leakage currents (10 pA) and high operating temperatures (300 °C) have been reported in the literature [Gildenblat 1991] using 100 nm of SiO_2 as the gate dielectric.

This technique has also been demonstrated using the hydrogen surface conductivity layer and a CaF_2 gate [Umezawa 2000]. However, it is not clear how adsorbates which are required for the conductivity can exist under a thermally evaporated material. It is suggested that the small gate width and high gate bias allow for the operation of this device. A typical device is shown in figure 4.6.
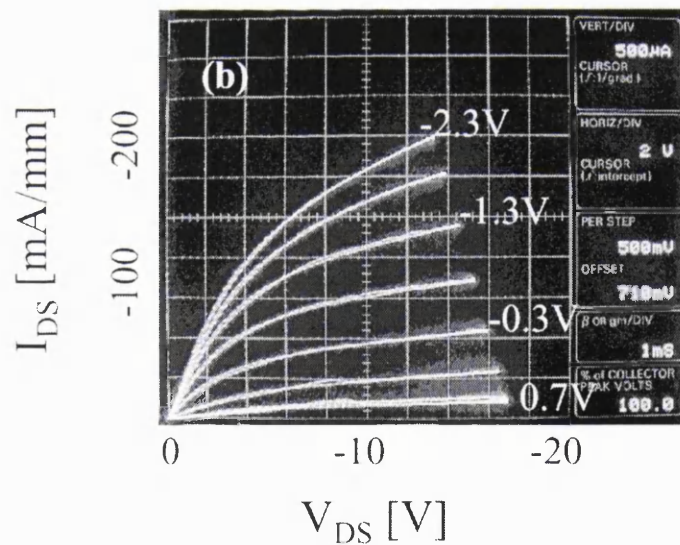
Figure 4.6 Diamond MOSFET [Umezawa 2000]

Section 4.5 MESFET Structures

MESFET structures do not suffer from diamonds inherent lack of a native oxide and can be fabricated with relative ease. Early devices fabricated on Boron doped CVD diamond suffered from high leakage [Shiomi 1989]. These devices were later improved using a type IIa diamond and solid state diffusion to create a 50 nm thick channel [Tsai 1991], this device gave a transconductance of 0.7 μS/mm. Further enhancements in doping control led to the first MESFET exhibiting pinch off and saturation [Shiomi 1994].

Far superior devices can be fabricated using the hydrogen surface conductivity layer. Transconductance values of 25μS/mm were reported using a simple Al gate and Au ohmics structure [Kawarada 1994]. The structure of these devices was refined further to yield transconductance values as high as 7mS/mm operating in enhancement or depletion mode depending of the gate metal electronegativity [Hokazono 1997]. These devices have also been demonstrated to handle high power levels (6W/mm) [Gluche 1997] and have been integrated into logic circuits [Hokazono 1997]. A typical device is shown in figure 4.7.
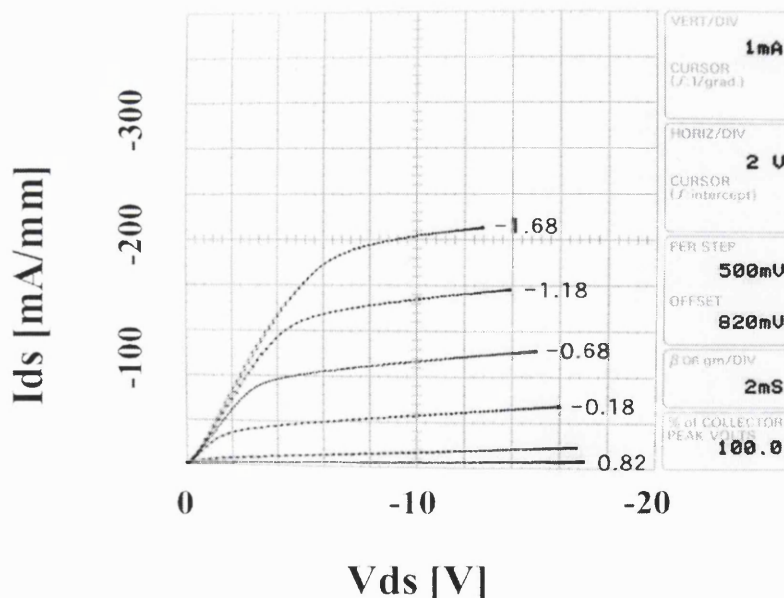
Figure 4.7 Diamond MESFET [Umezawa 1999]

References

Bogdanov A.V., Vikulin I.M. and Bogdanova T.V.,

Soviet Physics Semiconductors, **16** (1982) 720

Chen C.F., Chen S.H., Hong T.M. and Tsai M.H.,

Journal of Applied Physics, **77** (1995) 940

Collins A.T.,

Materials Science and Engineering, **B11** (1992) 257

Davies R.F., Sitar Z., Williams B.E., Kong H.S., Kim H.J., Palmour J.W., Edmond

J.A., Ryu J., Glassand J.T. and Carter J.,

Materials Science and Engineering, **B1** (1988) 77

Ferry D.K.,

Physical Review B, **12** (1975) 2361

Geis M.W., Efremow N.N. and von Windheim J.A.,

Applied Physics Letters, **63** (1993) 952

Geis M.W., Rathman D.D., Ehrlich D.J., Murphy R.A. and Lindley W.T.,

IEEE Electron Device Letters, **8** (1987) 341

Geis M.W., Rothschild M., Kunz R.R., Aggarwal R.L., Wall K.F., Parker C.D.,

McIntosh K.A., Efrenow N.N., Zayhowski J.J., Erlich D.J. and Butler J.E.,

Applied Physics Letters, **55** (1989) 2295

Gildenblat G. Sh., Grot S.A., Badzian A.R., Hatfield C.W. and Badzian T.,

IEEE Electron Device Letters, **12** (1991) 37

Gildenblat G. Sh., Grot S.A., Wronski C.R. and Badzian A.R.,

Proceedings of the IEEE, **79** (1991) 647

Gildenblat G.Sh., Grot S.A., Hatfield C.W. and Badzian T.,

IEEE Electron Device Letters, **11** (1990) 371

Glover G.H.,

Solid State Electronics, **16** (1973) 937

Gluche P., Aleksov A., Vescan A., Ebert W. and Kohn E.,

IEEE Electron Device Letters, **18** (1997) 547

Hayashi H., Yamanaka S., Okushi H. and Kajimura K.,

Applied Physics Letters, **68** (1996) 376

Hewett C.A. and Zeidler J.R.,

Diamond and Related Materials, **2** (1993) 1319

Hoffman A., Paterson P.J.K. and Prawer S.,

Nucleur Instrumental Methods in Physics Research B, **52** (1990) 63

Hokazono A., Ishikura T., Nakamura K., Yamashita S. and Kawarada H.,

Diamond and Related Materials, **6** (1997) 339

Johnson E.O.,RCA

Review **26** (1963) 163

Kawarada H., Aoki M. and Ito M.,

Applied Physics Letters, **65** (1994) 1563

Kawarada H., Aoki M. and Ito M.,

Applied Physics Letters, **65** (1994) 1563

Keyes R.W.,

Proceedings of IEEE, **63** (1975) 740

Lightlowlers E.C. and Collins A.L.,
Journal of Physics D, **9** (1976) 951

Looi H.J., Pang L.Y.S., Wang Y., Whitfiled M.W. and Jackman R.B.,
Diamond and Related Materials, **7** (1998) 565

Mead C.A. and McGill T.C.,
Physical Letters, **58A** (1976) 249

Moazed K.L., Nguyen R. and Zeidler J.R.,
IEEE Electron Device Letters, **9** (1988) 350

Mori Y., Kawarada H. and Hiraki A.,
Applied Physics Letters, **58** (1991) 940

Naseem H.A., Meyyappan I., Prasad C.S. and Brown W.D.,
International Journal of Microcircuits Electronic Packaging, **16** (1993) 257

Nishimura K., Das K., Iwase M., Glass J.T. and Kobashi K.,
MRS Symposium Proceedings, **162** (1990) 341

Pang L.Y.S., Chan S.S.M., Johnson C., Chalker P.R. and Jackman R.B.,
Diamond and Related Materials, **6** (1997) 333

Prins J.F.,
Journal of Physics D, **22** (1989) 1562

Shenai K., Scott R.S., and Baliga B.J.,
IEEE Transactions on Electron Devices, **36** (1989) 1811

Shiomi H., Nakahata H., Imai T., Nishibayashi Y. and Fuijmori N.,
Japanese Journal of Applied Physics, **28** (1989) 758

Shiomi H., Nakahata H., Imai T., Nishibayashi Y. and Fujimori N.,

Japanese Journal of Applied Physics, **28** (1989) 758

Shiomi H., Nishibayashi Y. Toda N., Shikata S. and Fujimori N.,

4th International Conference on New Diamond Science and Technology, Kobe,(1994) 661

Tachibana T., Williams B.E. and Glass J.T.,

Physical Review B, **42** (1992) 11972

Takeuchi D., Yamanaka S., Watanabe H. and Okushi H.,

Physica Status Solidi, **186** (2001) 269

Tisone T.S. and Drobek J.,

Journal of Vacuum Science Technology, **9** (1972) 271

Tsai W., Delfino M., Hodul D., Riaziat M., Ching L.Y., Reynolds G. and Cooper C.B.,

IEEE Electron Device Letters, **12** (1991) 157

Tsugawa K., Kitatani K., Noda H., Hokazono A., Hirose K., Tajima M. and Kawarada H.,

Diamond and Related Materials, **8** (1999) 927

Umezawa H., Taniuchi H., Arima T., Tachiki M., Tsugawa K., Yamanaka S., Takeuchi D., Okushi H. and Kawarada H.,

Japanese Journal of Applied Physics, **39** (2000) L908

Umezawa H., Tsugawa K., Yamanaka S., Takeuchi D., Okushi H., Kawarada H.,

Japanese Journal of Applied Physics, **38** (1999) L1222

Venkatesan V. and Das K.,

IEEE Electron Device Letters, **13** (1992) 126

Venkatesan V., Malta D.M., Das K. and Belu A.M.,

Journal of Applied Physics, **74** (1993) 1179

Werner M., Job R., Denisenko A., Zaitsev A., Fahrner W.R., Johnson C., Chalker P.R. and Buckley – Golder I.M.,

Diamond and Related Materials, **5** (1996) 723

Williams O.A., Nebel C.E. and Jackman R.B.,

Physica Status Solidi, **193** (2002) 577

Chapter 5

Experimental Methods

## Contents

Section 5.1: Scanning Electron Microscopy

Scanning Electron Microscopy or SEM as it is popularly known is a powerful extension of the principles of optical microscopy. Electrons have much smaller wavelengths than light (0.012nm for V=10,000V compared to 400 – 700 nm range of visible light [Schroder 1998, 653]), and this means that much larger magnifications are possible than with a conventional light microscope. By scanning a focused beam of electrons across a sample an image can be constructed by detecting the secondary and / or back scattered electrons.

Secondary electrons (SE) are generated by the interaction of the incident electron beam and weakly bonded electrons within the sample being studied. Secondary electrons are of low energy and are only emitted from the approximately the top 10 nm of the film. This low energy also means that they are influenced by electromagnetic fields and hence can be accelerated to the detector even if there emission is not in the direction of the detector.

Back scattered electrons (BSE) are of much higher energies as they are due to elastic collisions between the incident beam and relatively tightly bound electrons in the specimen. BSE emission intensity increase with increasing atomic number and can be used to differentiate regions of different elements.

A schematic of the apparatus is shown in figure 5.1. Electrons are generated by thermionic emission in the electron gun and are accelerated using a positive bias of around 20-40 keV on the condenser aperture. On passing through the aperture they are then focused into a tight beam by the condenser lens and scanned across the sample using the scanning lens. Focusing is assisted by the objective lens. Secondary electrons are collected by the detector and are amplified and projected on the CRT. The entire electron system has to be contained within a high vacuum to maintain a useable mean free path. Also, as electrons are emitted the sample can become charged thus reducing subsequent emission. Hence insulating samples are coated in a thin layer gold.
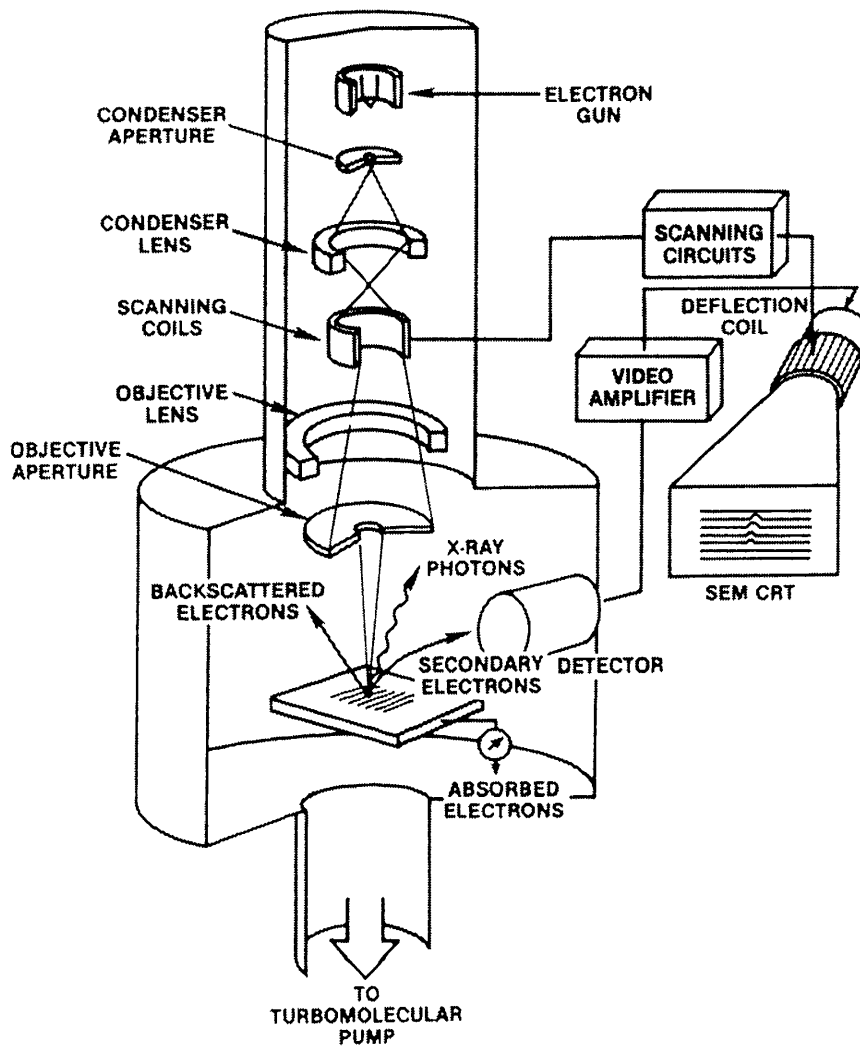
Figure 5.1 Standard SEM Apparatus [Young 1986]

Typical SEMs have a beam diameter of around 1 – 10 nm but resolution is ultimately limited by the broadening of the beam due to scattering at the sample surface. SEM in this work is used to measure grain size and morphology of the diamonds characterised.

Section 5.2: Scanning Tunnelling Microscopy

Scanning Tunnelling Microscopy or STM is a Nobel Prize winning technique based on a quantum mechanical process. The STM was developed by Gerd Binnig and Heinrich Rohrer in the IBM research laboratory, Ruschlikon, Switzerland [Binnig 1982]. A schematic of the basic implementation is shown in figure 5.2.
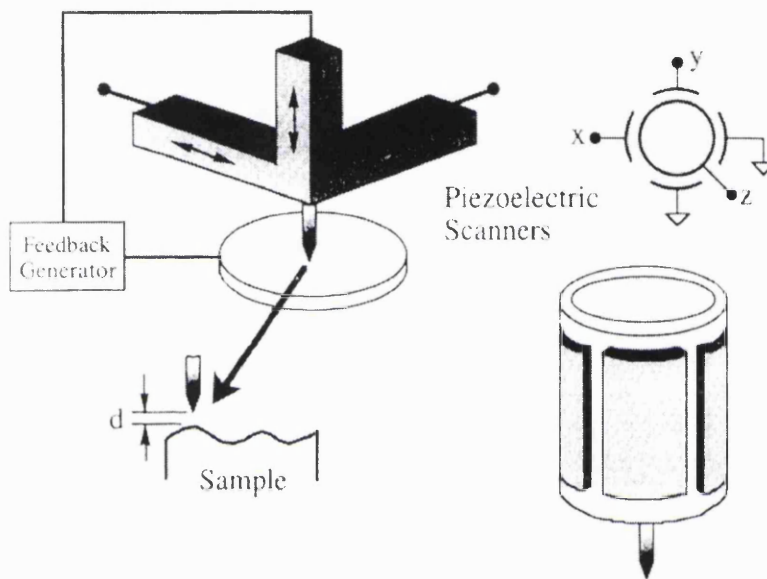
Figure 5.2 A Basic STM Setup [Schroder 1998]

A metallic probe tip is scanned across a sample using piezoelectric elements. The distance d between the tip and the sample is around 1 nm and is biased at around 0.05 V. As the tip is very close to the sample surface there is a small associated tunnel current of around 1 nA, which is in essence a measure of the overlap of the wave functions of the tip and sample within the gap between them. However, the current is largely determined by the distance between the tip and sample surface or the sample topography.

There are two basic modes of operation, constant current mode and constant height mode. In the constant current setup, the gap spacing and hence the current is held constant as the probe is scanned across the sample surface. This means that the piezoelectric voltage read from the Z transducer will be proportional to the vertical

displacement and hence a contour plot can be generated. In constant height mode the probe is scanned across the surface with no Z movement and hence the current varies as the gap spacing changes. A contour plot can be generated from the variation in current. Both of these techniques can be fooled by inhomogeneous surface conductivity as a region of lower conductivity will appear as a dip in the image.

As an idea of the sensitivity, for an effective work function of 4 eV, a gap spacing change from 1 nm to 1.1 nm changes the current density by a factor of eight [Schroder 1998]. The sharpness of the tip is also paramount, and it is commonly believed that it a single atom at the probe tip dominates the device function. This can also lead to problems when the tip "crashes" into the sample.

STM is often used as a method of imaging the surface termination of diamond surfaces at the atomic level. Kawarada et al [Kawarada 1996] showed dimmer rows and terraces due to hydrogen termination on various orientations of diamond surfaces. It has also been used to characterise the growth steps and terraces on single crystal [Tsuno 1994, Kuang 1995] and polycrystalline diamond [Godbole 1997, Lukins 2001]. Even if atomic resolution cannot be obtained, STM is a powerful technique for measuring surface roughness [Koslowski 1998].

One problem of STM measurements on diamond is the high intrinsic resistvity inherent in the films. This can either be solved by using boron doped films or the hydrogen surface conductivity layer. In a UHV environment however, the hydrogen surface conductivity layer is not stable and boron doped films are preferred. UHV is preferred for the use of Tungsten tips which are the standard, however, in air Pt – Ir tips can be used and the hydrogen surface conductivity layer yields more than enough conductivity to stop the films from becoming charged and hence compromising the measurement.

Section 5.3: Raman Spectroscopy

When light is scattered from the surface of a sample, the scattered light can be measured and contains mainly the wavelengths that were incident on it and this is called Rayleigh scattering. However, at much lower intensities, different wavelengths result due to the interaction with the material. Raman spectroscopy is based on the Raman effect [Raman 1928], where an incident photon loses some of its energy to the lattice via a phonon and hence emerges as a lower energy photon. A lower energy photon must have a lower frequency (as E = hf) and this shift is known as Stokes – shifted scattering. The opposite effect can also happen where the photon absorbs a phonon and hence emerges with a higher energy and thus higher frequency. This effect is much less pronounced and the Stokes – more scattering is usually monitored. The resulting energy distribution is shown in figure 5.3.
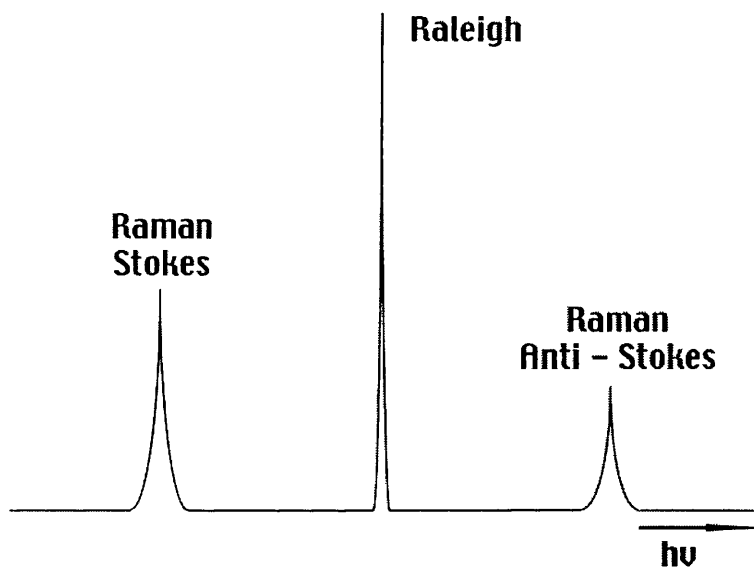
Figure 5.3 Energy Distribution of Scattered Light

The intensity of Raman scattered light is very weak and hence an intense monochromatic light source is generally used, most often a laser. The laser is focused on the sample surface using a conventional microscope, the power usually being held less that 5mW to reduce sample heating [Raptis 1983]. As seen in figure 5.3, the

scattered light must be passed through a sharp filter to remove the Rayleigh component and then a monocromator can be used to characterise the frequency shift.

Raman spectroscopy is used extensively in the diamond community. At room temperature diamond yields a sharp line at 1332 cm^{-1} which is very different from the spectra of other forms of carbon and hence is unambiguous evidence of diamond [Knight 1985]. This Raman line generally has a Full Width Half Maximum (FWHM) of around 2 cm^{-1} for natural type IIa diamond, increasing to 2-14 cm^{-1} for typical cvd material [Rutledge 1998].

Other important peaks are the so called D and G bands occurring at 1340 and 1580 cm-1 respectively. The D band is due to disordered carbon and the G band is due to single crystal graphite [Dillon 1984, Knight 1985]. Amorphous carbon yields a broad asymmetric band around 1500 cm^{-1} [Knight 1985] and nanocrystalline diamond around 1140 cm^{-1} [Nemanich 1989].

Other important experimental considerations are the relative intensities of the different carbon peaks. The Raman intensity of the graphite spectrum is 50 times that of the diamond spectrum. [Wada 1981], and amorphous carbon 233 times [Sails 1996]. The wavelength of the laser used to pump the sample is also of critical importance. The intensity and position of the non diamond carbon peaks are known to be affected by the wavelength of the laser [Wagner 1992, Yoshikawa 1989], and these effects have been attributed to either increased laser adsorption at shorter wavelengths [Wagner 1989] or resonance [Fayette 1994].

Raman spectroscopy has become the dominant technique for the analysis of the carbon bonding components in CVD diamond films. This is due to the high sensitivity of the technique to different carbon bonding types, but also the speed, simplicity and modest cost of the apparatus.

Section 5.4: Hydrogenation

Hydrogenation has become a controversial subject. Fundamentally it is related to diamond growth and this has inevitably led to the conditions under which it is performed. When hydrogen surface conductivity was first discovered, CVD diamond films were found to be conductive on removal from the growth chamber and this was attributed to the cooling of the films within a hydrogen plasma [Landstrass 1989]. As a result, many groups rehydrogenate films by immersing them in a hydrogen plasma at growth conditions and then cooling them to room temperature within the hydrogen plasma [Sauerer 2001, Jiang 1999, Maki 1992]

It is actually possible to rehydrogenate films in much shorter durations without cooling in a hydrogen plasma [Williams 2001]. It is also possible to rehydrogenate using a hot filament apparatus as a source for the atomic hydrogen [Ristein 2001, Sung Gi 1995]. Long duration hydrogenations lead to substantial surface etching [Kowlowski 1998] and should generally be avoided.

Early work during this PhD studied the effects of varying plasma conditions and found that there was little effect on the resulting surface conductivity. The standard conditions that are used during this thesis are 500° C, 40 torr, 800 watts, 5 mins. However, success has also been obtained with a wide range of conditions with pressures as low as 8 torr and durations as short as 2 seconds.
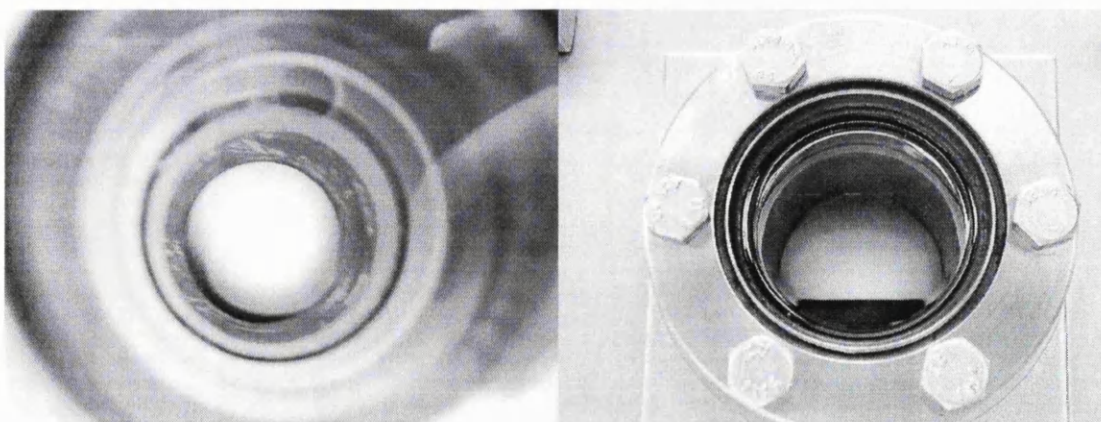
Figure 5.4 Pure Hydrogen Plasmas

Section 5.5: Van Der Pauw Resistivity

The Van der Pauw technique [Van der Pauw 1958] allows the derivation of the sheet resistivity of a sample of an arbitrary shape without any knowledge of the current flow paths. The following rules must be obeyed however:

a) The sample must be uniformly thick

b) The sample must be uniformly doped

c) The sample must be continuous with no isolated holes

d) The contacts must be placed at the sample circumference

e) The contact size must be small compared to the sample size

A schematic of an acceptable setup is shown in figure 5.5. It should be noted however, that in the case of diamond, a number of the above conditions will actually be violated due to the polycrystalline nature of the film (a), the non – uniformity of the hydrogen termination (b). Condition (e) can be particularly difficult to satisfy when the samples are small and of random shape. This means that there will be a small amount of error involved in this simplification but it is unavoidable.
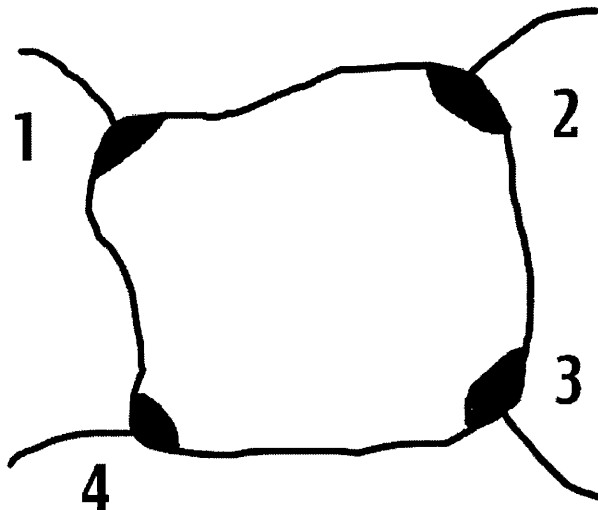
Figure 5.5 Typical Van der Pauw Configuration

Using the above technique the resistivity of the sample can be calculated by making just two measurements:

$$\rho_{sh} = \frac{\pi}{\ln(2)} \frac{R_{12,34} + R_{23,41}}{2} F$$

where $\qquad R_{12,34} = \frac{V_{12,34}}{I_{12}} \qquad$ and $\qquad R_{23,41} = \frac{V_{23,41}}{I_{23}}$

With reference to figure 5.5, The voltage $V_{12,34}$ is the open circuit voltage between terminals 3 and 4 and when a current (I_{12}) is passed between terminals 1 and 2, this gives $R_{12,34}$. Likewise the voltage $V_{23,41}$ is the open circuit voltage between terminals 4 and one when a current (I_{23})is passed through terminals 2 and 3, giving $R_{23,41}$. These measurements are best made by using a constant current source and a high impedence voltmeter. As this technique measures open circuit voltage, there is no potential drop across the contact resistance and the defined resistivity eliminates these contact complexities. Generally more measurements are made than just the minimum to remove any ambiguities in the ohmic nature of the contacts.

F is defined as the correction factor and is a function of $R_r = R_{12,34} / R_{23,41}$ and is equal to unity when these values are identical.
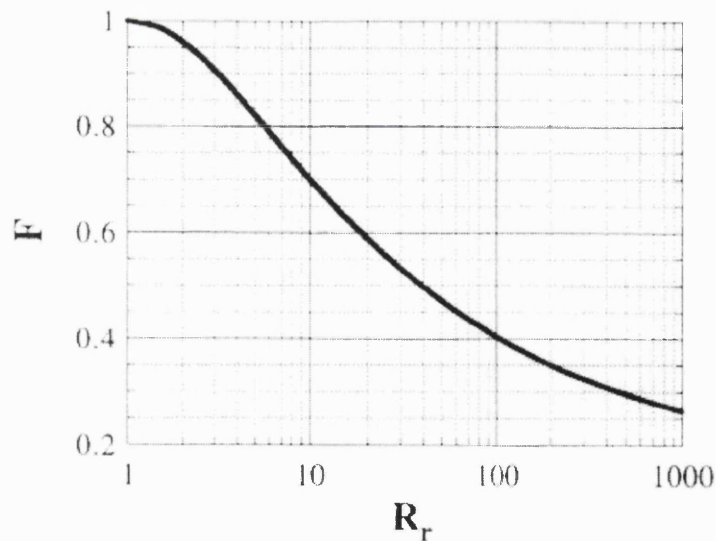
Figure 5.6 Correction Factor

Section 5.6: Hall Effect

In 1879 Hall discovered a potential difference across two sides of a metal when a current was being passed through it under a magnetic field [Hall 1879]. This phenomenon is now named after him as the Hall Effect. This is an extremely powerful technique as it can quantify the number of charge carriers in a material and their type. When combined with a resistivity measurement the mobility can also be derived. Figure 5.6 shows this phenomenon schematically:
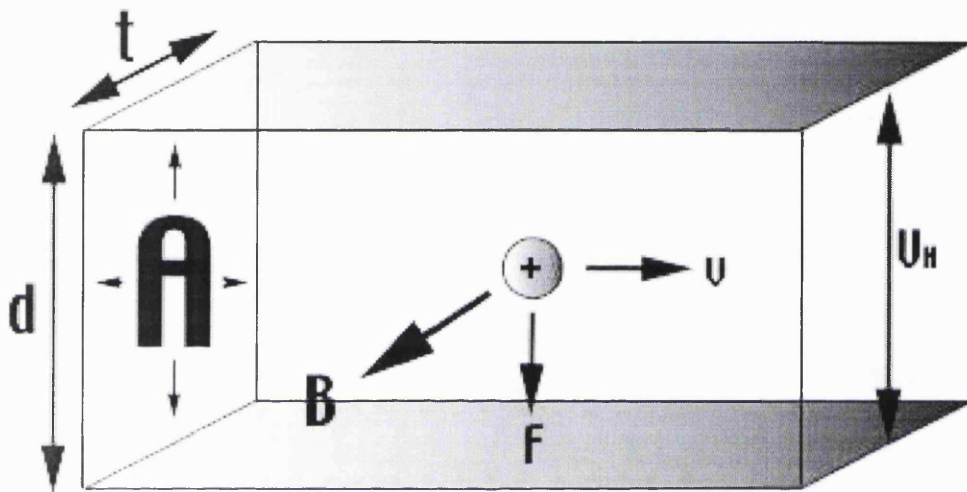
Figure 5.6 The Hall Effect

Figure 5.6 shows a p –type semiconductor with a carrier (hole) moving from left to right. The field is perpendicular to the the motion of the carrier, coming out from the page. According to Fleming's left hand rule there will be a resultant force downwards on the carrier. The force on a particle due to a magnetic field is given by:

$$F = Bqv$$

where B = Magnetic Field Strength,

  q = The charge on the hole,

  F = The force exerted on the carrier,

  v = The drift velocity of the charge carriers.

As more and more carriers move towards the bottom of the figure, a positive charge builds up and thus a potential difference is established between the top and bottom of the semiconductor. The build up of charge increases until the potential difference becomes so large that it prevents any further increase. This potential difference is called the Hall voltage V_H. Therefore it follows:

$$F = qE = \frac{qV_H}{d} = Bqv$$

(where E = electric field strength, d = distance between top and bottom)

$$\therefore V_H = Bvd$$

and also:

$$I = nAvq \rightarrow v = \frac{I}{nAq}$$

where n = number of charge carriers per unit volume,

A = cross – sectional area of material

$$\therefore V_H = \frac{BdI}{nAq} = \frac{BI}{nqt}$$

Hence from the hall voltage one can deduce the number of free carriers in the material and their type from the polarity. If we also know the resistivity of the material from the Van der Pauw method then we can also deduce the mobility:

$$\mu = \frac{1}{nq\rho}$$

where μ = The mobility of the free carriers

ρ = The resistivity of the material

Section 5.7 Device Fabrication

The devices fabricated in this thesis are rather simple in comparison to those made on other materials. Much of the work carried out was on polycrystalline material which, unless it is polished, makes the utilisation of photolithography rather problematic. It is also very difficult to use photolithography on very small samples due to "beading" effects at the sample edges. However it is very possible to build decent schottky contacts and Au ohmics by using basic shadow masking, which has been used extensively in this thesis. Figure 5.7 illustrates the principle of shadow masking:
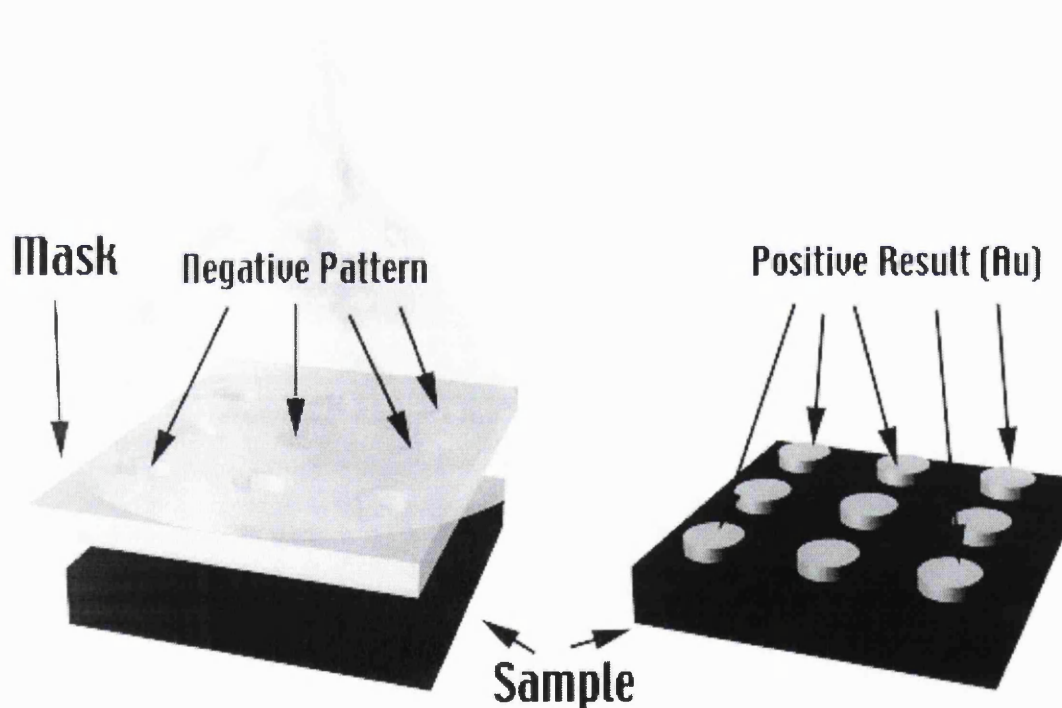
Figure 5.7 Shadow Masking

A mask with the negative pattern of that desired is drilled / laser cut etc and placed over the sample. On evaporation, only the exposed areas of the sample receive the metal coating. This method can be used to make structures down to around a few hundred micron. Crude shadow masking can also be performed with aluminium foil, and this technique is essential for samples of irregular shapes.

Photolithography can be used to fabricate far smaller structures. The procedure is ultimately very similar to shadow masking, but the mask is made of a photoresist. There are two main techniques, "liftoff" and "etching". Liftoff is demonstrated in figure 5.8:
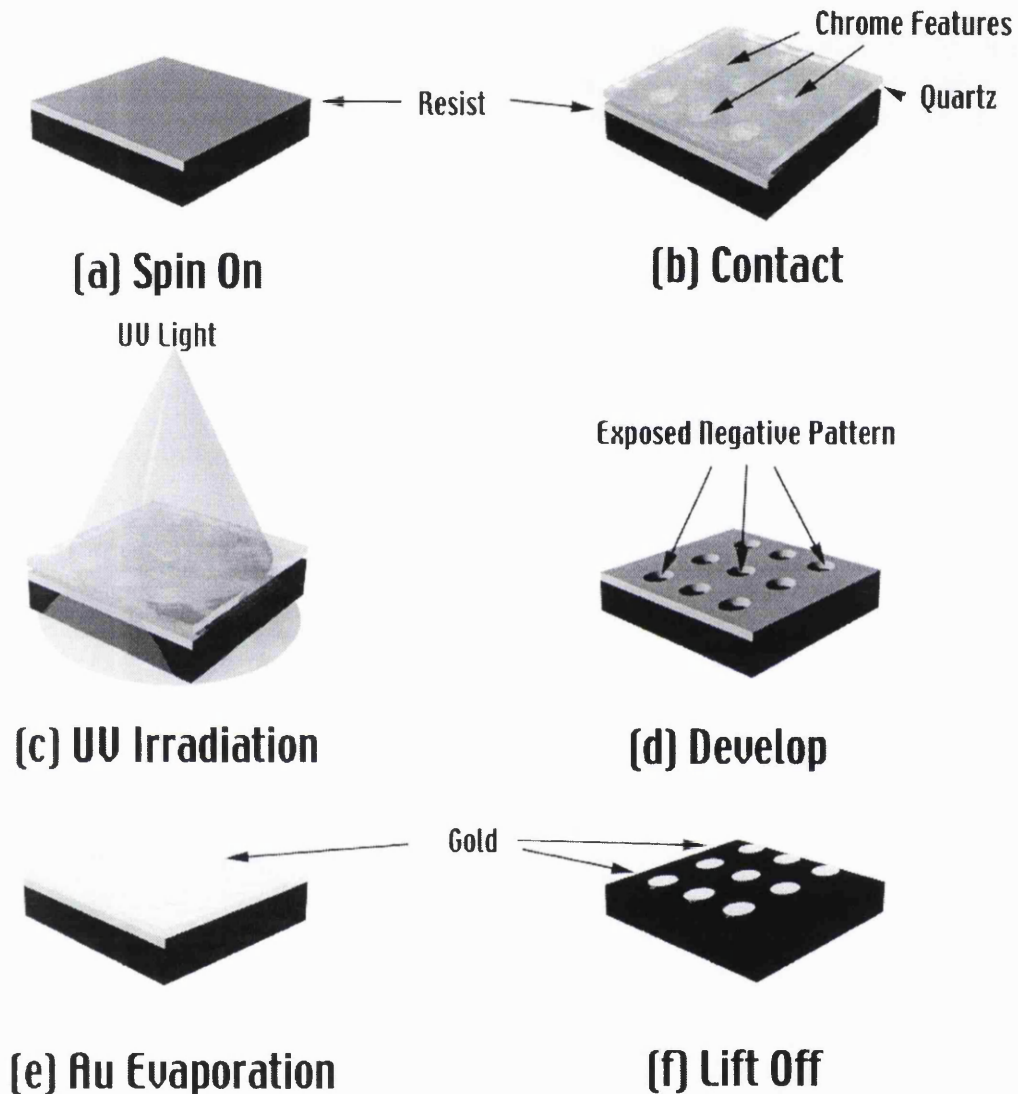
Figure 5.8 Photolithography "Lift Off'

Photolithography uses electromagnetic radiation to pattern photosensitive material. The procedure varies depending on the type of resist but basically involves the spinning on of a suitable resist (Figure 5.8 (a)), contact (Figure 5.8 (b)) with a quartz mask with chrome patterns facing down. The sample is then exposed to UV radiation and the light is masked by the chrome areas (figure 5.8 (c)). This process is performed

using a mask aligner which has high quality optics and ensures a good contact between the mask and the resist layer. This is crucial for good resolution as otherwise there will be a shadowing effect and the resulting pattern will be blurred. On developing (figure 5.8 (d)) the patterned structure is realised and the rest of the resist is destroyed. This procedure depends on the resist; with positive resist, areas exposed to UV will be destroyed, but with negative resist the areas masked will be destroyed. The resist then acts like a very high resolution shadow mask and after evaporation (figure 5.8 (e)) the resist is removed by acetone rinsing (figure 5.8 (f)), a process called "lift off". Etching is the inverse of this process where the metal is evaporated and then the resist is spun on. The resist is then patterned and then the sample etched. Photoresist can be hard baked to protect the relevant areas of the sample from the etchant.

Photoresists are polymers in liquid solution, UV exposure forces chemical changes to the resist which can be developed due to the differential solubility of exposed and unexposed regions.

Evaporation of metal in this work is performed by thermal evaporation. This is the simplest technique, which utilises a refractory metal as a heating element. A high current is passed through the element and thus heat is generated and is used to melt the metal on it. The element is chosen to have a very melting point and it is preferable than it sublimes to avoid contamination with the metal that is evaporated. This procedure must be carried out within a high vacuum (better than 10^{-6} torr) to minimise oxidation of the evaporated metal, contamination with water vapour and other contaminants present within the atmosphere. The quality of the resulting metal layer is crucial to the performance of the contact, i.e. a highly contaminated metal will not yield a good schottky diode or ohmic contact. Also as diamond is very inert and hence if the sample is not very clean the metal will not adhere very well to it and float off in a subsequent rinse. This is a line of sight technique and can be used to deposit very thick films (500nm easily).

Figure 5.8 Atom Beam Bombardment

This technique utilises a saddle field source to generate low energy neutral particles from a gas source. The chosen gas source in this case was argon but the source can also be used with acetylene or other hydrocarbon containing gases [Franks 1989, Evans 1991] to grow diamond like carbon. The beam is essentially defocused and is used to remove the hydrogen termination, shadow masking can also be used as a crude form of patterning.
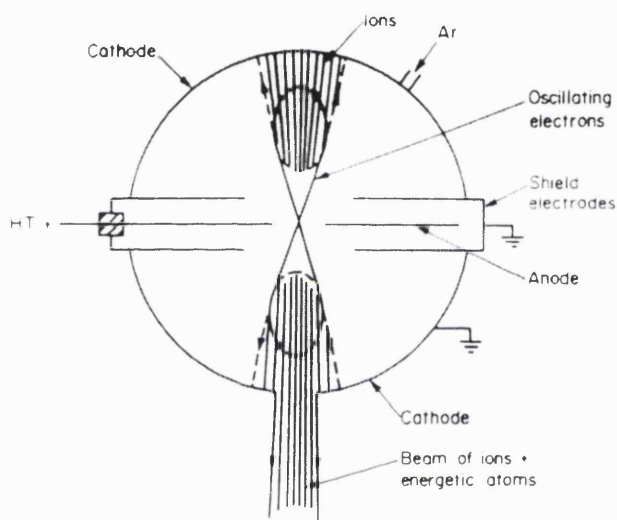
Figure 5.8 Fast Atom Beam Source [Franks 1984]

A Schematic of the fast atom beam source is shown in figure 5.8. Electrons are induced to oscillate between two cathodes under the action of a dc field [Franks 1979]. Electrons which travel through the anode are repelled by the opposite cathode sector and hence oscillate around a central saddle point. This means the electrons have long trajectories before being captured by the anode. The probability of ionisation is very high because of these long electron trajectories and the ions formed are accelarted to a cathode grid where they recombine with secondary electrons (resulting from the grid bombardment) to form a 99 % neutral atom source at around 100 eV [Franks 1979].

References

75

Binnig G., Rohrer H., Gerber Ch. And Weibel E.,

Applied Physics Letters, **40** (1982) 178

Dillon R.O., Woolam J.A. and Katkanant V.,

Physical Review B, **29** (1984) 3482

Evans A.C., Franks J. and Revell P.J.,

Surface and Coating Technology, **47** (1991) 662

Franks J.,

Journal of Vacuum Science Technology, **16** (1979) 181

Franks J.,

Journal of Vacuum Science Technology, **7** (1989) 2307

Franks J.,

Vacuum, **34** (1984) 259

Godbole V.P., Sumant A.V., Kshirsagar R.B. and Dharmadhikari,

Applied Physics Letters, **71** (1997) 2626

Hall E.H.,

American Journal of Mathematics, **2** (1879) 287

Jiang N. and Ito T.,

Journal of Applied Physics, **85** (1999) 8267

Kawarada H.,

Surface Science Reports, **26** (1996) 205

Knight D.S. and White W.B.,
Journal of Materials Research, **4** (1985) 385

Knight D.S. and White W.B.,
Journal of Materials Research, **4** (1989) 385

Koslowski B., Strobel S., Wenig M.J., Martschat R. and Ziemann P.,
Diamond and Related Materials, **7** (1998) 322

Koslowski B., Strobel S., Wenig M.J., Martschat R. and Ziemann P.,
Diamond and Related Materials, **7** (1998) 322

Kwang Y., Wang., Lee N., Badzian A., Badzian T. and Tsong T.T.,
Applied Physics Letters, **67** (1995) 3721

Landstrass M.I. and Ravi K.V.,
Applied Physics Letters **55**(1989) 975

Lukins P.B., Zareie M.H. and Khachan J.,
Applied Physics Letters, **78** (2001) 1520

Maki T., Shikawa S., Komori M., Sakaguchi Y., Sakuta K. and Kobayshi T.,
JapaneseJournal of Applied Physics, **31** (1992) L1446

Nemanich R.J., Glass J.T., Lucovsky G. and Shroder R.E.,
Journal of Vacuum Science and Technology, **A6** (1988) 1783

Raman C.V. and Krishna K.S.,
Nature, **121** (1928) 501

Raptis J., Liarokapis E. and Anastassakis,
Applied Physics Letters, **44** (1983) 125

Ristein J., Maier F., Riedel M., Stammer M. and Ley L.,

Diamond and Related Materials **10** (2001) 416

Rutledge K.M. and Gleason K.K.,

Handbook of Industrial Diamonds and Diamond Films, Marcel Dekker Inc, New York, USA

Sails S.R., Gardiner D.J., Bowden M., Savage J. and Rodway D.,

Diamond and Related Materials, **5** (1996) 589

Sauerer C., Ertl F., Nebel C.E., Stutzmann M., Bergonzo P., Williams O.A. and Jackman R.B.,

Physica Status Solidi 186(2001) 241

Schroder D.K.,

Semiconductor Material and Device Characterisation (Second Edition), John Wiley and Sons, New York, 1998

Sung Gi R., Mizumasa T., Akiba Y., Hirose Y., Kurosu T. and Iida M.,

Japanese Journal of Applied Physics, **34** (1995) 5550

Tsuno T., Tomikawa T., Shikata S. and Fujimori N.,

Journal of Applied Physics, **75** (1994) 1526

Tsuno T., Tomikawa T., Shikata S., Imai T. and Fujimori N.,

Applied Physics Letter, **64** (1994) 572

Van der Pauw L.J.,

Phillips Research Reports, **13** (1958) 1

Wada N. and Solin S.A.,

Physica B, **105** (1981) 353

Wagner J., Ramsteiner M., Wild C. and Koidl P.,

Physical Review B, **40** (1989) 1817

Wagner J., Wild C., Muller – Sebert W., and Koidl P.,

Applied Physics Letters, **61** (1991) 1284

Williams O.A., Whitfield M.D., Jackman R.B., Foord J.F., Butler J.E., Nebel C.E.,

Diamond and Related Materials, **10** (2001) 423

Yoshokawa M., Katagiri G., Ishida H., Ishitani A., Ono M. and Matsumara K.,

Applied Physics Letters, **55** (1989) 2608

Young R.A. and Kalin R.V.,

Microelectronic Processing: Inorganic Material Characterization, American Chemical

Society, Symposium Series 295, Washington DC, 1986, 49-74

Chapter 6

Low Temperature Hall Effect Characterisation

Contents

Section 6.1 Introduction

The exposure of diamond to a hydrogen plasma yields a surface conductivity layer of p-type character. Various models exist for the explanation of this phenomenon including surface graphite, upward band-bending due to the surface dipole, the formation of shallow acceptor states, transfer doping through the hydrogen bond and the manipulation of the Fermi level at metal / diamond interfaces.

This layer has been extensively characterised by the Hall Effect at room and liquid nitrogen temperatures [Jiang 1999], however as the carriers have not been frozen out, it is a natural progression to expand the temperature range. This information can shed new light on the origin of the surface conductivity layer and its carrier transport mechanism.

Section 6.2 Experimental Aims

The aim of the work described in this chapter was to search for the possibility of "freeze out" of carriers in the surface conductivity layer. This information can lead to the calculation of the activation energy, information that is not available in the literature. Various films were characterised over the 10 - 300K temperature range, using a hall signal (offset plus hall voltage) tracking procedure. The advantages of this technique are demonstrated and the pitfalls of not using this procedure are expressed. This information should be noted when reviewing the literature, as this technique is generally not used as most commercial hall systems are designed for use with silicon and other standard materials which do not exhibit high contact drift.

As the hydrogen conductivity is a surface property, it is particularly sensitive to the environment and temperature variations. This can lead to enough drift in the hall signal to imply a negative hall coefficient and hence n – type conductivity. Numerous papers have been withdrawn and rejected due to the misinterpretation of this effect.

Section 6.3 Experimental Methods

Free standing polycrystalline MWPECVD diamond films were used throughout. Diamond films are generally cooled in a hydrogen plasma after growth which leads to the surface conductivity layer, however in this work the films were first immersed in a strong oxidising solution known to remove all contaminants and graphite [Baral 1996], this procedure also destroys the hydrogen conductivity. The films were then rehydrogenated in a pure hydrogen plasma at 500°C, 40 torr, 100 sccm, 800 W for 5 mins. This procedure was used as some of the wafers supplied were not grown in the same lab, thus this procedure provides a kind of normalisation allowing hall data from different films to be compared having been hydrogenated from the same initial state. None of the chambers in which the diamond films were grown had ever been used to grow doped material, hence contamination due to boron etc can be ruled out.

SEM images were taken with a JEOL microscope and RAMAN spectra with a RENISHAW 2000 system with red (He-Ne) laser excitation. Au contacts were deposited in the van der Pauw configuration [van der Pauw 1956] by thermal evaporation under pressures better than 6×10^{-7} mbar, the ohmic nature of which was confirmed with a HP4145B parameter analyser. Samples were then packaged and edge bonded.

Hall measurements were carried out in three different hall systems in two different labs. The main systems was located at the Walter Schottky Institute, part of the Technishe Universitat Munich. This system comprised of a two tesla electromagnet with very large poles (an ex-NMR magnet) and hence high uniformity. The cryostat was a liquid helium based open loop system, this limits the maximum experimental time due to the finite nature of the helium supply. However, for basic 30 hour measurements this is not a significant issue. The instrumentation was a standard Keithley setup, controlled by a computer with Fourier transform capabilities for hall voltage extraction under high noise levels. For ultra low temperatures (0.32K) a 17 tesla superconducting magnet with helium three / helium four interchange cryostat was used.

The third system was situated at University College London, comprising of a more modest 0.32 tesla electromagnet and Keithley instrumentation. This system had a closed cycle refrigerator based cryostat and hence experimental time is not limited by helium supply. Both systems operate under high vacuum (better than 2×10^{-5} mbar) to reduce the effect of water depositing on the surface and hence affecting measurements.

Section 6.4.1 Experimental Results: RAMAN and SEM

SEM and optical micrographs of the growth surface of the films investigated are shown in figure 6.1.

a) SEM of WD8   (b) SEM of WD95

(c) Optical Micrograph of WD139   (d) SEM of NRL5K260
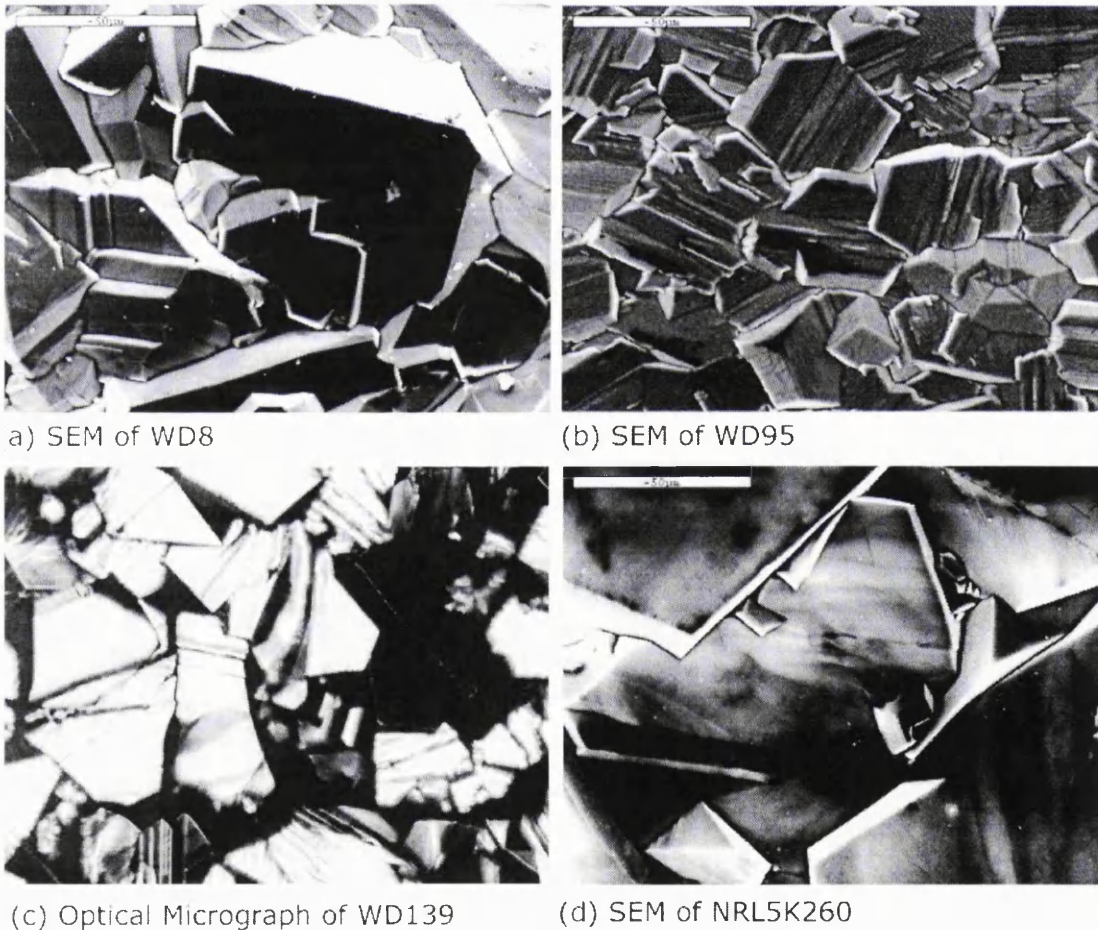
Figure 6.1 SEM / Optical Micrographs

Measurements on four films are documented in this chapter, as seen from the micrographs, they all exhibit randomly aligned grains of various sizes. All films were

grown by GEC Marconi in an Astex PDS-18 except WD139 and NRL 5K260 which was grown at the Naval Research Laboratories Washington in a similar Astex reactor. The ranges of grain sizes being for WD8 30-60μm, WD95 10-30μm, WD139 20-40μm and NRL5K250 60-80μm. Grain size being roughly proportional to sample thickness, all being 100μm except WD8 at 300μm and NRL5K260 at 500μm. Samples WD95, NRL5K260 and WD139 were laser cut tiles, WD8 was mechanically cut from respective wafer.

Raman Spectra of the above films are displayed in Figure 6.2.

(a) Raman Spectra of WD8   (b) Raman Spectra of WD95

(c) Raman Spectra of WD139   (d) Raman Spectra of NRL5K260
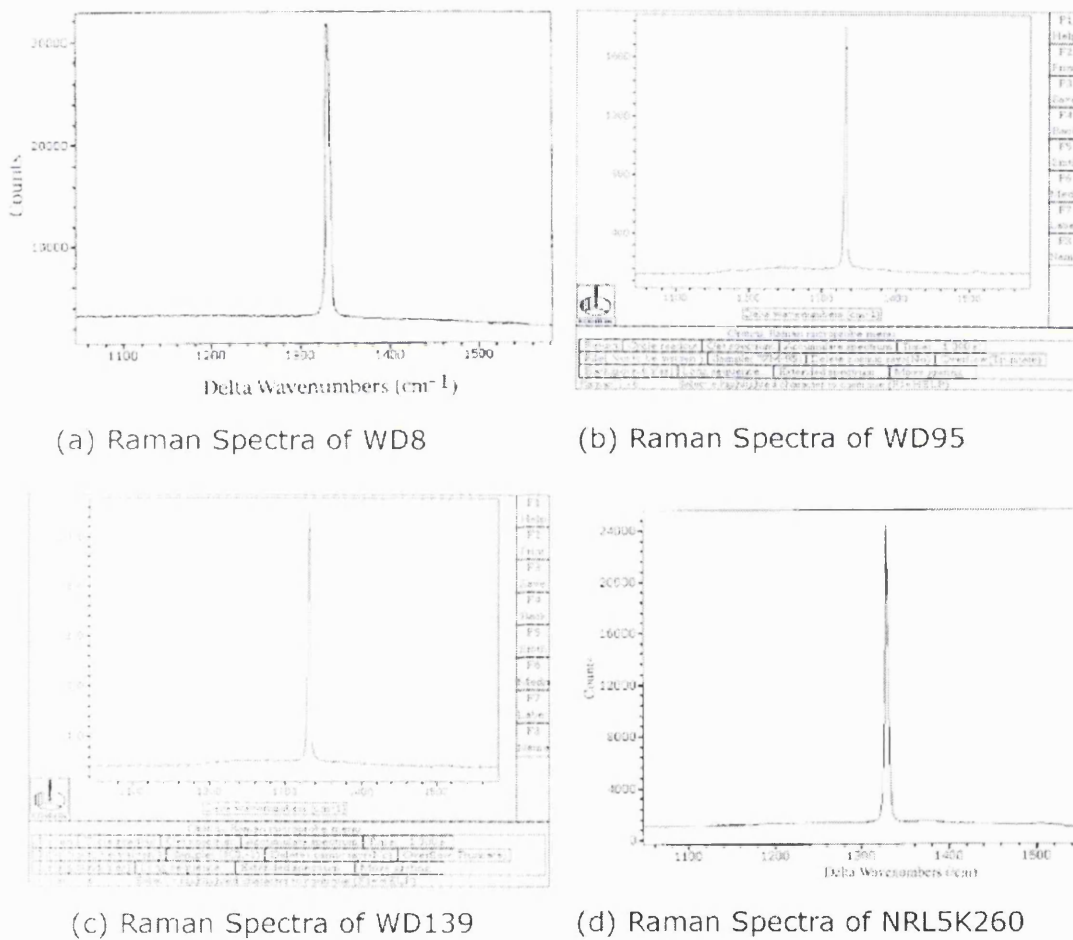
Figure 6.2 Raman Spectra

The spectra for all the films are almost identical, displaying a sharp peak at 1332cm^{-1} with no other features, such as the G and D bands evident. This is indicative of high quality films, the laser used was a He-Ne (633nm), which is very sensitive to non – diamond carbon, and hence there relatively few sp^2 phases. As all films were grown

under very similar conditions albeit in different labs, this is to be expected with modern diamond growth procedures reaching high levels of reproducibility.

## Section 6.4.2 Experimental Results: Hall Signal Tracking

Figure 6.3 shows a typical hall measurement where the variation in the Hall Offset voltage is small compared to the hall voltage. Here it is obvious that standard hall techniques, where the voltage is calculated from just two measurements (positive and negative field) would suffice.
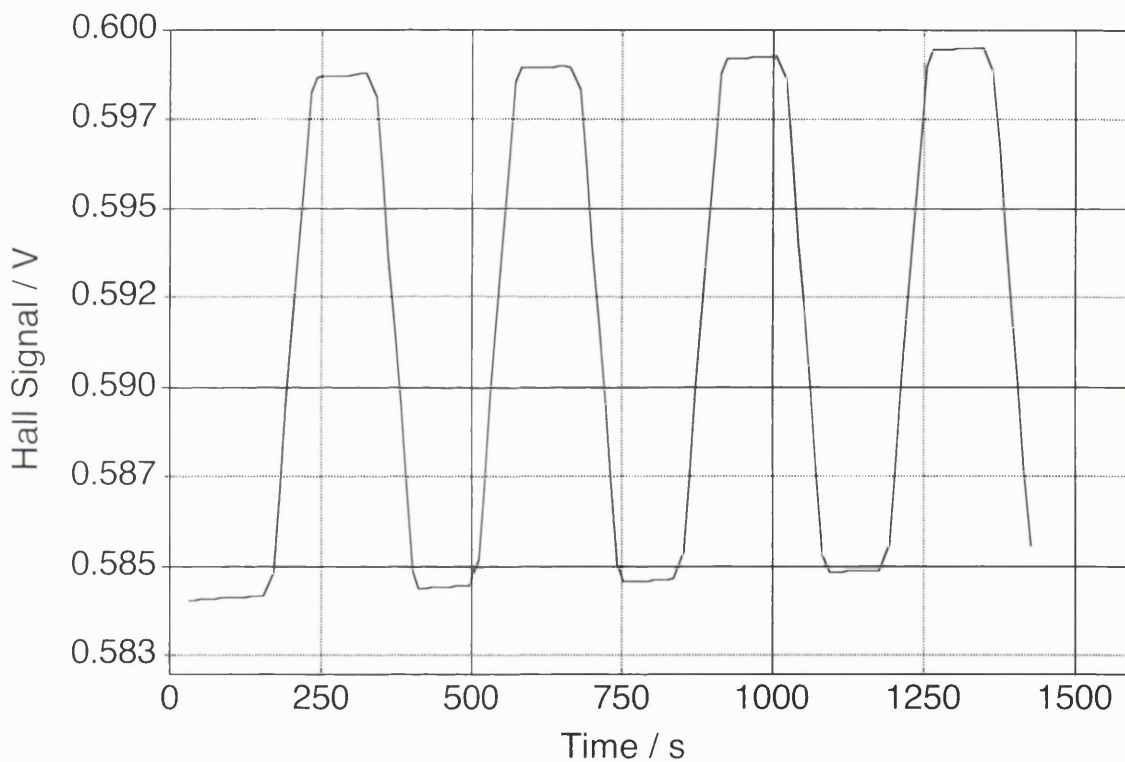
Figure 6.3 Stable Hall Data

The characteristic "square wave" of hall signal is observed where the periodicity of the field yields periodicity in the hall signal - this is the ideal case. It can be seen from this data that the signal offset is increasing slightly, this is due to the measurement being made in the dark. Hydrogenated diamond takes an exceptionally long time to settle at a constant resistivity in the dark, but the variation is very small. Figure 6.4 shows a more drastic case where the variation in the offset voltage is large compared to the hall voltage.
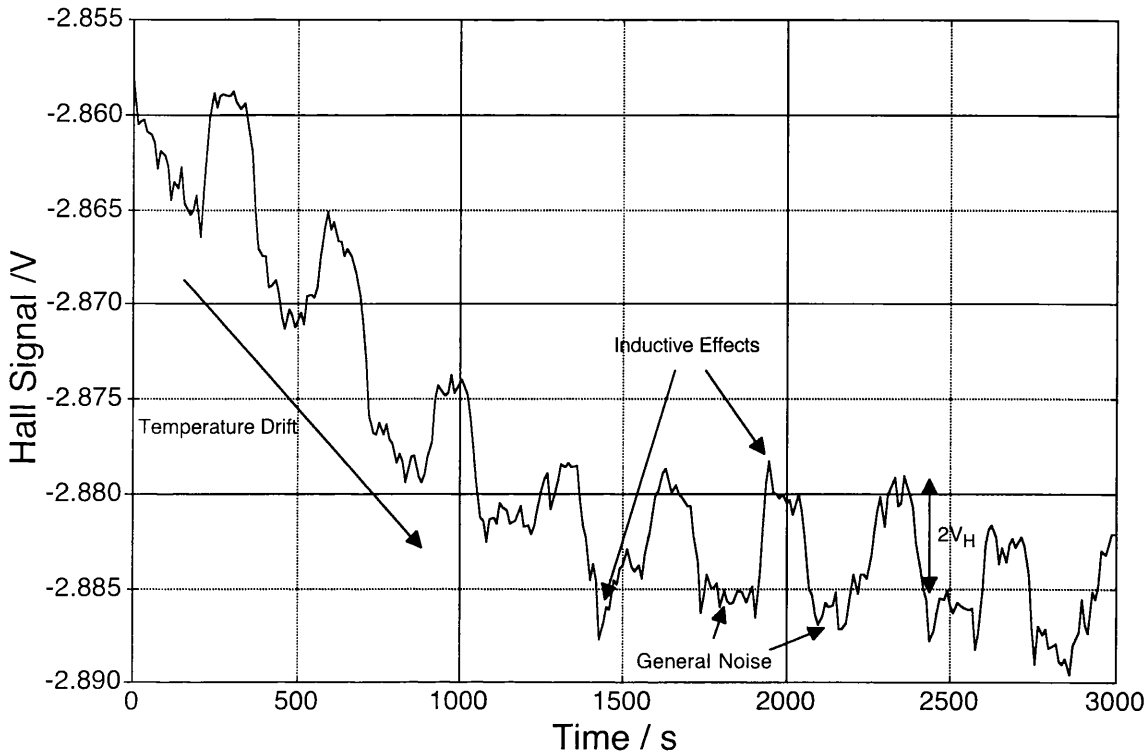
Figure 6.4 Unstable Hall Data

It can be seen from Figure 6.4 that a large drift in temperature can lead to very large errors in the measured hall voltage. At the top of the slope (time=0) the signal can be seen to be almost identical to the voltage where the field is first reversed (time = 200s), this would yield a very small hall voltage and in extreme cases can yield an opposite polarity hall coefficient. Inductive effects are also very common at low signal levels and are due to small voltages being induced by the variation in field in the cables measuring the system. General noise is very common at lower temperature and signal levels. The sample in Figure 6.4 actually had a higher carrier concentration than that in Figure 6.3, as the hall voltage is inversely proportional to the carrier concentration. This effect is also exaggerated by the fact the higher carrier concentrations usually lead to lower mobilities, hence it is generally easier to measure lower carrier concentrations. It should also be mentioned that the polarity of the hall signal is only related to the non – uniformity of the sample and not the polarity of the hall coefficient, the later being related to the polarity of the field only. Figure 6.4 is far from the worst case scenario.

Section 6.4.3 Experimental Data: Hall Data

Figure 6.5 displays the variation of sheet conductivity with temperature of the above samples.
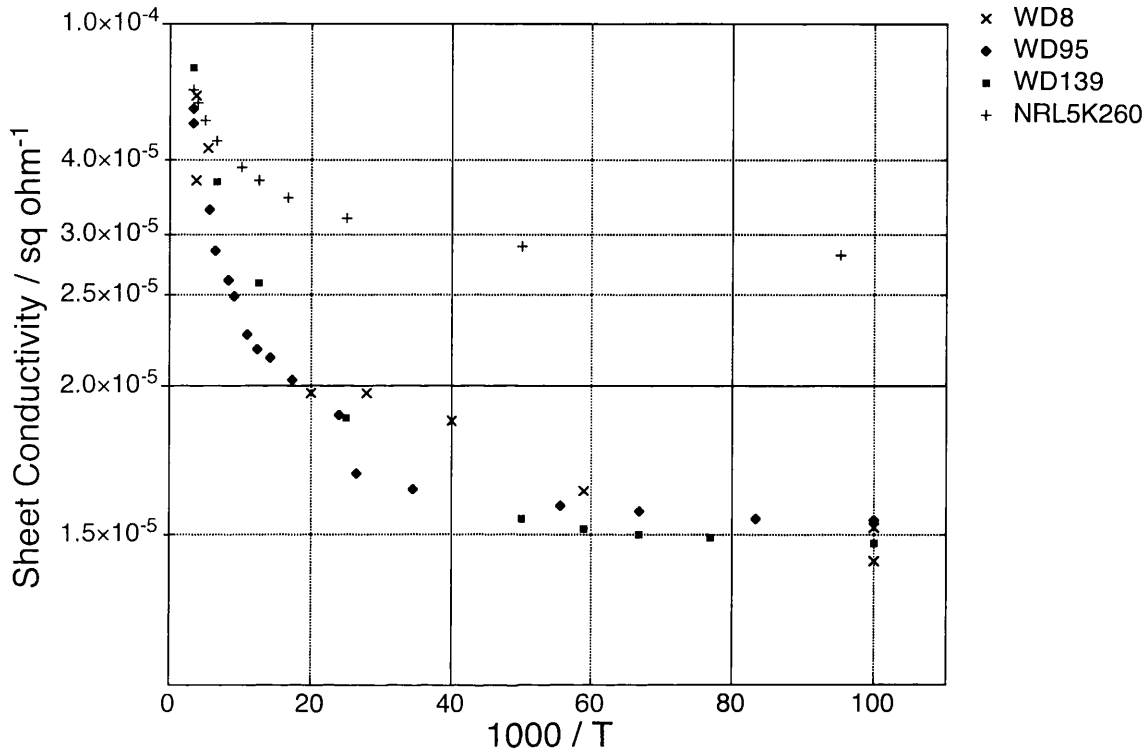
Figure 6.5 Sheet Conductivity Against Reciprocal Temperature

The sheet conductivity for all samples decreases with decreasing temperature for all samples, however no single activation energy can be fitted to the above data. It is also obvious that sample NRL5K260 varies significantly less over the entire temperature range than the other samples. The maximum variation of all samples is less than an order of magnitude, so the conductivity is far from being "frozen – out" at 10K.

Figure 6.6 shows that the sheet carrier concentrations for all samples actually increase as the temperature is decreased.
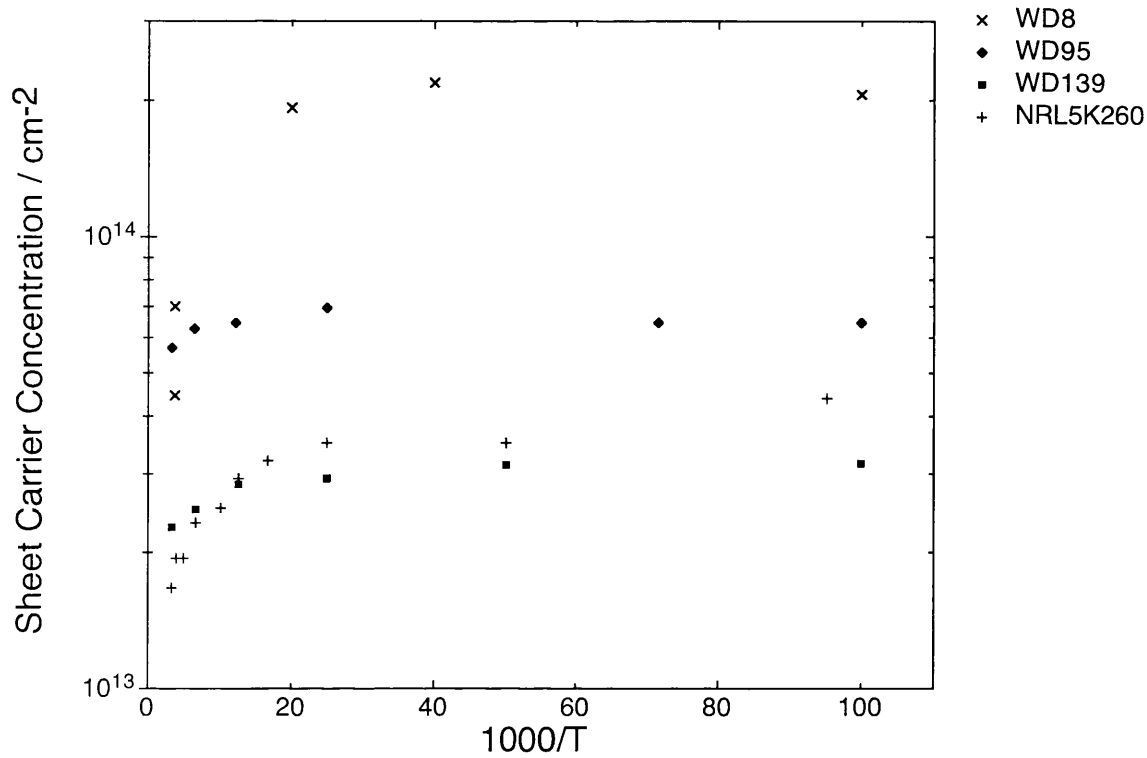
Figure 6.6 Sheet Carrier Concentration Against Reciprocal Temperature

Again the variation of sheet carrier concentration is sample dependant, with the variation of all the samples being rather small. The greatest increases observed were on samples WD8 and NRL5K260, the samples with the greatest grain size. Samples WD95 and WD139 show smaller increases in sheet carrier concentration. As the opposite trend to convention is observed it is again impossible to attempt to fit an activation energy, however it can be stated that the carriers do not freeze out above 10K, and thus is corresponding activation energy must be lower as there is also no indication of a possible freeze out around this temperature.

Fiqure 6.7 shows the corresponding mobility (derived from the resistivity and carrier concentration values) of the four samples against reciprocal temperature.
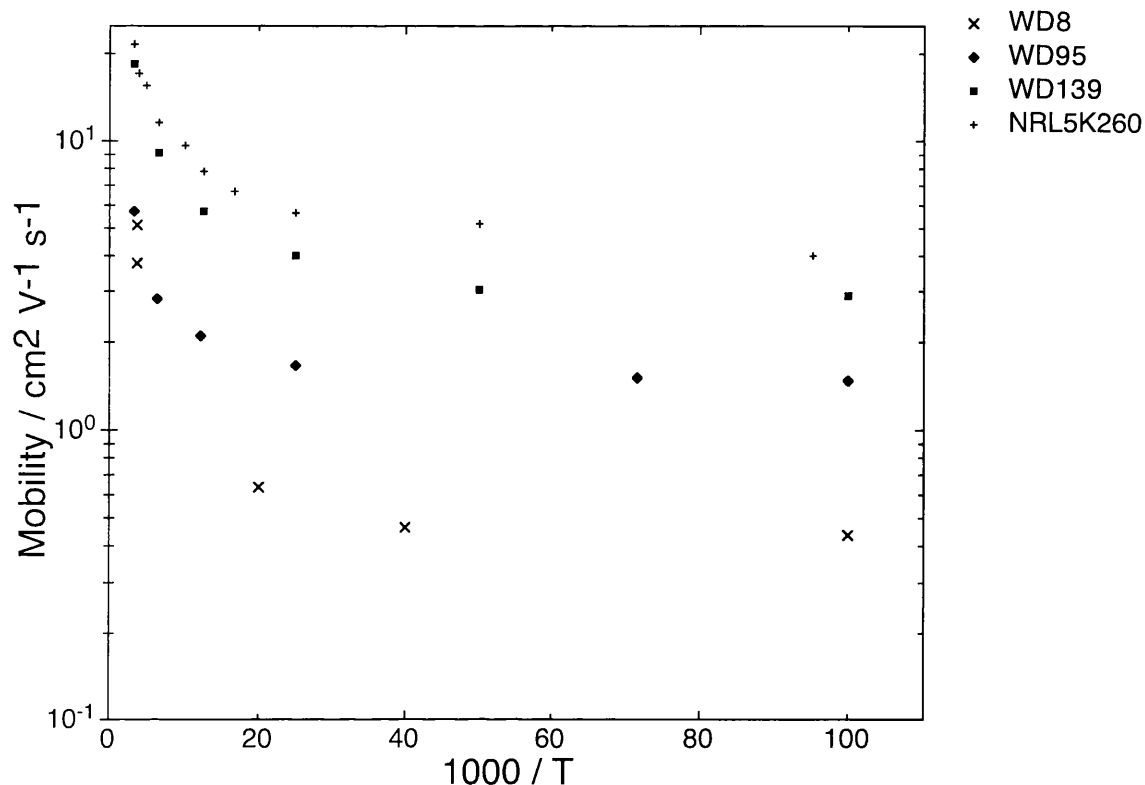
# Figure 6.7 Mobility Against Reciprocal Temperature

As the sheet conductivity decreases and the sheet carrier concentration increases with decreasing temperature then it stands to reason that the mobility must decrease and is the dominant mechanism for the conductivity decrease, this is observed in Figure 6.7. Mobilities vary from above 20 cm^2 V^{-1} s^{-1} down to below 0.5 cm^2 V^{-1} s^{-1}, which is approaching the limit of the hall system used. The greatest variations are again in the samples with the largest grain sizes (WD8 and NRL5K260) but all samples show a significant reduction. It should be noted that all the mobility values recorded are significantly above those expected with a carrier hopping transport mechanism.

Figure 6.8 shows the variation in activation energy with atmosphere, this measurements was performed on the same single crystal diamond. It can be seen that the activation energy increases with prolonged vacuum exposure and that the lowest value is obtained in He ambient. It can also be seen that the reduction in conductivity is much more drastic on this diamond, decreasing three orders of magnitude in vacuum.
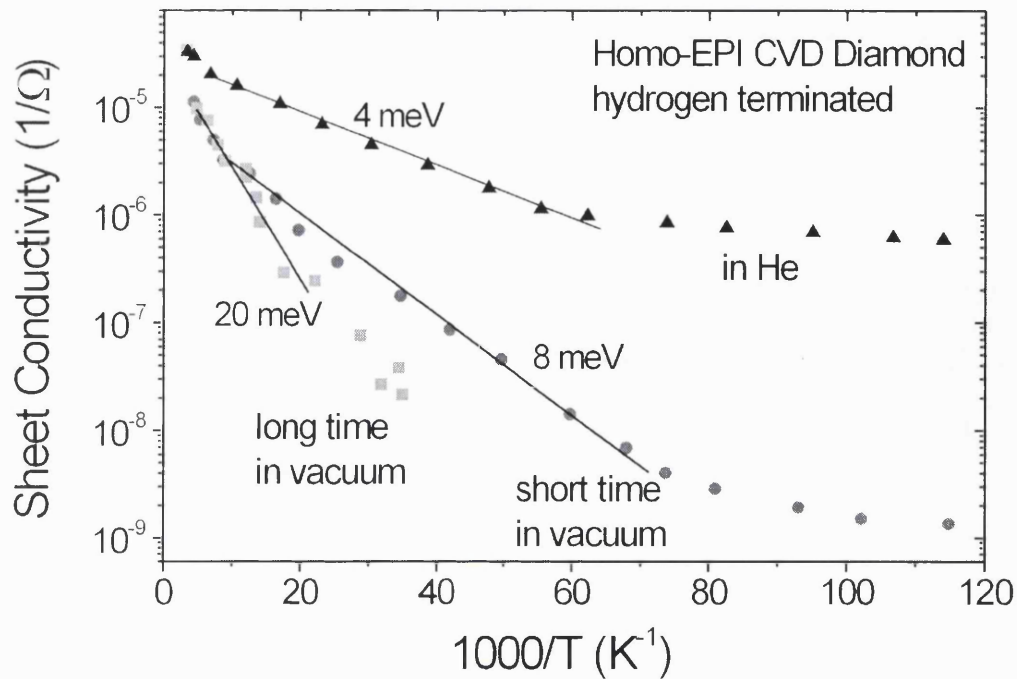
Figure 6.8 Variation of Activation Energy With Environment

The effect of very low temperatures on the surface conductivity layer can be seen in figure 6.9.
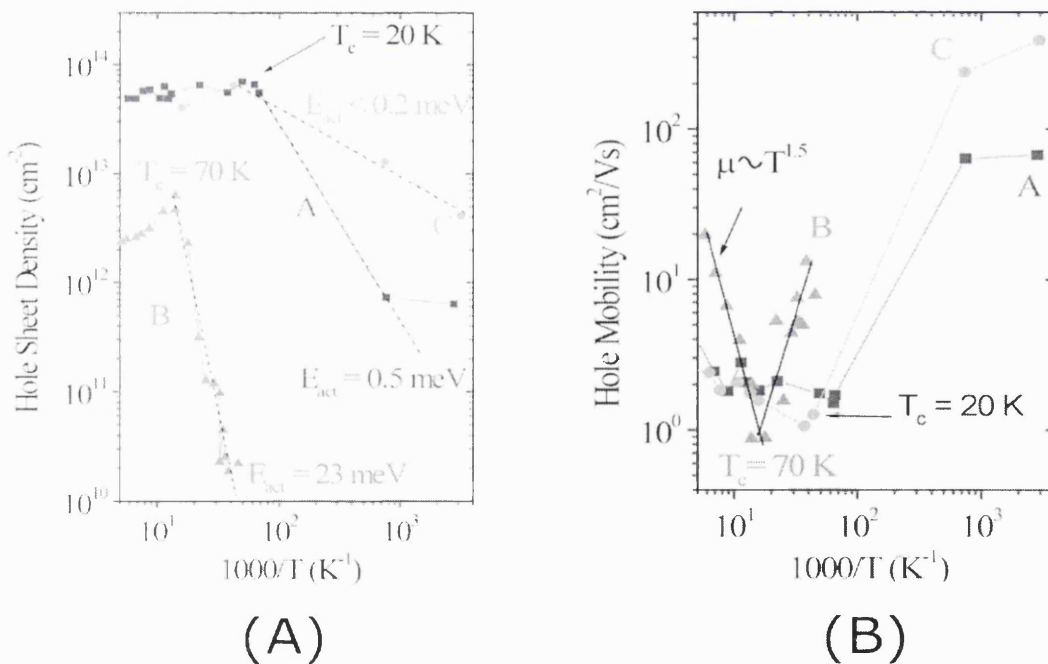
Figure 6.9 Ultra Low Temperature Hall

It can be seen from figure 6.9 (a) that the carriers begin to freeze out under very low temperatures (towards 0.32 K). Under these extreme regimes, the holes also propagate at very high mobilities (> 400 $cm^2V^{-1}s^{-1}$).

Section 6.5 Discussion

The Raman data of all films display sharp peaks with no observation of the g and d bands. This means that the amount of graphitic phases in the films must be too low to yield the observed conductivity. Also, films can be rehydrogenated after growth many times so the etching of this plasma should remove any surface graphitic layer very quickly. In fact the author has also hydrogenated various types of natural diamonds. Therefore the proposal that the origin of the conductivity is due to surface graphite can be ruled out [Stallcup 1995]. The thickness required to support such levels of graphite is of the order of 30 nm [Shirafuji 1996] which should easily be detected by Raman and XPS measurements and has not been [Graupner 1994]. In fact, a layer of this thickness would also inhibit continuous growth of diamond films which is not the case and hence it does not exist.

The first recorded observation of this surface conductivity [Landstrass 1989] attributed it to the passivation of defects in the bulk diamond. Hydrogen does not passivate defects at GaAs interfaces [Kampen 1991], in fact it creates surface acceptors. Theoreticians [Mehandru 1992] have calculated the activation energy of hydrogen moving between bond centres in diamond to be 1.9eV which is well in excess of that reported here(>20meV), hence a diffusion model is inadequate. As the conductivity can also be switched by chemical cleaning [Muto 1991], the effect must be predominantly on the surface and not due to bulk hydrogen. The speed at which the conductivity can be switched (2s in hydrogen plasma by the author) also cast serious doubt on any serious amount of diffusion into the bulk. It is not clear how this would increase conductivity anyway as diamond is naturally highly resistive, i.e. passivation of defects should lead to a lower conductivity as defects usually provide a mechanism for carrier transport rather than hinder them.

Maki et al [Maki 1992] verified the p –type nature of the conductivity by the Seebeck effect, however, this thermal type of measurement can lead to problems when dealing

with a non – stable surface conductivity mechanism, as the conductivity will decrease if the film is annealed. Maki et al also verified the crystalinity of the films after hydrogenation was not adversely affected by utilising various surface science techniques. The resistance of their films were also rather high (10^6 Ω) and they were unable to obtain a stable hall voltage, presumably due to limits in their apparatus / method as these resistances are quite possible with the hall effect.

The aforementioned results conflict with the conventional theory of semiconductor doping. Principally, sheet carrier concentrations should be constant with decreasing temperatures until the temperature becomes insufficient for activation and hence the concentration begins to drop. This does not happen above, the sheet carrier concentrations actually increase with decreasing temperature implying an alternative conductivity mechanism is involved. Jiang el al [Jiang 1999] characterised many films down to liquid nitrogen temperature showing very little variation over the temperature range. They reported similar results to the data here but on single crystal, the mobility values being no greater.

Hayashi et al [Hayashi 1997] proposed that the surface conductivity is due to hydrogen incorporation in the sub-surface region, promoting the formation of shallow acceptor states near the valence band maximum. Hall measurements confirmed the p-type nature of the conductivity, SIMS measurements also showed high concentrations of hydrogen in the first 20nm of the diamond. Again the hall measurements showed little variation over the liquid nitrogen temperature range.

The results here shed serious doubt on the shallow acceptor states theory, as no single activation energy can be derived and the carriers do not "freeze out", even under extreme temperature (0.32K) as shown in figure 6.9. The environmental dependence on the activation energy shown in figure 6.8 also conflicts with this.. The fact that the carrier concentration rises with deceasing temperature is a particular contradiction. The author has also shown that it is possible to hydrogenate diamond films in durations as short as 2 seconds, which makes the idea of hydrogen diffusion into the bulk unlikely. It is very possible that the presence of hydrogen in the near surface is inconsequential and is just a by product of the technique used to terminate the surface.

The SIMS measurements performed by various authors [Hayashi 1997, Looi 1998] were on CVD diamond which is known to have a high density of point defects and vacancies in the near surface [Won 1996] and hence these could provide sites for hydrogen. SIMs performed by Looi et al [Looi 1998] was also performed on polycrystalline material which is very difficult to interpret due to grain boundary effects and other surface scattering phenomenon. Data for SIMS on hydrogenated natural diamond is not available and this is a crucial control measurement.

It is possible for carrier concentrations in conventionally doped materials to increase with decreasing temperature, and this has been reported on Ge and GaN [Look 1997]. Mott and Twose [Mott 1961] proposed a model where transport through both defect centres and the conduction band can lead to an increase in carrier concentrations as the energy of the impurity band is below that of the conduction band. However, this is not an adequate explanation of the observed phenomenon as the mobility is too high for impurity band hopping conduction. It is also not obvious where an impurity band might originate from in a well terminated diamond.

Far more satisfactory explanations can be reached when the surface dipole due to the hydrogen termination is considered. Due to the electronegativity of carbon, the electrons involved in the carbon hydrogen bond are more likely to be situated near the carbon atom, this leads to a dipole and hence a negative potential which could explain the accumulation of holes, and hence upward band bending of the valence band at the surface of the diamond [Kawarada 1995]. An illustration of this band bending is shown in figure 6.10.
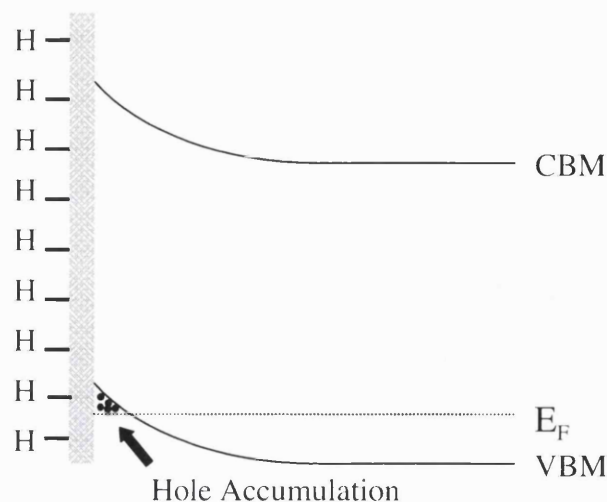
Figure 6.10 Surface Band Bending Due to Hydrogen Termination

The illustration of the band bending in figure 6.10 is applicable to all models of the surface conductivity, as if there is a high concentration of holes at the surface the bands must bend upwards to satisfy charge neutrality. The presence of this band bending has been confirmed by XPS and Kelvin probe techniques [Shirafuji 1996]. The depth of the conductivity layer is controversial, values varying from 2-20nm in the literature [Hayashi 1997, Looi 1998].

This negative surface dipole driven accumulation can also explain the hall results described in this chapter. At 300K some holes have enough energy to be situated away from the surface, but as the sample is cooled down their energy is reduced. This means that they are now more effected by the dipole and hence attracted to the surface leading to a slight increase in the overall carrier concentration as measured by the hall effect. However, the sheet resistivity increases and the temperature decreases as with conventional semiconductors, and thus the mobility must be decreased by some mechanism. This is again explained by the dipole interaction, as when the holes are increasingly confined to the surface they experience far more coulomb interaction with the surface dipole and hence are scattered more. This adds to conventional scattering by impurities and lattice phonons.

At very low temperatures the carrier begin to "freeze out" as shown in figure 6.9 (a). This reduces scattering and at low hole concentrations this allows the holes to propagate with very high mobilties ($> 400 \text{cm}^2\text{V}^{-1}\text{s}^{-1}$).

The variation between hall characterisitics and films thickness (and hence grain size) / morphology is difficult to interpret. After hydrogenation all samples have rather similar conductivities, but on cooling, NRL5K260 exhibits less of a decrease in conductivity than the other samples. However, as in all three hall plots, the differences are minimal and are probably due to grain boundary effects. A rather more drastic variable however is the non – reproducibility of plasma treatments.

Section 6.6 Summary

The work detailed in this chapter sheds new light on the mechanism behind hydrogen surface conductivity. For the first time, various forms of hydrogenated diamond have been systematically studied to very low temperatures. This data has shown that the mobility is the driving force behind the reduction in conductivity on cooling hydrogen surface conductive films. The fact that the holes do not "freeze out" even at 0.32 K is of particular interest, and the mobility at these temperatures is very impressive. The dependency on the environment also adds further doubt to the shallow acceptor state model, and this will be addressed in the next chapter.

References

Baral B., Chan S.S.M. and Jackman R.B.,
Journal of Vacuum Science and Technology **14**(1996) 2303

Graupner R., Stockel R., Janischowski K., Ristein J., Hundhausen M., Ley L.,
Diamond and Related Materials, **3**(1994) 891

Hayashi K., Yamanaka S., Watanabe H., Sekiguchi T., Okushi H. and Kajimura K.,
Journal of Applied Physics **81**(1997) 744

Jiang N. and Ito T.,
Journal of Applied Physics **85**(1999) 8267

Kampen T.U., Koenders L., Smit K., Ruckscloss M. and Monch W.,
Surface Science **242**(1991) 314

Kawarada H., Sasaki H. and Sato A.,
Physical Review B **52**(1995) 11351

Landstrass M.I. and Ravi K.V.,
Applied Physics Letters **55**(1989) 975

Looi H.J., Jackman R.B. and Foord J.S.,
Applied Physics Letters **72**(1998) 353

Looi H.J., Pang L.Y.S., Molloy A.B., Jones F., Foord J.S. and Jackman R.B.,
Diamond and Related Materials **7**(1998) 550

Look D.C., Molnar R.J.,
Applied Physics Letters **70**(1997) 3377

Maki T., Shikama S., Komori M., Sakaguchi Y., Sakuta K. and Kobayashi T.,

Japanese Journal of Applied Physics **31**(1992) L1446

Mehandru S.P., Auderson A.B., Angus J.C.,

Journal of Materials Research, **7**(1992) 689

Mott N.F. and Twose T.D.,

Advanced Physics **10**(1961) 107

Muto Y., Sugino T., Shirafuji J, Kobashi K.,

Applied Physics Letters **59**(1991) 843

Sauerer C., Ertl F., Nebel C.E., Stutzmann M., Bergonzo P., Williams O.A. and Jackman R.B.,

Physica Status Solidi **186**(2001) 241

Shirafuji J. and Sugino T.,

Diamond and Related Materials **5**(1996) 706

Stallcup R.E., Aviles A.F. and Perez J.M.,

Applied Physics Letters **66**(1995) 2331

Van der Pauw L.J.,

Philips Reseach Report **13**(1956) 1

Won J.H., Hatta A., Ito T., Sasaki S., Hiraki A.,

Applied Physics Letters **69**(1996) 4179

Chapter 7

Atmospheric Effects on Surface Conductivity

Contents

Section 7.1 Introduction

In the previous chapter, hall measurements showed the unusual transport mechanism behind hydrogen surface conductivity. Resistivity measurements showed the sensitivity of the conductivity to various environments and this chapter investigates this phenomenon further. This chapter is complementary to the previous chapter in that it discusses the possible origin of the holes governed by the aforementioned transport mechanism.

Hydrogen-induced surface conductivity is highly sensitive to the gaseous environment and temperature. Wide band-gap semiconductors are particularly sensitive due to the large screening length associated with these materials [Kawarda 1996]. Hydrogen termination provides a means for adsorbates to interact electrically with the near surface via the surface dipole.

Early work has shown the effect of annealing hydrogenated diamond in air [Landstrass 1989, Looi 1998], leading to a permanent reduction in sheet conductivity. However, in vacuum this effect is reversed on the admittance of air [Ristein 2001] and this metastability is investigated further in this chapter.

Section 7.2 Experimental Aims

The aim of work outlined in this chapter is to investigate the stability and atmospheric sensitivity of the hydrogen surface conductivity layer. This is essential for the utilisation of hydrogenated diamond for device fabrication. The viability of passivation of the surface conductivity will also be addressed. The measurements used include simple two contact measurements and four contact hall measurements.

## Section 7.3 Experimental Methods

Free standing high quality polycrystalline diamond was used throughout. Samples were immersed in a strong oxidising solution known to remove all contaminants and graphite [Baral 1996], this procedure also destroys the hydrogen conductivity. The films were then re-hydrogenated in a pure hydrogen plasma at 500°C, 40 torr, 100 sccm, 800 W for 5 mins in a purpose built reactor. No other gases other than

hydrogen (and air for venting) have been introduced into this reactor. Au contacts were deposited with 1mm seperation by thermal evaporation under a pressure better than 10^{-7} mbar. Au contacts were deposited in the van der Pauw configuration for hall measurements under identical conditions. For conductivity measurements, a constant 5V bias was applied using a Keithley 657 Source Measure Unit and the current was read continuously using National Instruments Labview software while the environmental conditions were adjusted.

Hall measurements were performed using a vacuum based hall system with a two tesla magnet. This system has several advantages over conventional hall systems, principally being the ability to vary the field periodically and control the system base pressure. In this way the effects of the atmosphere can be observed in both the drift in hall signal voltage which indicates resistivity variations, and variations in the hall voltage alone. Combining this data will indicate the mechanism responsible for the change in resistivity. Unless otherwise stated all of these measurements were performed in the dark.

Section 7.4.1 Experimental Results: Conductivity Data

Figure 7.1 shows the decrease in conductivity due to pumping down the sample from room pressure to 4 x 10^{-5} mbar.
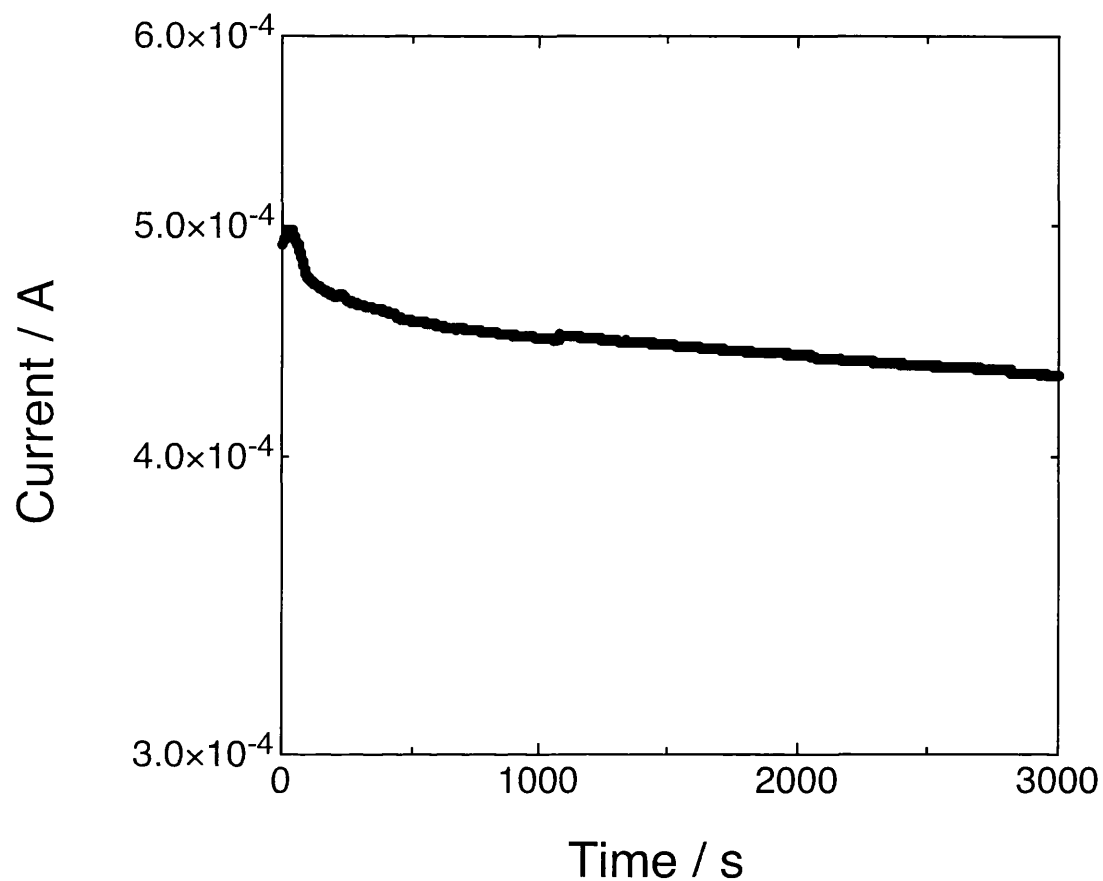
Figure 7.1 Conductivity Due to Evacuation of Sample

It can be seen from this figure that after an initial decrease the sample conductivity stabalises to a value around 10% of it's initial value. Upon heating the conductivity of the sample decreases even further as shown in figure 7.2.
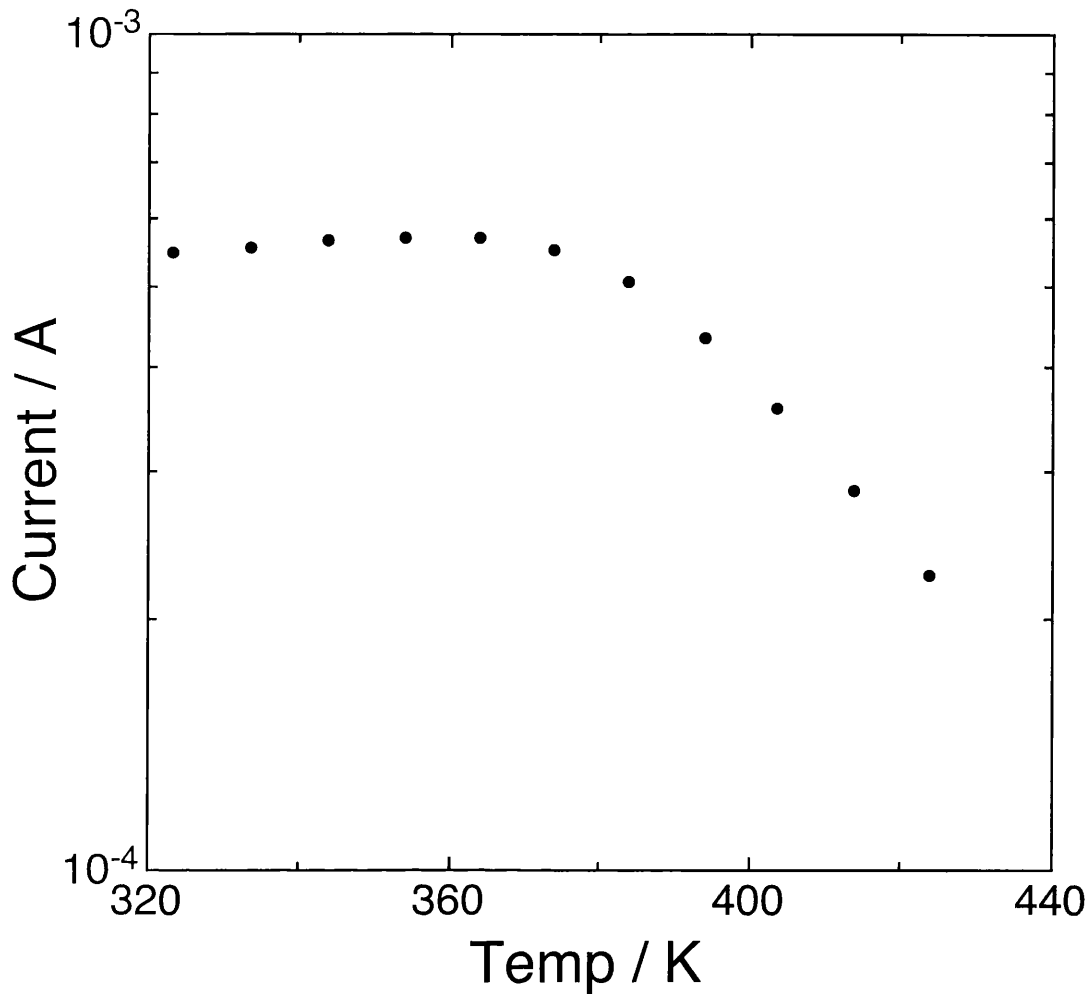
Figure 7.2 Heating the Sample Under Vacuum

From this figure (7.2), it can be seen that after a small initial rise up to around 360K, the conductivity of the sample starts to decrease again as the temperature increases. The apparent linearity of the higher temperatures is of no consequence, as there is a finite duration between temperature during which the sample conductivity is also decreasing.

However, the decrease in conductivity stops after a certain duration at a given temperature as shown in figure 7.3. It can be seen that after about 7000s the samples conductivity is approaching a stable equilibrium value.
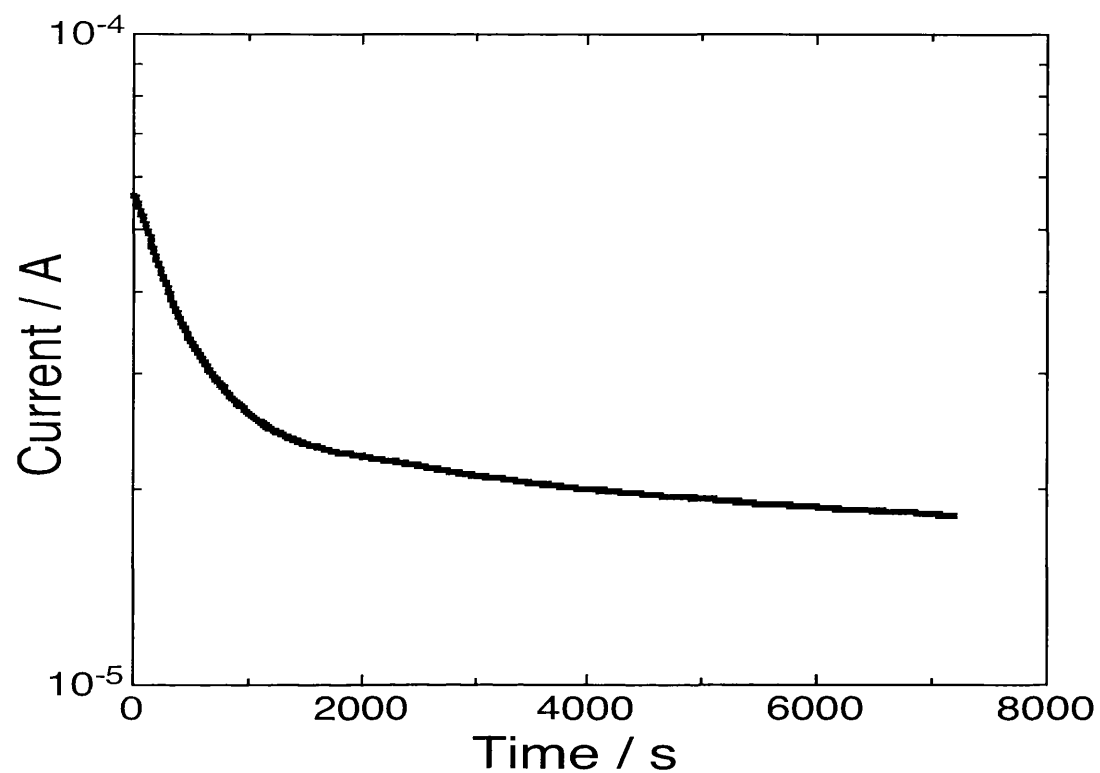
Figure 7.3 Decrease in Conductivity at 470K

The sample was then cooled to room temperature as seen in figure 7.4.
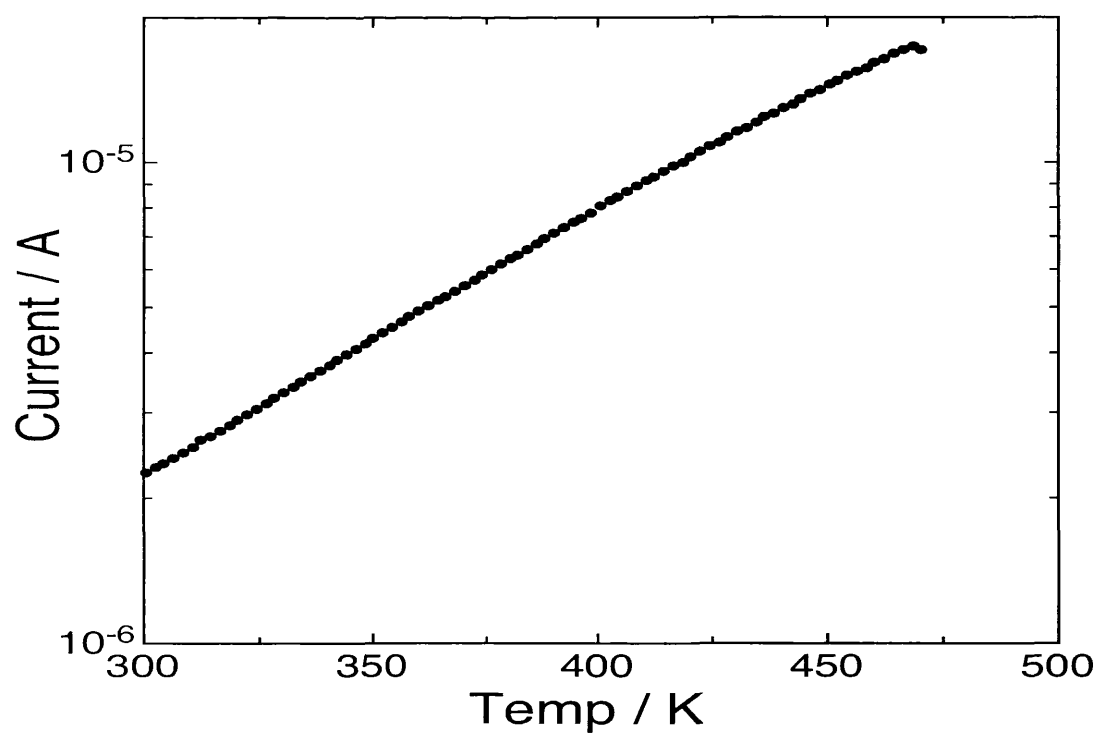
Figure 7.4 Decrease in Conductivity from Cooling

Upon cooling the conductivity decreases again as the thermally stimulated current is frozen out. The sample is now at much more resistive state than before heating, the decrease is over two orders of magnitudes. To investigate the stability of the conductivity further the sample was vented to air at room temperature, the resulting increase in conductivity is shown in figure 7.5
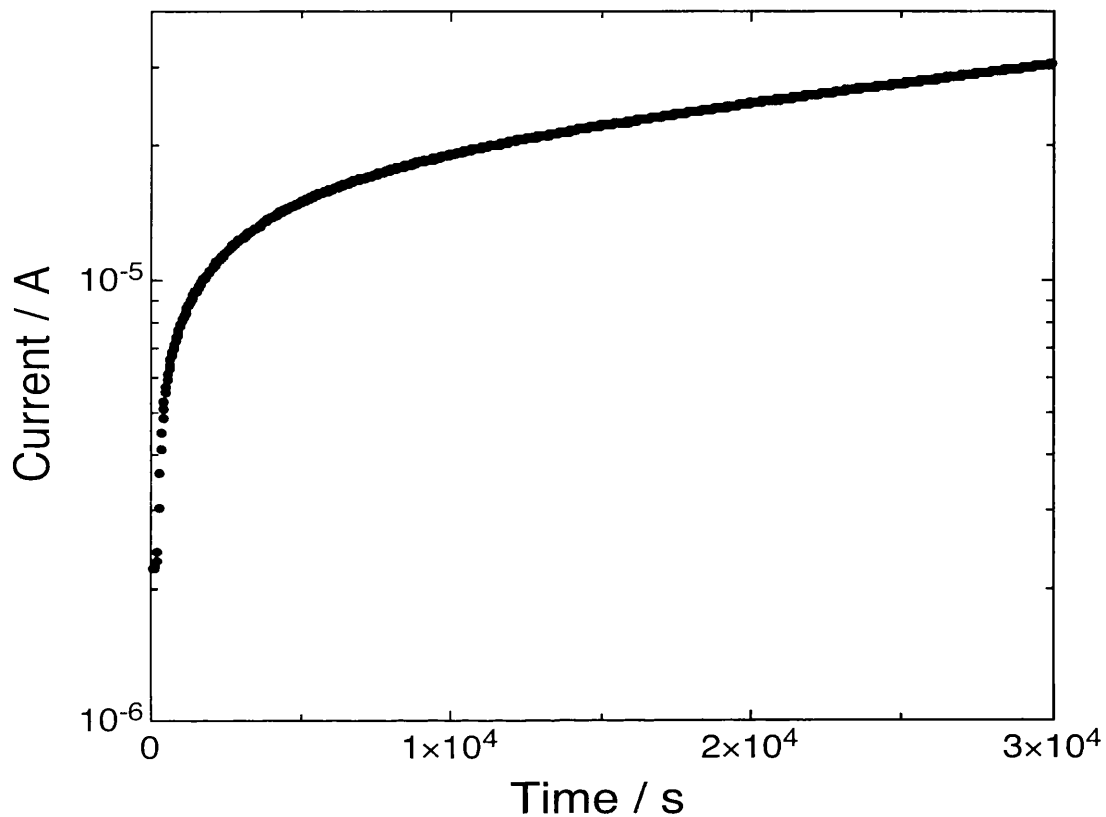
Figure 7.5 Venting the Sample at 300K

The samples conductivity increases over an order of magnitude in 30000s and is still increasing after this duration. If the sample is left for a day it will return to its initial value. Figure 7.6 summarises this repeatable phenomenon, it is possible to travel around this cycle of conductivity indefinitely provided the sample is under vacuum when being annealed. Higher temperatures yield much faster decreases in conductivity and still yield reproducible cycles of conductivity as seen in figure 7.7.
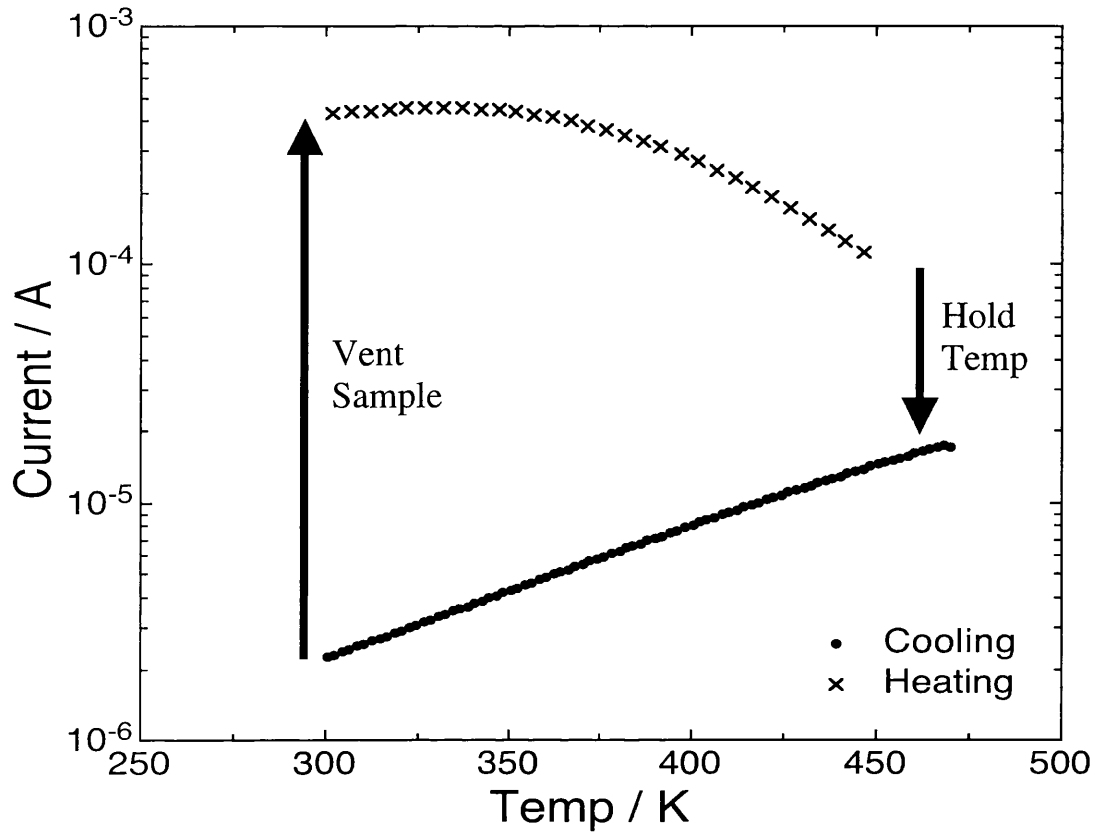
Figure 7.6 Cycle of Conductivity
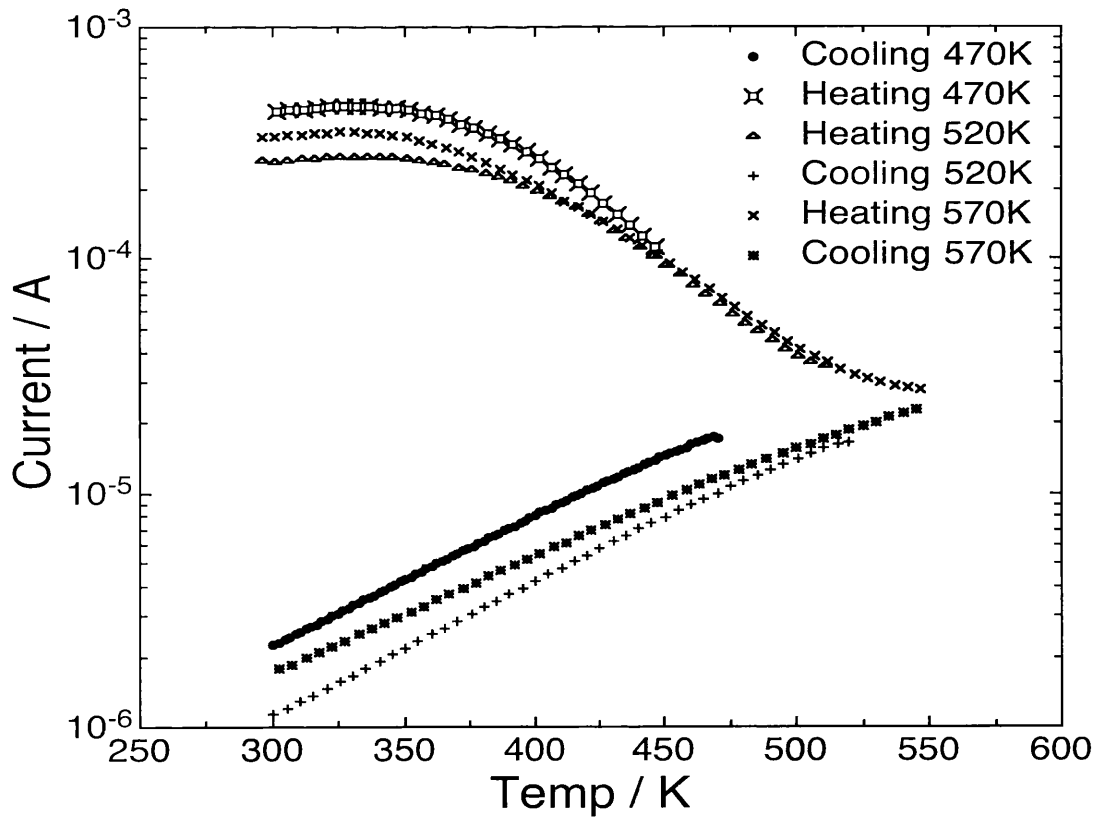
Figure 7.7 Multiple Temperature Cycles

Figure 7.7 shows that at higher temperatures it is unnecessary to hold the sample at the high temperature to reach stability, this is due to the elevated temperature and the time it takes to ramp to this temperature. The value of conductivity which the sample returns to after venting can be seen to be almost identical as is the value after cooling.
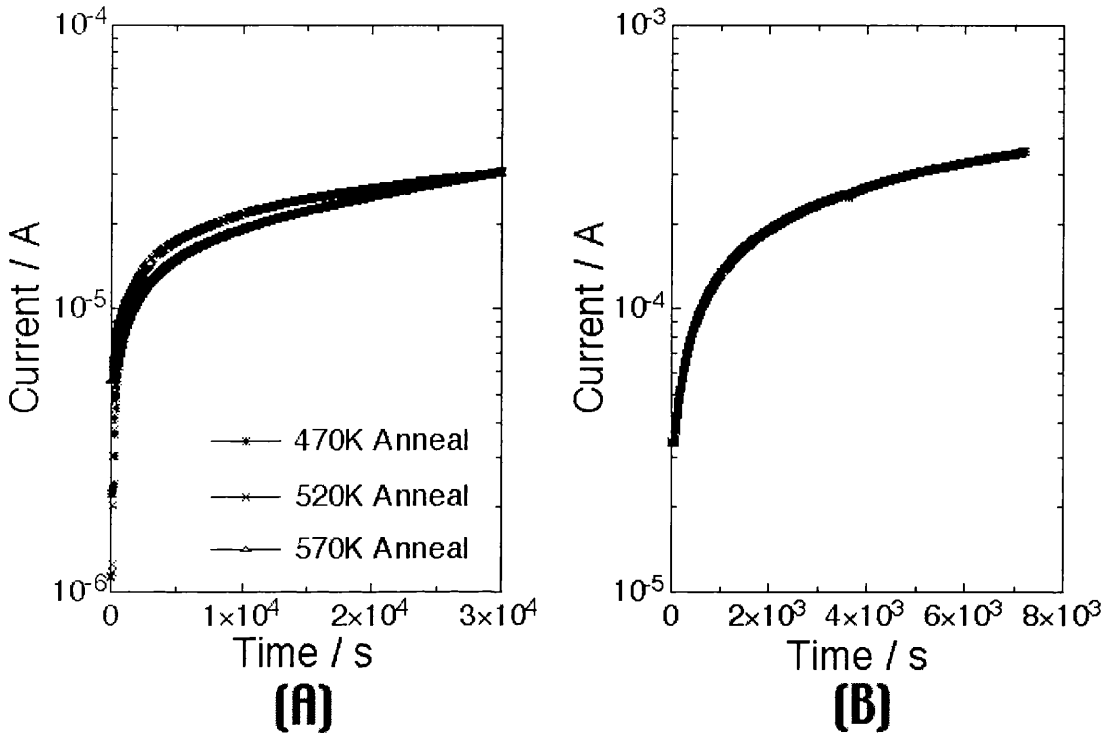
Figure 7.8 Sample Venting

Venting the sample after annealing at various temperature results in almost identical approaches to the original conductivity value as shown in figure 7.8 (A). Figure 7.8 (B) shows the continual increase in conductivity towards the original conductivity value over an extended duration. All of the above conductivity measurements were made using the same polycrystalline sample and it should be noted that there are significant sample dependancies with these kinds of measurements.

Another curiosity of the hydrogen surface conductivity layer is its sensitivity to light. All of the previous measurements were carried out in the dark, bur figure 7.9 shows the effect on conductivity of exposing the sample to different wavelengths of light. Figure 7.9 (A) shows a moderate increase in conductivity due to ambient light and

figure 7.9 (B) shows a much more significant increase (plotted on a log scale compared to 7.9 (A) on a linear scale due to pumping with UV light.
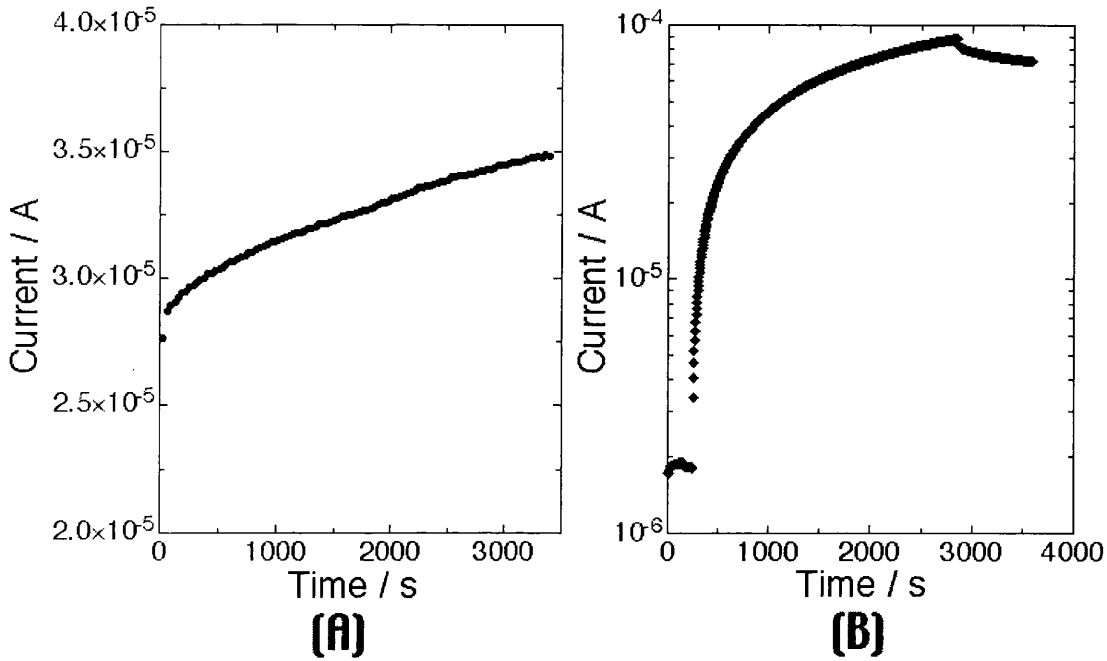
Figure 7.9 Light Effects on Surface Conductivity
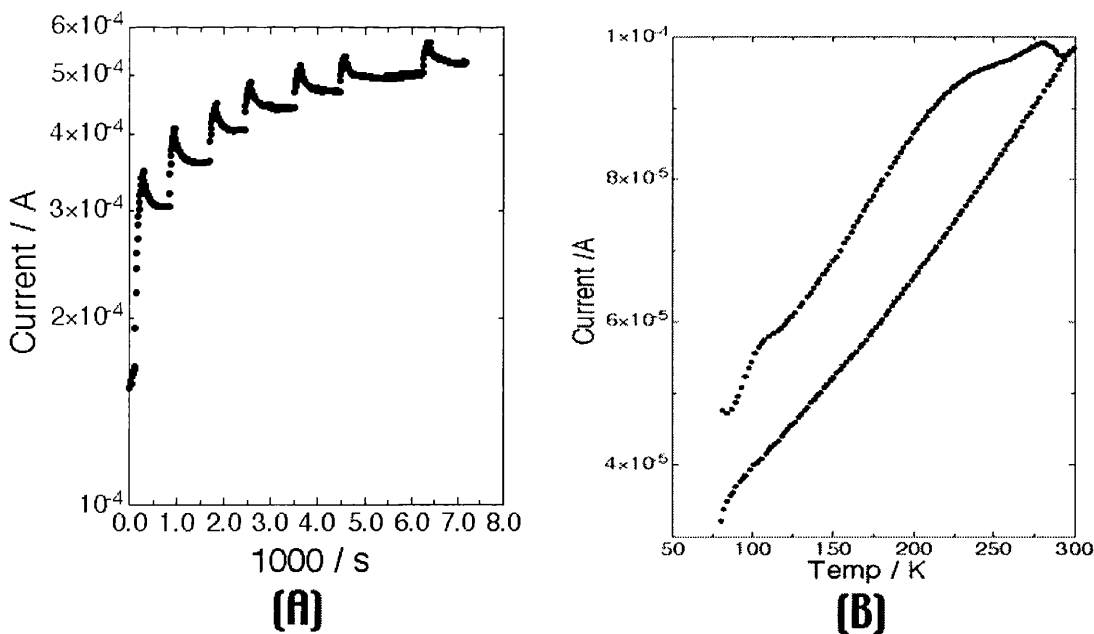
Figure 7.10 Multiple Pumping

Rather more unusual is the stability after pumping the sample with UV light, the small decrease after pumping is due to the slight decrease in temperature after pumping.

106

This effect as better seen in figure 7.10 (A), the pumping effect seems to decrease asymptotically reaching a stable value and then the sample can be pumped again. Obviously there is a maximum conductivity value obtainable by this effect which is also evident in this figure. Figure 7.10 (B) shows a pumped sample at low temperatures, as it is heated the pumped increase in conductivity is lost and the sample cools to a lower value.

It is possible to remove the conductivity of a sample very quickly using a sputtering technique. Figure 7.11 shows the effect of exposing the sample to an atom beam with 100 eV Ar atoms.
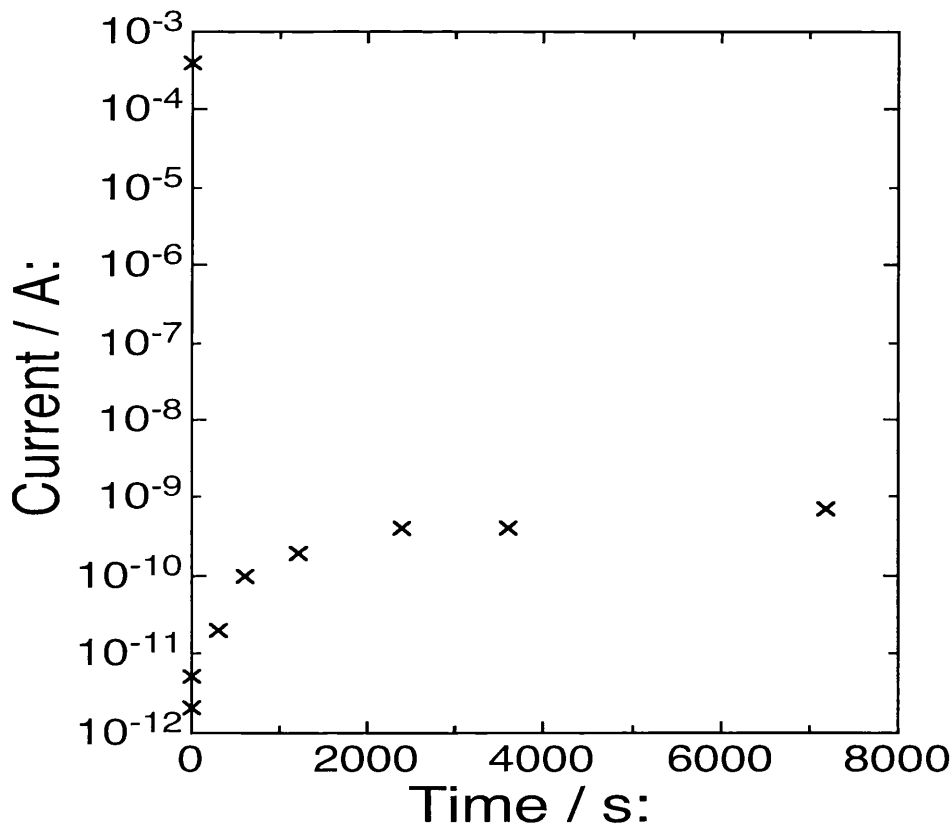
Figure 7.11 Conductivity After Ar Sputtering

After 1 second of Ar bombardment the conductivity has been reduced to intrinsic levels. After this period the conductivity slowly rises but nowhere near the original value.

Section 7.4.2: Hall Data

In order to investigate the mechanism behind the reduction in conductivity due to the application of a vacuum one must look at the hall data. Figure 7.12 displays the hall signal (Hall voltage plus offset) as the sample is pumped down from room pressure to 10^{-5} mbar vacuum.
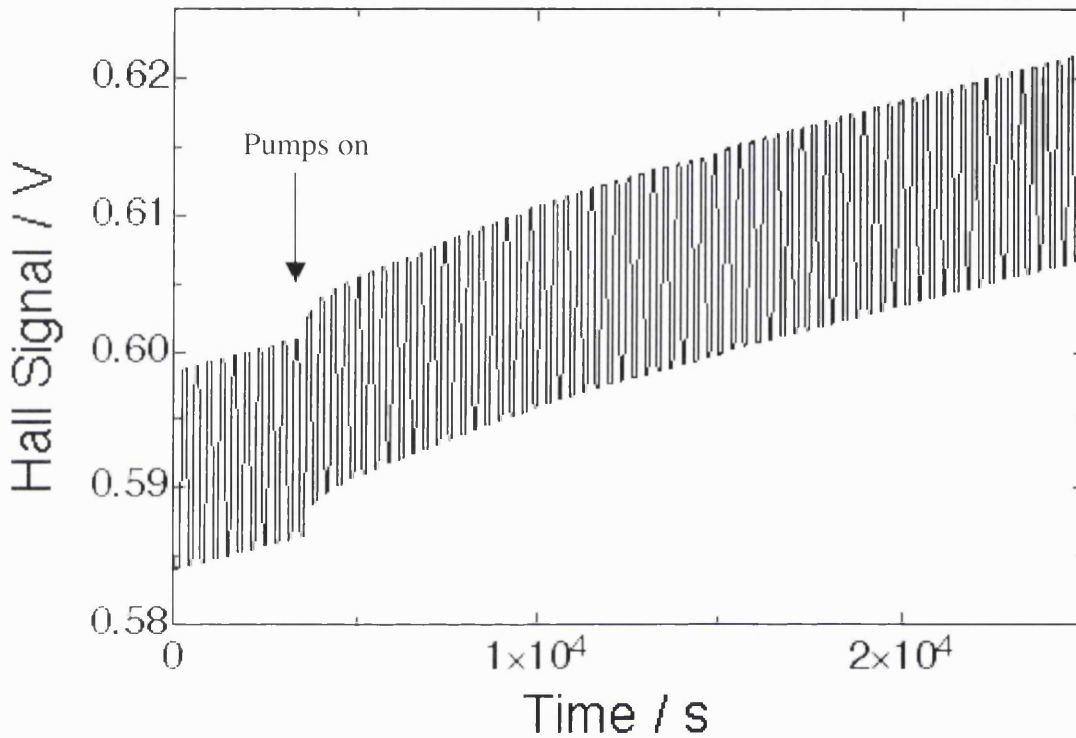
Figure 7.12 Hall Signal Under Vacuum

The hall signal rises immediately on application of vacuum an can be seen to increase asymptotically. This is identical to the rise in the resistivity displayed in previous figures. However, if the individual hall oscillations are analysed it turn, one can derive the variation in carrier concentration as displayed in figure 7.13 (A). The decrease observed is slight but coincides with the timing of the application of vacuum. Figure 7.13 (B) shows the effect on mobility and it can be seen to be almost constant, hence the decrease in resistivity is due to a decrease in the carrier concentration.
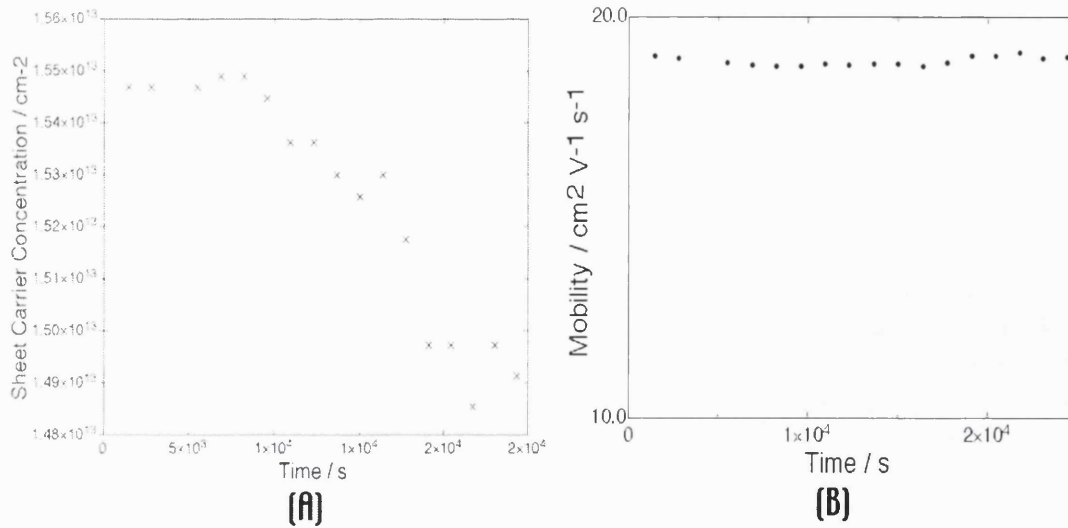
Figure 7.13 Hall Analysis in Vacuum

This experiment can also been run in reverse, that is, the hall signal can be measured as air is let back into the chamber. Figure 7.14 shows this and it can be seen that it is rather more difficult to analyse.
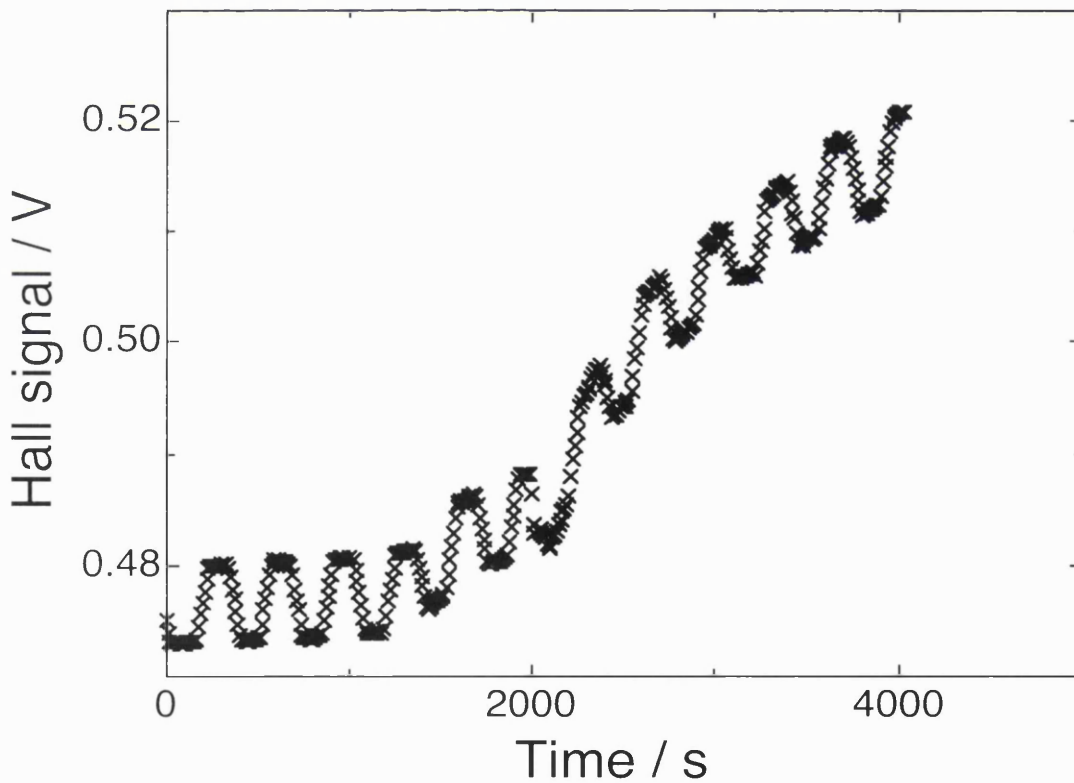
Figure 7.14 Hall Signal During Venting

It be seen from this figure that the signal is not stable enough to be analysed in any more detail. This is due to the cooling of the sample during venting at the same time as the small increase in conductivity due to venting.

The effect of annealing can also be investigated by analysing the hall signal, and this is shown at various temperatures in figure 7.15.
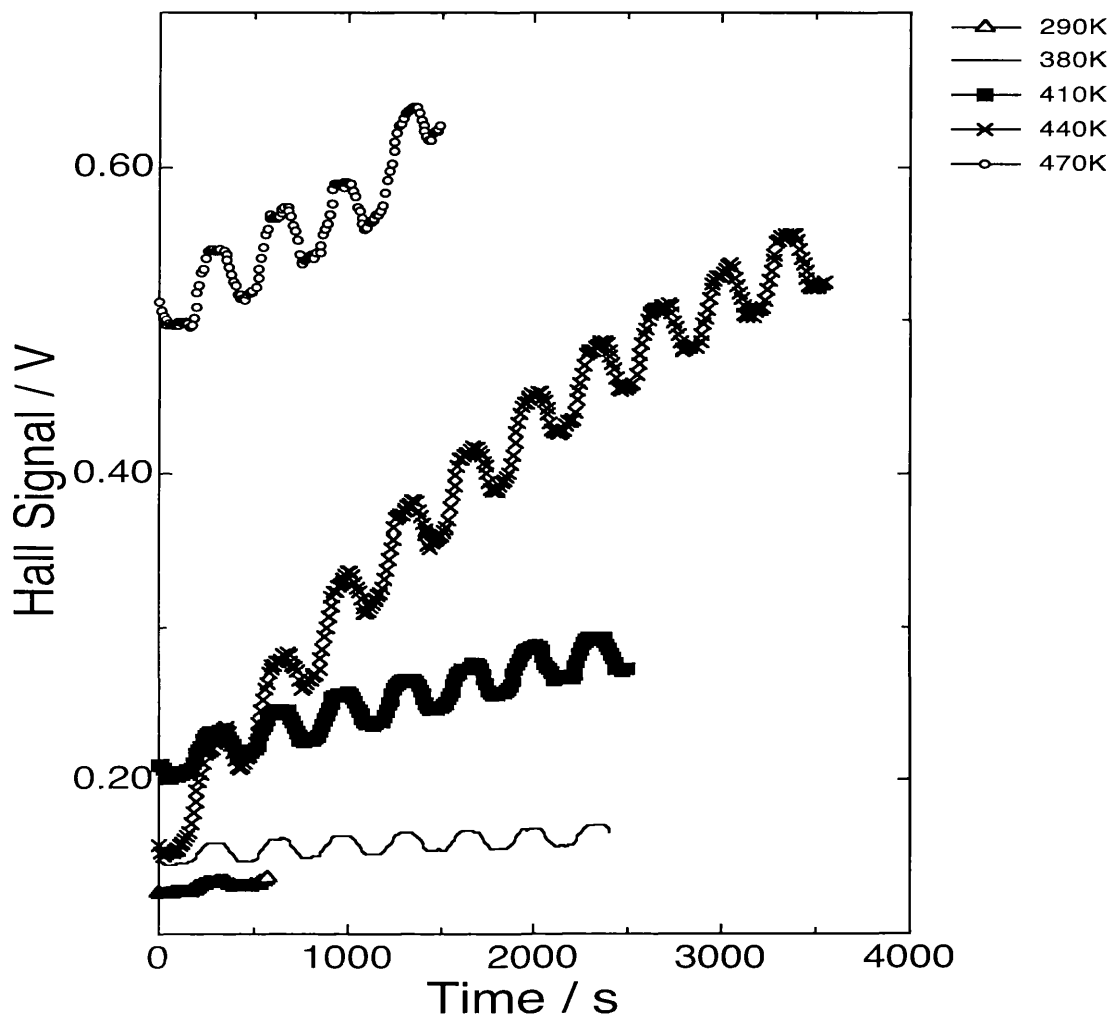
Figure 7.15 Hall Signal Whilst Annealing

A relatively small increase in the hall voltage is clearly visible with increasing temperature marking a decrease in the carrier concentration. The analysis of the above figure is detailed in figure 7.16.
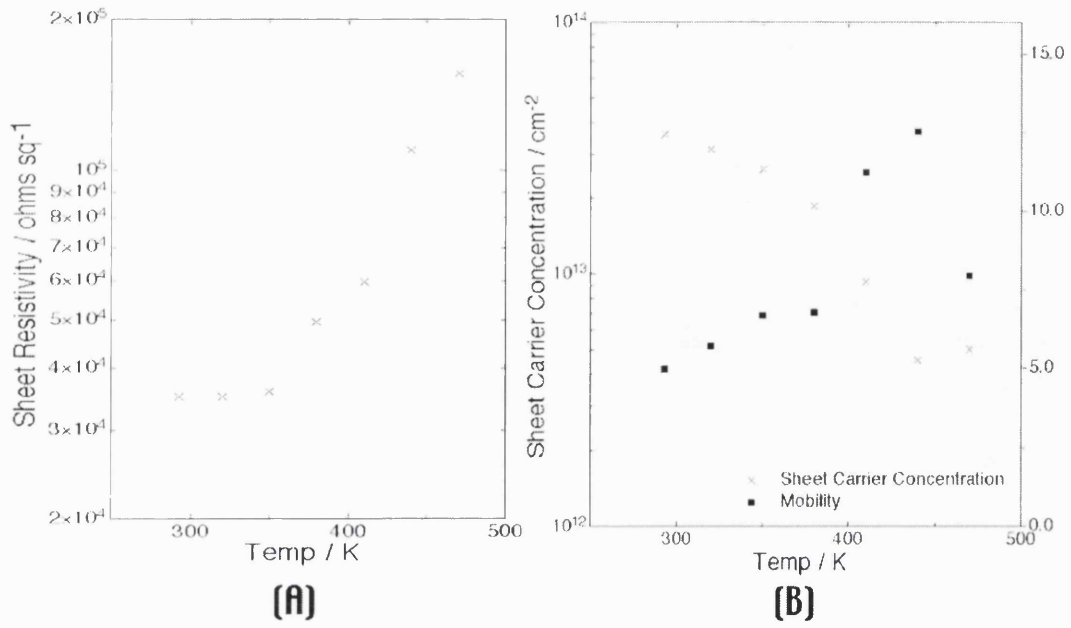
Figure 7.16 High Temperature Hall Analysis

It can be seen from the above figure that the sheet resistivity rises with temperature. Figure 7.16 shows that this is due to a drop in sheet carrier concentration, however there is an accompanied increase in mobility.

Section 7.5 Discussion

The results above show a clear variation of conductivity with respect to the surrounding environment. Figure 1 shows a similar trend to that shown by Sung Gi et al [Sung Gi 1995], where the samples conductivity decreases under applied vacuum, and increases upon venting as in figure 7.5. It stands to reason that to explain this effect there must be something on the surface or in the surrounding air as the bulk should not be affected by applied vacuum.

It has been shown that diamond does not become conductive after hydrogenation until the sample is vented to air [Sung Gi 1995, Ristein 2001]. Sung Gi et al [Sung Gi 1995] vented a hydrogenated sample into various atmospheres and showed that the conductivity did not rise with nitrogen, oxygen, carbon dioxide or hydrogen gas. Furthermore they also showed that dry air had no effect on the conductivity, nor did ultra pure water. This lead to the hypothesis that some contaminant in the air dissolves into water vapour and so they tested the effect of hydrochloric acid (HCl) and sodium chloride (NaCl) as they are typically present in the air. A marked decrease in resistivity was observed in HCl vapour, as was in H_2SO_4 and HNO_3 , i.e. acids make diamond more conductive after hydrogenation. This effect is also suppressed by sodium hydroxide (NaOH) and ammonia (NH_3). Washing the diamond surface with ultra pure water decreases the conductivity, and it returns when the sample is exposed to air again. The below equation shows how HCl could react to water vapour to create oxonium ions (H_3O):

$$ HCl + H_2O \rightarrow H_3O^+ + Cl^- $$
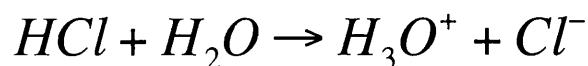
These oxonium ions can accept an electron from a hydrogen atom on the hydrogen terminated surface. Thus the hydrogen atoms on the diamond surface become positively charged attracting a valence electron and thus creating a hole in the valence band. This process is shown schematically and with a band diagram in figure 7.17 (A).
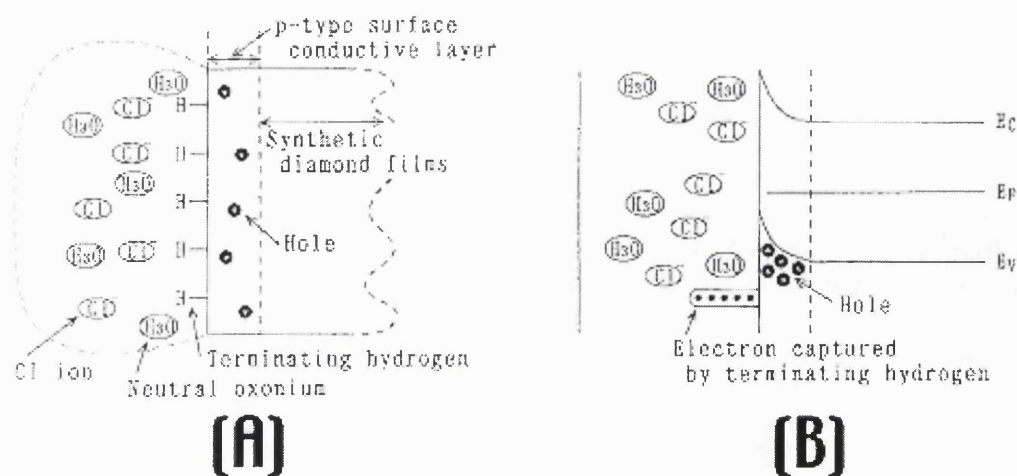
Figure 7.17 Schematic of Sung Gi Model

Figure 7.17 (B) shows the effect this will have on the band bending structure, i.e. the bands must bend up at the surface as has been measured by Shirafuji et al [Shirafuji 1996].

Ristein et al calculated the extent of this upward band bending and showed that in order to satisfy experimental hall sheet carrier density values, the valence band must bend up far enough to reach the Fermi - level at the surface [Ristein 2001]. This was also confirmed by XPS. In order for this to happen the adsorbates must have an electron affinity higher than the ionisation energy (bandgap energy plus electron affinity) of diamond to create states below the valence band maximum to localise valance band electrons. As diamond has an unusually large band gap, this ionisation is also large. However, hydrogen terminated diamond is helped by its substantial negative electron affinity (-1.27eV± 0.07eV [Cui 1998]), and subtracting this from the band gap energy gives an ionisation energy of around 4.2eV. This is still a very high electron affinity to expect from an adsorbate commonly found in the atmosphere, with halogen atoms not exceeding 3.7eV. This means that electron transfer from the diamond to an atmospherically occurring adsorbate is impossible. It is possible for protons screened by water molecules to have this affinity and oxonium atoms as mentioned above fit this description.

This model can easily explain the effect of exposing a sample to vacuum as the adsorbates are "pumped off" the surface and hence the conductivity decreases as shown in figure 7.1. When the sample is vented, water vapour in the air containing these species redeposit on the surface and the conductivity increases as in figure 7.5. Figures 7.12 and 7.13 confirm that this change in conductivity is due to changes in the carrier concentration which is also consistent with the pumping off or deposition of adsorbates (and hence the holes donated by them) from the diamond surface.

Upon heating the situation is slightly different. Previous reports [Landstrass 1989] have shown a five orders of magnitude decrease in resistivity when annealing in air at 570K. However, this effect is only reversible by rehydrogenation and so is different from in vacuum. The reason for this is clearly the presence of oxygen in air, which can react with the surface and displace the hydrogen termination. In vacuum, hydrogen termination is known to be stable up to around 1000K [Su 1998, Cui 1999], but in air the value is much lower [Mantel 2000]. Figure 7.18 shows that the hydrogen termination and conductivity are removed at the same temperatures in air by Fourier Transform Infra - Red Spectrocopy [Mantel 2001].
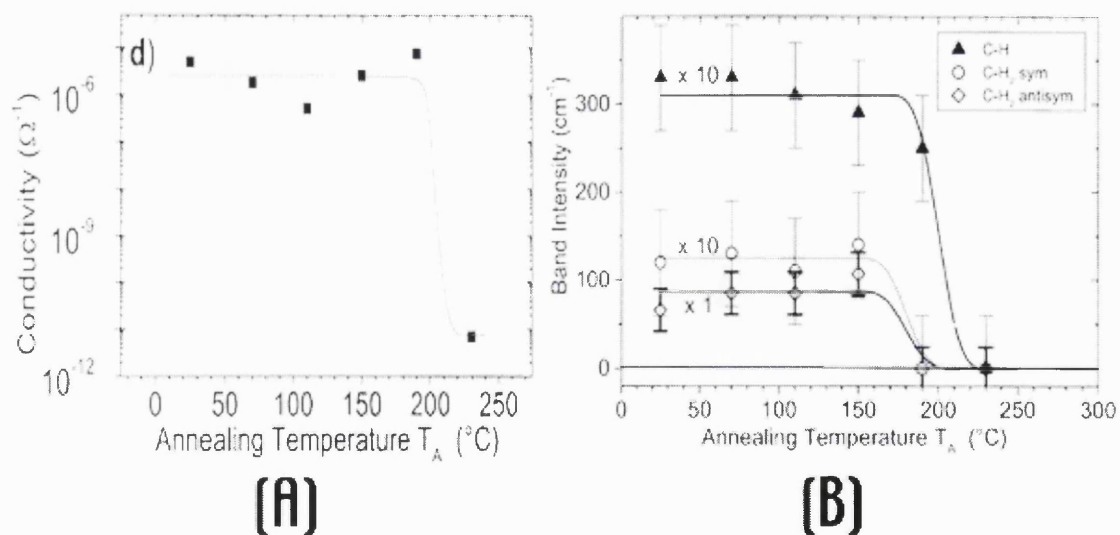
Figure 7.18 Annealing C - H Dipole

This means that there must be two processes in air, the displacement of the hydrogen dipole and the dislodging of adsorbates. This explains how diamond can be partially

annealed [Looi 1998], as at lower temperatures some but not all of the hydrogen termination is removed and thus there is less transfer doping through dipoles.

In vacuum the hydrogen termination is not exposed to significant amounts of oxygen and hence it is far more stable. Obviously, as the sample is heated, adsorbates will be dislodged and the conductivity will decrease as seen in figures 7.2 and 7.3. when the diamond is cooled after annealing, it stabalises at a much lower value of conductivity as the adsorbates are no longer present. The trend in figure 7.4 is just thermally stimulated current, as there are far fewer adsorbates the dominant process on cooling is the freezing out of thermally generated bulk charge carriers. Figure 7.5 shows how the conductivity is replaced by venting the sample to air, this is due to the redeposition of adsorbates at the surface of the diamond, a phenomenon also seen by Sung Gi and Ristein [Sung Gi 1995, Ristein 2001]. Figures 7.7 and 7.8 show the reproducibility of this effect and hence the stability of the hydrogen dipole under this vacuum. Looi et al [Looi 1998] suggested that the annealing process was identical in air and in vacuum, however, they did not measure the sample after the chamber had been vented to air and hence did not see the conductivity return. Szameitat et al [Szameitat 2000] reported similar observation to those above but found that the rate of return of conductivity was very low. It is not clear why their results conflict with those above or reported in the literature [Ristein 2001]. They suggest that the adsorbate required to induce conductivity is not very common in atmospheric air, in contradiction with the model [Sung Gi 1995]. Another possibility is that the air in their lab had a very low humidity or there was very poor circulation in their vacuum chamber and hence the sample took a long time to saturate.

Figures 7.9 and 7.10 show persistent photoconductivity in hydrogenated diamond films. Figure 7.9 (A) shows that the film is in fact sensitive to even visible light, but this is not entirely surprising as the film is polycrystalline and hence contains many defects. Figure 7.9 (B) shows the increased sensitivity expected to UV light and a clear persistent photoconductivity effect, this effect has been observed in other wide bandgap materials including diamond [Gonon 1997, Horng 1999]. The decrease in current after pumping is due to small heating effect from the illumination. There is also the effect of the negative electron affinity (NEA) of the hydrogen terminated

diamond surface, if an electron can reach the conduction band, i.e. through pumping then it can leave the sample and enter the vacuum. However, it has been shown that the NEA of hydrogen terminated diamond is not maintained unless under UHV conditions [Ristein 1998]. It is therefore more likely that the UV effect is related to persistent photoconductivity, as defect states in the films can be used to "ladder" electrons into the adsorbate layer.

This model so far requires the presence of the hydrogen dipole, but this alone is not sufficient. Figure 7.11 shows the effect of removing the hydrogen dipole under vacuum. The conductivity is totally annihilated after 1 second of argon bombardment and does not return upon venting the sample to air. This means that the atom beam is not just removing the adsorbates from the diamond surface as they would come back as air was let into the chamber. The increase in conductivity after 1 second is slight and due to damage on the surface from the atom bombardment. After bombardment it is impossible to rehydrogenate the sample without prior surface treatments to remove surface damage. This damage can be removed by oxygen plasma treatment or just annealing at high temperatures in air to "burn off" the near surface. A similar result is recorded in the literature where one side of a sample was electron bombarded and another not; upon contact with air, the un-irradiated side became conductive while the electron irradiated area did not [Ristein 2001]. As the energy of the electrons was very low (1KeV), any argument about the bombardment effecting the bulk is void.

Hall measurements have also been used to quantify the effects of gases on the surface conductivity layer [Sung Gi 1999]., these measurements showed an increase in carrier concentration in oxidising gas (NO_2) and a decrease in reducing gas (NH_3) atmospheres.

Figures 7.12 and 7.13 show direct evidence of the reduction in carrier concentration due to applied vacuum and the relative stability of the mobility under these conditions. Figure 7.15 shows the increase in hall voltage during annealing and hence the decrease in carrier concentration, the offset also increases marking the increase in the sheet resisitivity. The value at 440K in this figure shows the signal before the film has been stabalised, that is, the annealing is still effecting the film so the oscillation is

sloped. Figure 7.16 shows the analysis of this data, the mobility is seen to increase slightly as the carrier concentration decreases. The carrier concentration obviously decreases because of the desorbtion of adsorbates, and at higher temperatures there are also thermally stimulated carriers. When the sample is brought back to room temperature without venting, the carrier concetration drops further still due to the loss of the thermally stimulated carriers. Annealing has a rather more subtle effect on the mobility values. As the sample is heated the carriers have more thermal energy and hence are less confined by the surface dipole. This means that they will experience far less coulomb scattering and surface scattering and hence the mobility increases. This increase is ultimately limited by phonon scattering. When the sample is brought back down to room temperature the mobility value drops because the thermal energy is decreased leading to enhanced confinement and the associated increased scattering.

Section 7.6 Summary

This chapter has focused on the peculiar stability of hydrogen terminated diamond under various atmospheric conditions. This data has been correlated with published work and a possible model for the surface conductivity layer has been proposed. This model requires the presence of adsorbates within a water layer on the hydrogen terminated diamond surface. This layer can act as an "electron sink" to create holes within the near surface region of the diamond film.

This work also has a profound impact on the realisation of commercial devices from this conductivity layer as their inherent instability will have to be addressed. If the model proposed in this chapter is correct then it stands to reason that most forms of diamond could be used with this conductivity layer.

References

Baral B., Chan S.S.M. and Jackman R.B.,
Journal of Vacuum Science and Technology **14** (1997) 2303

Cui J.B., Ristein J. and Ley L.,
Physical Review B, **59** (1999) 5847

Cui J.B., Ristein J., Ley L.,
Physical Review Letters, **81** (1998) 429

Gonon P., Prawer S., Boiko Y. and Jamieson D.N.,
Diamond and Related Materials **6** (1997) 860

Horng R.H., Wuu D.S., Wei S.C., Chan S.H. and Kung C.Y.,
Thin Solid Films, **343-344** (1999) 642

Kawarada H.,
Surface Science Reports, **26** (1996) 205

Landstrass M.I. and Ravi K.V.,
Applied Physics Letters, **55** (1989) 975

Looi H.J., Jackman R.B. and Foord J.S.,
Applied Physics Letters, **72** (1998) 353

Mantel B.F., Stammler M., Ristein J. and Ley L.,
Diamond and Related Materials, **10** (2001) 429

Mantel B.F., Stammler M., Ristein J. and Ley.L.,
Diamond and Related Materials, **9** (2000) 1032

Ristein J., Maier F., Riedel M., Stammer M. and Ley L.,
Diamond and Related Materials **10** (2001) 416

Shirafuji J. and Sugino T.,
Diamond and Related Materials **5**(1996) 706

Su C. and Lin J.C.,
Surface Science, **406** (1998) 149

Sung Gi R., Mizumasa T., Akiba Y., Hirose Y., Kurosu T. and Iida M.,
Japanese Journal of Applied Physics, **34** (1995) 5550

Sung Gi R., Tashiro K., Tanaka S., Fujisawa T., Kimura H., Kurosu T. and Masamori
I.,
Japanese Journal of Applied Physics, **38** (1999) 3492

Szameitat M., Jiang X. and Beyer W.,
Applied Physics Letters, **77** (2000) 1554

Chapter 8

Hydrogenated Black Diamond

Contents

Section 8.1 Introduction

Black diamond is considered to be low grade "thermal management" material not suitable for active device applications. However, in previous chapters it has been shown that even highly twinned material can be used for devices application when utilising the hydrogen surface conductive layer. Also, it was shown that polycrystalline material performs comparably to high quality single crystal homoepitaxial and natural diamond films.

Black diamond is commercially available from a multitude of suppliers and the distribution is not with strained by any patents. Black diamond is available is many shapes and sizes, grown by various techniques. The utilisation of such a material for electronic applications would therefore have huge cost implications.

Section 8.2 Experimental Aims

The aim of the work detailed in this chapter is to assess the viability of the utilisation of black diamond for active device applications. Standard electrical characterisation techniques have been used on various films and devices fabricated. Comparisons will be made with both white polycrystalline and single crystal diamond films. Simple devices have also been fabricated and tested.

Section 8.3 Experimental Methods

All samples studied here were free standing diamond and grown by CVD techniques from a dilute hydrocarbon in hydrogen gas mixture. Sample types A, B and C were grown by MWPECVD, whilst sample type D was produced using HFCVD. Scanning electron microscope (SEM) images were taken with a Joel microscope and RAMAN spectra with a RENISHAW 2000 system with red (He-Ne) laser excitation.. Prior-to hydrogenation all samples were immersed in a boiling ammonium persulphate / sulphuric acid mixture which is known to result in a contaminant free oxidised surface [Baral 1997]. Hydrogenation was performed using pure atomic hydrogen plasma generated within a purpose built MWPECVD chamber (sample temperature 500°C,

800W, 40torr, 5 minutes). This chamber has never been intentionally contaminated with any other gases. Samples were then removed from the chamber and Au contacts deposited in an Edwards A306 evaporator with a base pressure better than 4×10^{-7} mbar. Hall effect measurements were carried out in a vacuum better than 6×10^{-6} mbar (10-300K *in-vacuo*, 0.3-1.8 T magnetic field strength). It should be noted that on this visit to the WSI Munich, only liquid nitrogen was available and so sample samples were measured over a smaller temperature range. Schottky contacts were fabricated on MWPECVD black diamond by thermally evaporating $500 \mu m$ aluminium diameter dots with a simple shadow mask under pressures better that 4×10^{-7} mbar. I / V tests were performed with a Hewlett Packard HP4145B parameter analyser with a Signatone heated probe station.

Section 8.4 Experimental Results

Section 8.4.1 RAMAN and SEM

SEM images of the black diamond films are shown in figure Y.1 the white bar representing 50μm.
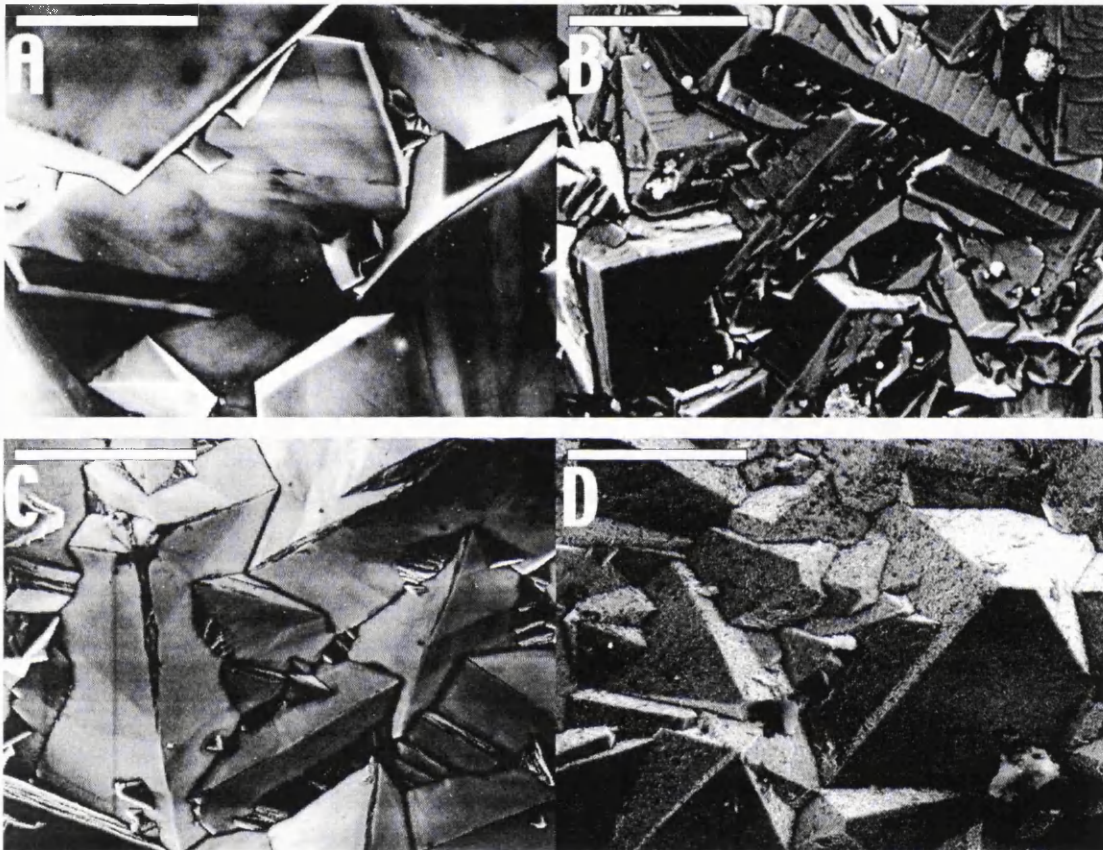
Figure 8.1 SEM Images

Sample types A, B and C were grown by MWPECVD, whilst sample type D was produced using HFCVD. Sample A was an MWPECVD grown 500μm thick film and consisted of large (50-100μm) randomly aligned grains, being 'white' in colour due to light scatter from the rough top surface of the film. Samples B and C were also MWPECVD grown, but differed in thickness, being 800μm and 1mm respectively. In both cases the grains were randomly oriented with grain sizes of 50-100μm,

however sample C displays much cleaner faceting. Both samples were densely black when observed under optical illumination. This effect is normally associated with high levels of graphite inclusion when higher percentages of hydrocarbon are used within the gas used to grow the film, which dramatically enhance the growth rate. Sample D was grown by HFCVD and was 500μm thick, graphitic inclusions can clearly be observed within the grains which otherwise show clear faceting.

Raman spectra of the above films are displayed in figure 8.2
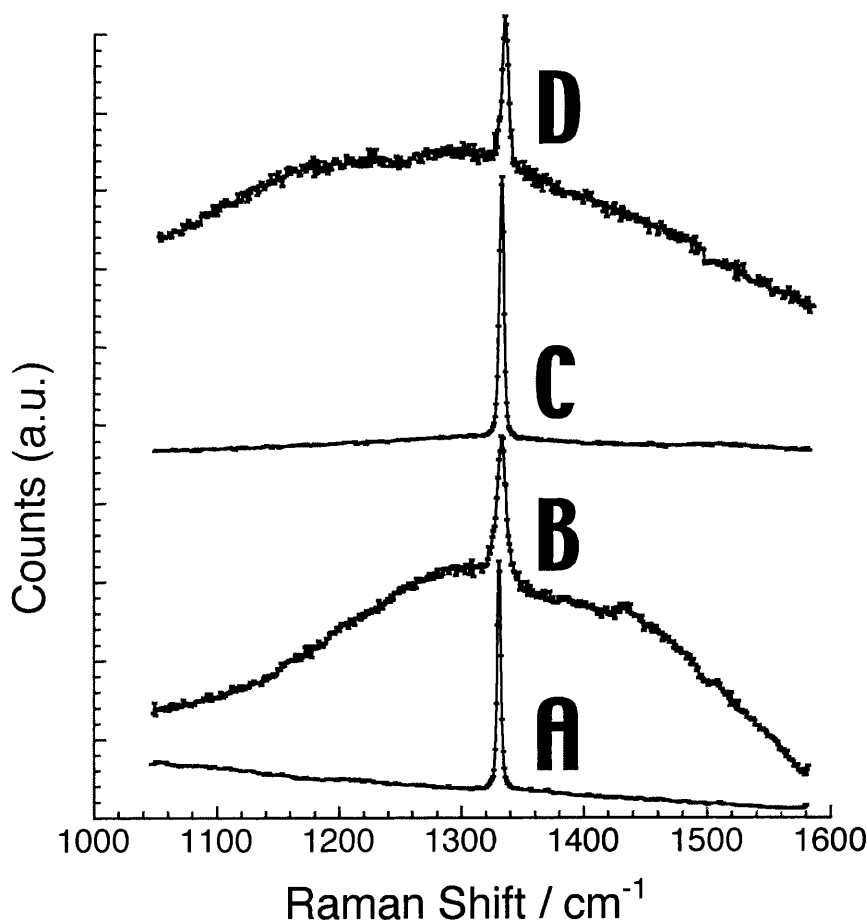
Figure 8.2 Raman Spectra

Samples A and C show intense 1332cm^{-1} peaks, indicative of high quality diamond [1], whilst samples B and D show a 1332cm^{-1} peak imposed on a broad feature between 1100 and 1500cm^{-1}, implying significant non-diamond carbon content within the films. These films also showed non diamond inclusions in the SEM images displayed previously.

Section 8.4.2 Hall Data

Figure 8.3 shows the variation of sheet resistivity against temperature for the four films.
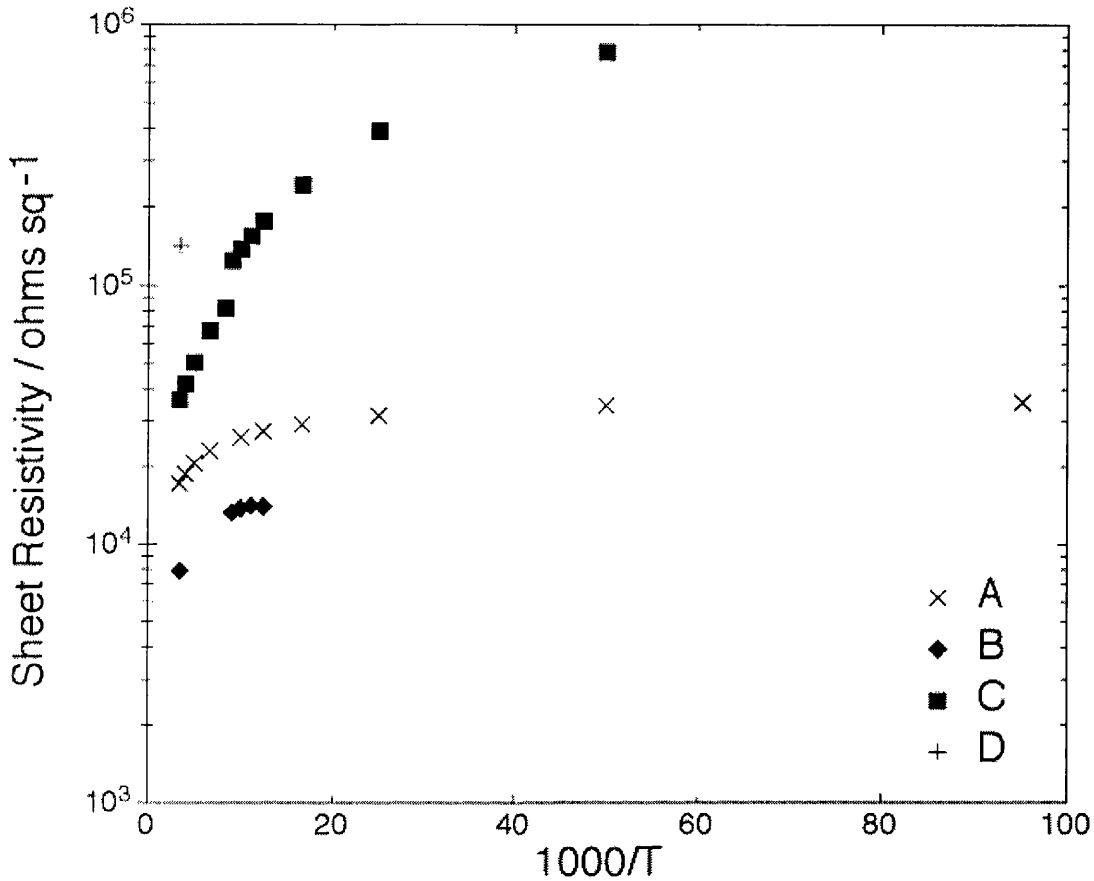
Figure 8.3 Sheet Resistivity Against Reciprocal Temperature

As with the white diamond films previously studied, all films show and increase in sheet resistivity (decrease in sheet conductivity) with decreasing temperature. Again no single activation energy is apparent. The largest variation is shown by sample C (1mm thick) and the smallest by sample A. Sample D was too resistive to measure at lower temperatures.

Figure 8.4 shows the variation of the sheet carrier concentration of the above samples with decreasing temperatures.
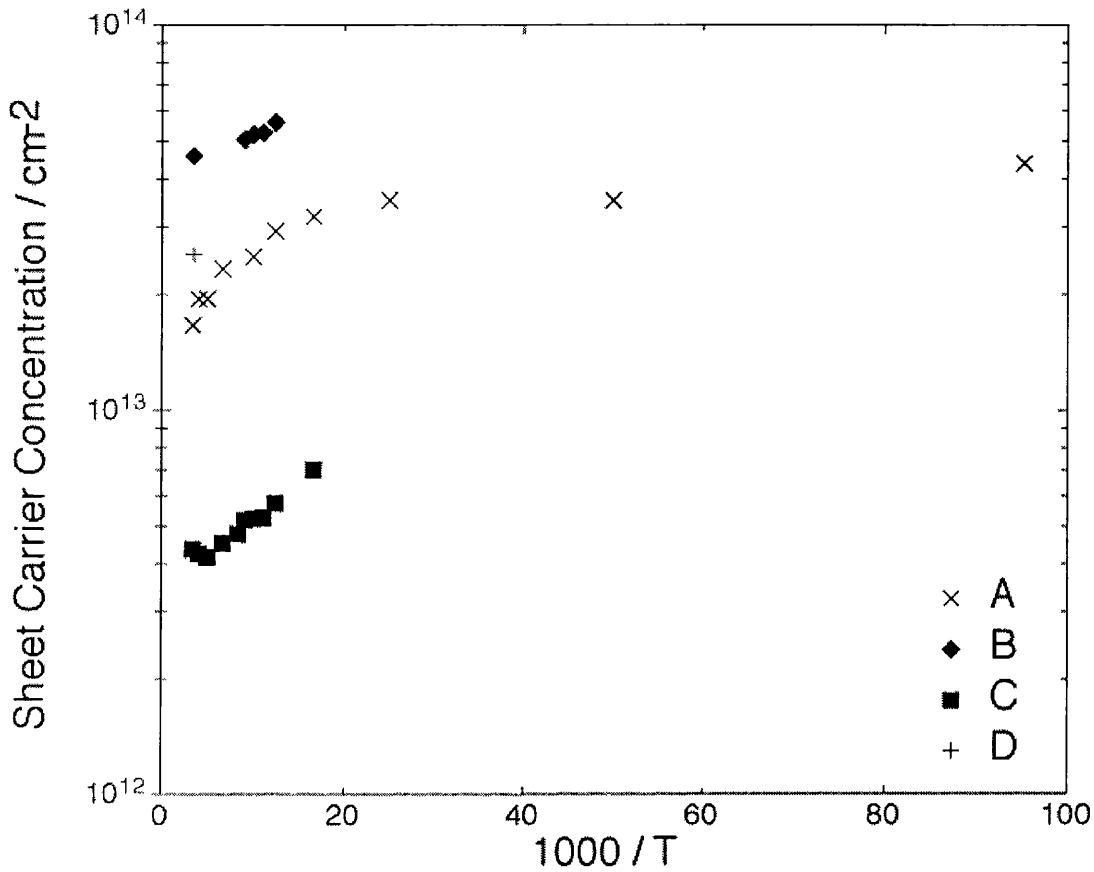
Figure 8.4 Sheet Carrier Concentrations Against Reciprocal Temperature

All samples display an increasing sheet carrier concentration with decreasing temperature except sample D which could not be measured at lower temperatures. The variation of all samples is slight, the greatest being sample A the 500µm white diamond. The highest carrier concentration is upheld by sample B and the lowest by sample C. The three black diamonds can be seen to show similar carrier concentrations to the white diamond control.

Figure 8.5 shows the variation of the hall carrier mobility of each of the diamond films.
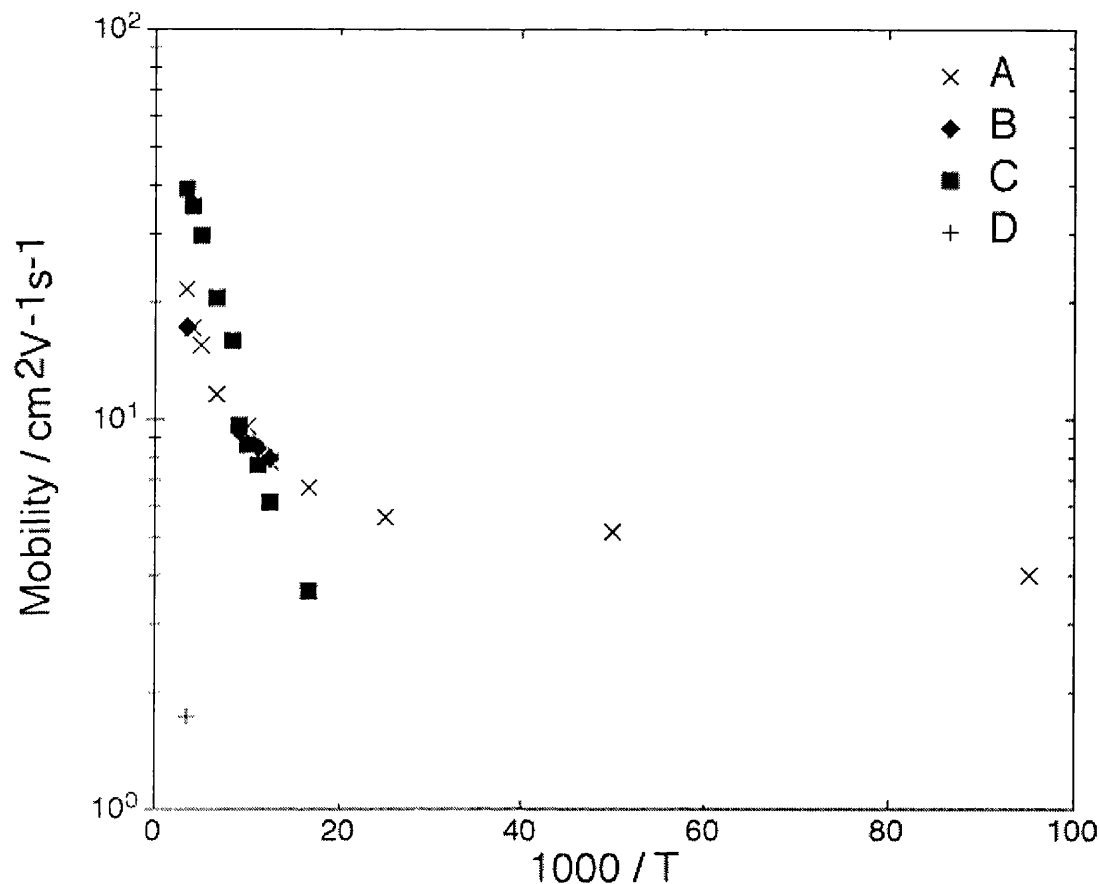
Figure 8.5 Mobility Against Reciprocal Temperature

The mobility values of all samples can be seen to decrease with decreasing temperature except for sample D which could not be measured at lower temperatures. This sample had a low mobility at room temperature and hence was exceptionally difficult to measure at lower temperatures. Sample C Shows the highest mobility at room temperature ($46\text{cm}^2\,\text{V}^{-1}\,\text{s}^{-1}$) which is also the highest measured by the author on polycrystalline diamond. It can be seen that again the mobility varies much more than the respective carrier concentrations over the temperature range and is the driving force behind the variations in the sheet resistivity.

Figure 8.6 shows a comparison of the black diamonds studied at room temperature, it can be seen that black diamond yields similar mobility and carrier concentration values as the white diamond in previous chapters. As it is to be expected, higher carrier concentrations result in lower mobilities.
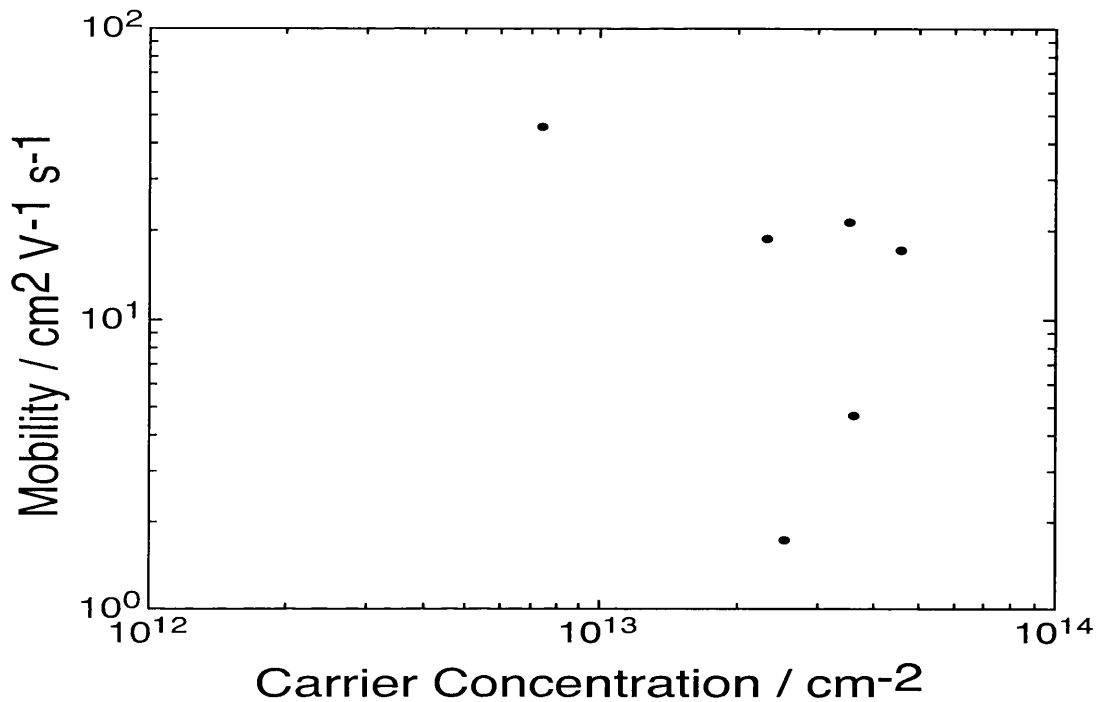
Figure 8.6 Hall Data Comparisons

Section 8.4.3 Device Characteristics

Figure 8.7 shows the I/V characteristics of an Al schottky diode fabricated on MWPECVD black diamond. This diode has an ideality factor of around 3 and a low reverse bias leakage of around 10^{-10} A, limitations in the screening setup make it difficult to read current values much lower. The forward current is around $40\mu A$ which yields a rectification ratio of between five and six orders of magnitude. The series resistance of the diode begins to dominate at 5V.

The high temperature characteristics of this diode are shown in figure 8.8. Upon heating the diode the reverse bias current increases but the forward bias current is unaffected – hence the rectification ratio drops dramatically. When the device is returned to room temperature the reverse bias leakage only improves by around one order of magnitute from the 470K result and hence the device is damaged by the process.
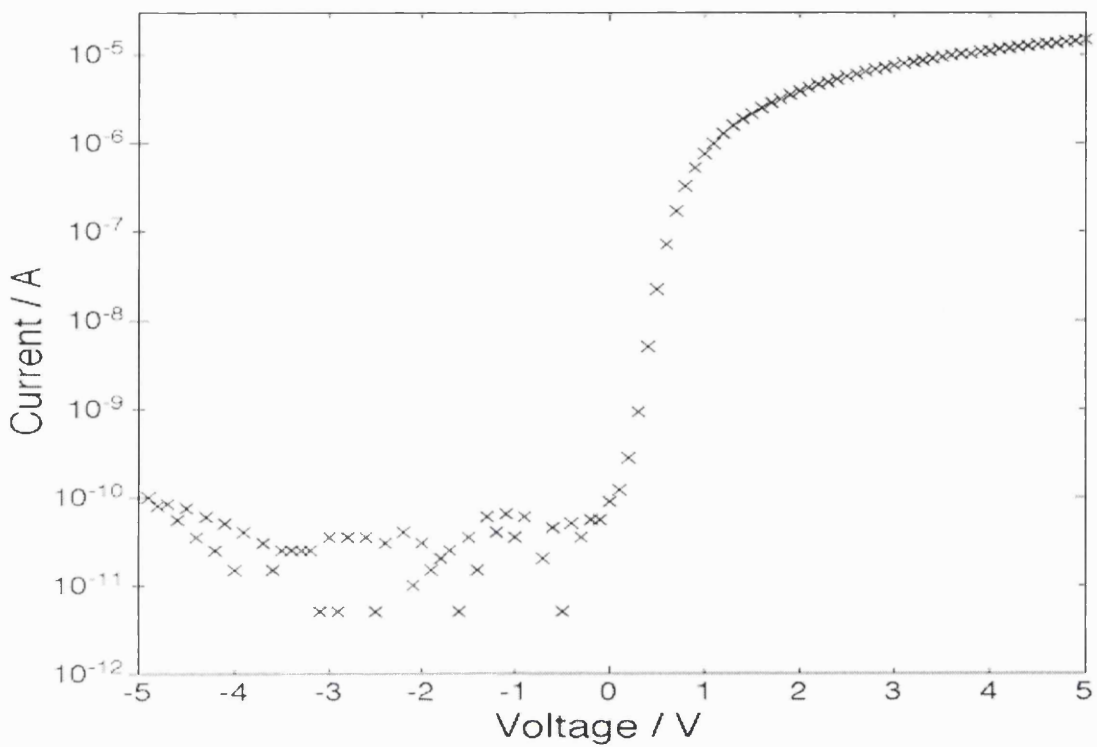
Figure 8.7 Schottky Diode I / V Characteristics
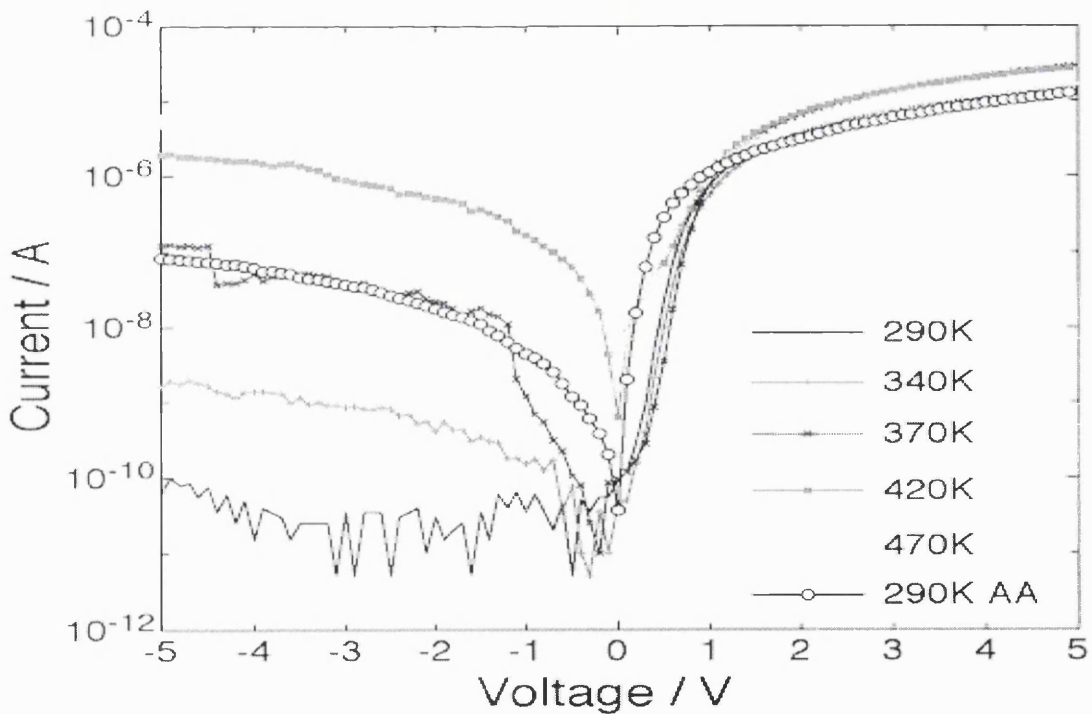
Figure 8.8 High Temperature I / V Characteristics of Black Diamond Schottky Diode

Devices can also be fabricated on HFCVD diamond and an example of a similar schottky to Figure 8.7 is shown in figure 8.9.
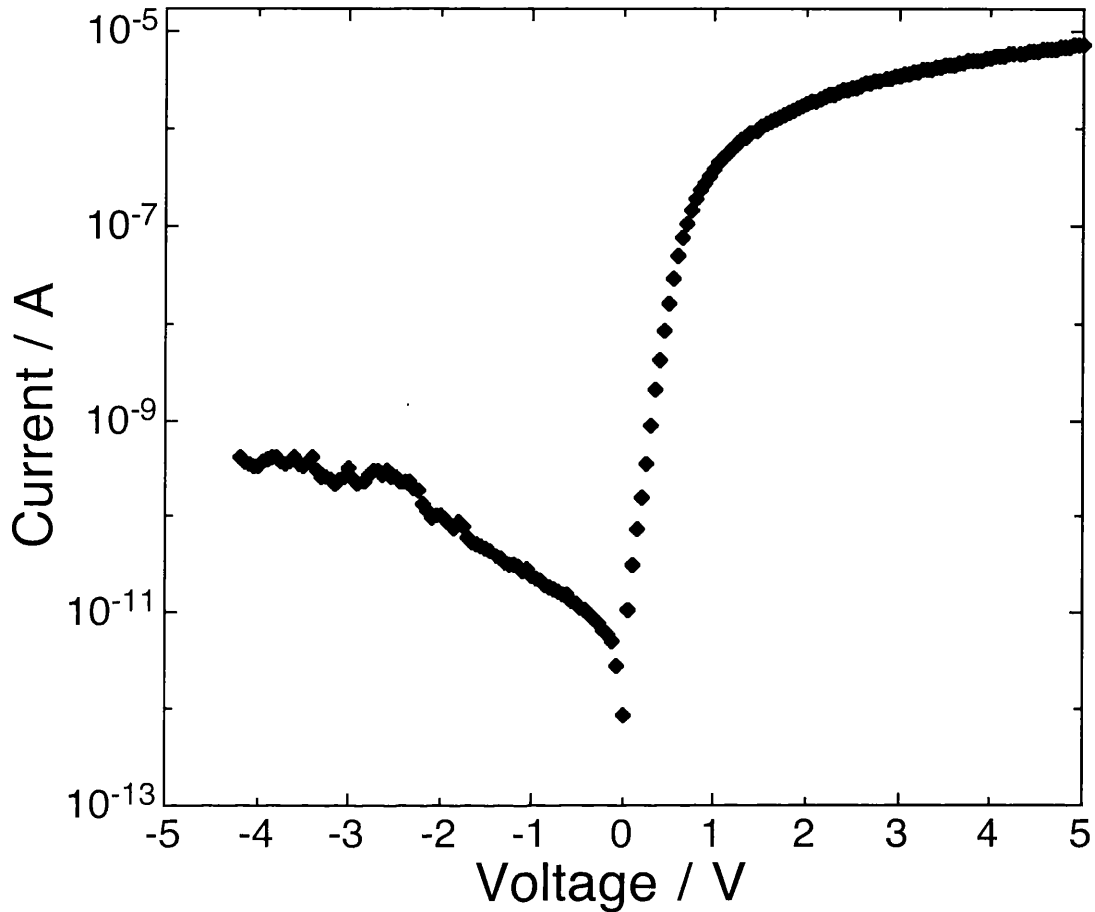
Figure 8.9 Al Schottky contact on HFCVD

It can be seen that this diode shows increased leakage and reduced forward bias current, hence the rectification ratio is reduced to 4 orders of magnitude.

MISFETs were also attempted but it was found that the CaF_2 gate significantly reduced conductivity. Figure 8.10 shows the test structure designed to confirm this and figure 8.11 shows I/V measurements between contacts.

(A)   **(B)**
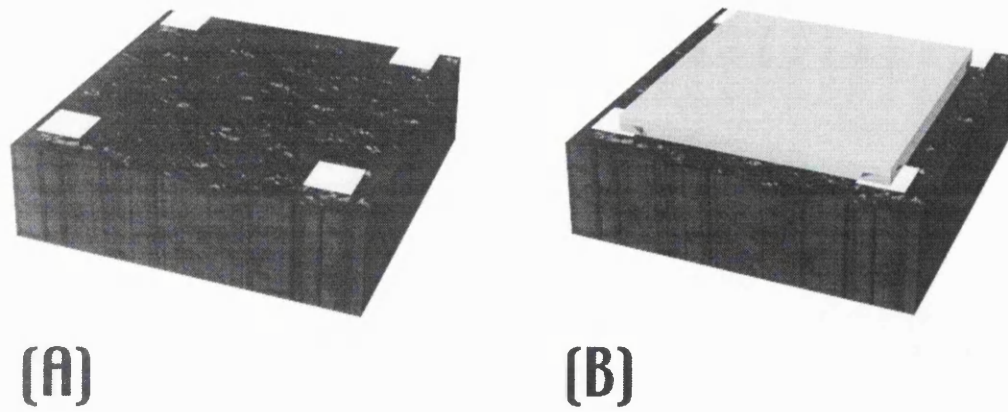
Figure 8.10 CaF$_2$ Test structure
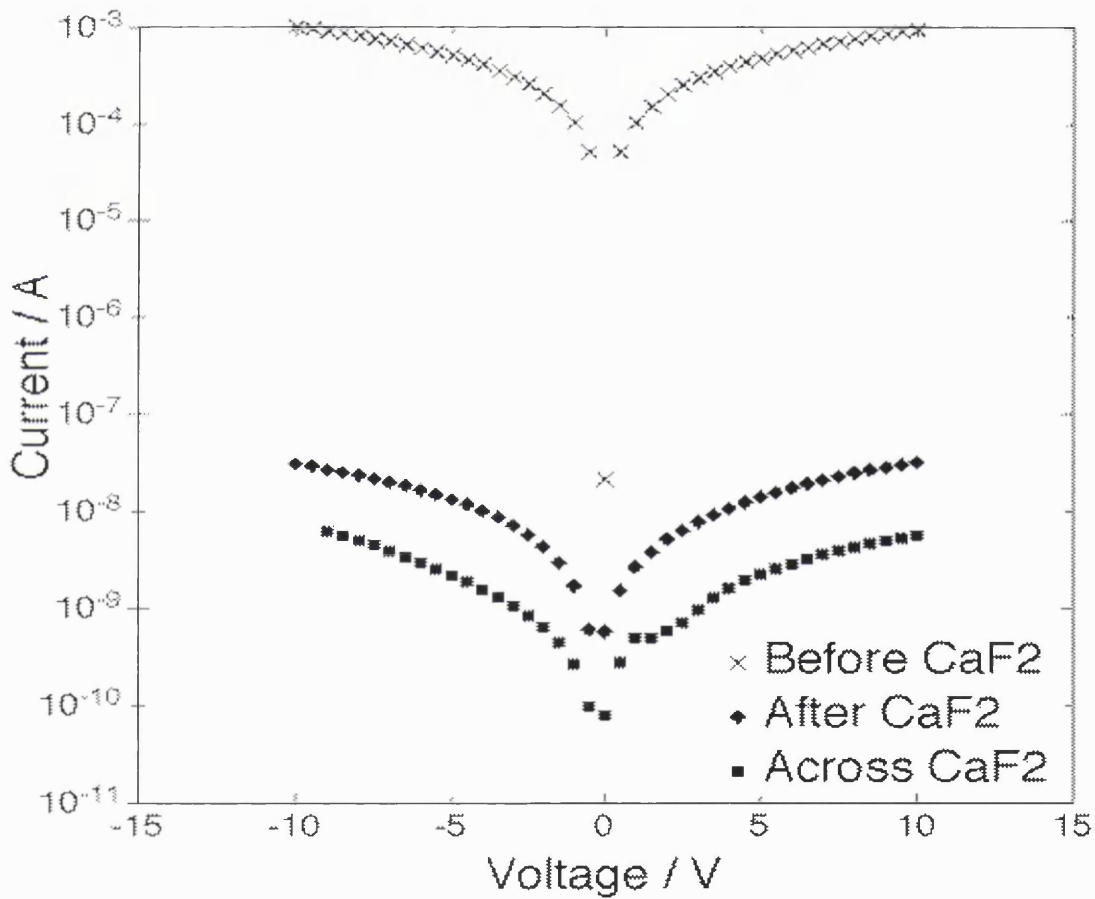
Figure 8.11 I/V Measurements of CaF$_2$ Test Structure

It can be seen in figure 8.10 (A) that the Au contacts were deposited inside the edges of the diamond film to avoid edge effects, the current between two of the four

contacts (diagonal) can be seen in figure 8.11. After CaF_2 deposition (figure 8.10 (B)), the current has decreased five orders of magnitude.

Section 8.5 Discussion

Very little information is available about black diamond within the literature and none utilising the hydrogen surface conductivity layer. Hot filament material has been used in the past [Sung Gi 1995], as have hot filament reactors for hydrogenation [Ristein 2001]. In general it is considered more desirable to grow white diamond for electronic applications due to the high level of defects in black material.

Hot filament and Microwave Plasma Enhanced Chemical Vapour Deposited material (HFCVD and MWPECVD respectively) can be grown faster at higher methane concentrations, and this results in a black material.

Figures 8.1 and 8.2 correlate in that the samples with clear faceting (A and C) also show clear Raman Spectra with no evidence of graphitic phases. Sample B is heavily twinned and it's Raman Spectra reflects this. Sample D shows clear evidence of inclusions and it's Raman Spectra is reminiscent of this. These inclusions are assumed to be graphitic, but there are generally high amounts of Tantulum from the filament as measured by SIMS [Barnes 2002]. Although it is initially surprising that a black diamond can show a very flat Raman Spectra (sample C), the fact that Raman Spectroscopy uses a highly focused beam which could be entirely positioned on a large grain explains this phenomenon. The SEM of sample C is also very clear and there is no evidence of grain inclusions, this sample was fundamentally black however. It has been shown by others that higher methane / oxygen ratios lead to poorer facetted diamond and a higher percentage of non – diamond components [Sanchez 1994, Liou 1994], and that these ratios also produce a higher growth rate. It is not possible to confirm the growth gases here as the samples were commercially supplied.

Figure 8.3 shows that the sheet resistivity of all samples increases with decreasing temperature as is to be expected, the room temperature values being comparable with those available in the literature [Looi 1998, Williams 2001]. The variation is very

similar to that measured on white diamond in previous chapters, and as the samples were very resistive prior to hydrogenation this is clear evidence of the hydrogen surface conductivity layer. Black diamond can show lower resistivity than white diamond if grown without oxygen and at high methane concentrations [Lux 1994]. The volume resistivity is generally assumed to be lower for black diamond [Lux 1994], but the surface resistivity is generally very similar. In these experiments we are measuring the surface resistivity as hydrogenation is a surface phenomenon. Black diamond is too highly resistive to perform hall measurements before hydrogenation, and no time of flight data exists in the literature to calculate its mobility.

Figure 8.4 shows that the variation of the sheet carrier concentration values with temperature for all samples are similar to that of white diamond [Jiang 1999, Williams 2001, Looi 1998, Saurer 2001]. The characteristic increase in sheet carrier concentration with decreasing temperature has been discussed in previous chapters. This measurement confirms that black diamond can yield high carrier concentrations.

The mobility values are displayed in figure 8.5. It is intriguing that in fact the highest mobility value recorded on polycrystalline diamond in this thesis is on black diamond (sample C). The only substantially worse sample is the HFCVD diamond, which is presumably due to Ta filament inclusions. Again the trend observed over the temperature range is identical to that seen in previous chapters on white diamond.

The comparison of the black diamond samples studied at room temperature in figure 8.6 shows a general trend of higher mobilities at lower carrier concentrations. However, the common trend of ionised impurity scattering is not observed, this is not expected as explained in previous chapters and this is more evidence for the Sung Gi model [Sung Gi 1995], as there multiple scattering mechanisms.

The device characteristics of the Al schottky on black diamond (figure 8.7) are surprising. Although the device is far from the best possible on single crystal or high quality polished white diamond [Gluche 1997], it demonstrates over five orders of magnitude rectification ratio. In forward bias the series resistance is clearly visible, but this is a rather crude structure and the probe was used as the ohmic contact, which

always leads to more resistive device characteristics. At lower voltages the diode shows clear evidence of thermionic emission due to the exponential behaviour and in reverse bias the current is very low. The device does break down at higher voltages (around - 20V), and this is a substantially lower value than on the best white diamond devices [Gluche 1997]. It is conceivable that this is due to the effect of the grain boundaries and grain inclusions as the contact will cover several of these on the diamond surface.

By extrapolating the exponential region of the I/V curve to the y axis the Schottky Barrier Height (SBH) is estimated to be around 0.67 eV which is comparable with values in the literature [Mori 1991]. However, this technique is a highly unreliable at calculating the SBH and should be treated with caution. The ideality factor of this device is around 3.2 which is much higher than white diamond and single crystal devices, with typical values around 1.24 [Kiyota 1995].

The HFCVD device shows less ideal characteristics, the rectification ratio is around 4 orders and the ideality factor is simular at 3.8. The SBH is 0.67 eV, identical to the device fabricated on MWPECVD black diamond. This shows that even this material can be used for lower performance device application and is particularly interesting considering it is commercially available at $5 for a 4mm x 4mm tile.

Hayashi et al [Hayashi 1997] reported a SBH of 0.6 eV which is very similar to the values reported here and found that the barrier height changed with oxidised surfaces to 1.1 eV. Mori et al [Mori 1991] showed that the adsorption of oxygen substantially changed the electrical properties of the interface between the diamond and metal, suggesting that oxygen induces surface states that pin the Fermi level. Before oxidation, the SBH's of various metals showed dependence on the electronegativity, but after oxidation this dependence vanished. This is shown in figure 8.12.
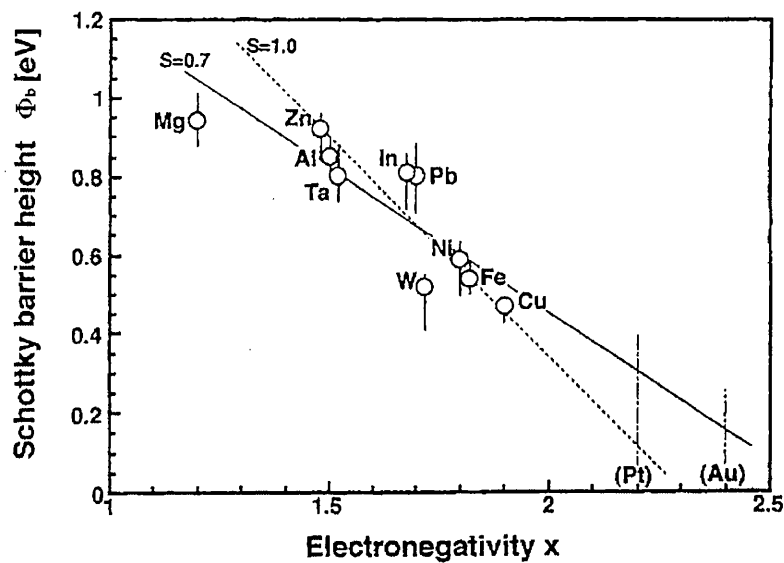
Figure 8.12 Schottky Barrier Height dependence on Metal Electronegativity [Kawarda 1996]

Heating a surface conductive device leads to a rather curious behaviour which is related to the atmospheric effects detailed in previous chapters. Figure 8.8 shows that as you heat the diode, the reverse bias current increases but the forward bias current does not. The reverse bias current obviously increases due to basic thermionic emission, as holes can more easily traverse the barrier at higher temperatures. However the forward current is dominated by the series resistance of the film and this does not decrease with increasing temperature, on the contrary it increases as the adsorbtes are desorbed from the film and at higher temperatures the desorption of the hydrogen dipole. A side effect of the depsorption of the hydrogen termination is the pinning of the Fermi level due to the surface states induced by oxygen termiation [Mori 1991].

This has serious consequences on the application of the surface conductivity layer, and without some mechanism of passivation renders the devices useless for higher temperature operation. There is obvious degradation in the Al contact too as the device is permanently damaged on returning to room temperature.

The depostion of CaF_2 onto black diamond shows that the conductivity is near destroyed under the layer (figure 8.11). This is due to the dislodging of adsorbates at

136

the surface, as CaF_2 is thermally deposited. This is a serious problem for the fabrication of MISFET structures and devices that have been shown to work in the literature [Umezawa 2000] presumably rely on their small gate sizes and high gate bias voltages.

Section 8.6 Summary

Black diamond has been demonstrated as a material capable of both high carrier concentrations and mobilities, comparable with that of the best single crystal diamond. It is very surprising that this is possible in such a highly defective material. It has been suggested that this may be due to the application of the hydrogen surface conductivity layer, as this is situated in the near surface of the diamond. As this conductivity is also activated by a hydrogen plasma, the possibility of the surface being etched of contaminants has also been raised.

If it is possible to passivate the surface conductivity layer to remove such atmospheric effects as detailed in chapter seven, then black diamond could be seen as a cheap and effective alternative to white / single crystal material.

References

Barnes R.,

(2002), Private discussion

Gluche P., Aleksov A., Vescan A., Ebert W. and Kohn E.,

IEEE Electron Device Letters, **18** (1997) 547

Hayashi K., Yamanaka S., Watanabe H., Sekiguchi T., Okushi H. and Kajimura K.,

Journal of Applied Physics, **81** (1997) 744

Jiang N. and Ito T.,

Journal of Applied Physics **85**(1999) 8267

Kawarada H.,

Surface Science Reports, **26** (1996) 205

Kiyota H., Matsushima E., Sato K., Okushi H., Ando T., Kamo M., Sato Y. and Iida M,

Applied Physics Letters, **67** (1995) 3596

Liou Y. and Ma Y.R.,

Diamond and Related Materials, **3** (1994) 573

Looi H.J., Jackman R.B. and Foord J.S.,

Applied Physics Letters, **72** (1998) 353

Lux H.,

Diamond and Related Materials, **3** (1994) 277

Mori Y., Kawarada H. and Hiraki A.,

Applied Physics Letters, **58** (1991) 940

Ristein J., Maier F., Riedel M., Stammer M. and Ley L.,

Diamond and Related Materials **10** (2001) 416

Sanchez O., Gomez-Aleixandre C., Agullo F and Albella J.M.,

Diamond and Related Materials, **3** (1994) 1183

Sauerer C., Ertl F., Nebel C.E., Stutzmann M., Bergonzo P., Williams O.A. and Jackman R.B.,

Physica Status Solidi **186**(2001) 241

Sung Gi R., Mizumasa T., Akiba Y., Hirose Y., Kurosu T. and Iida M.,

Japanese Journal of Applied Physics, **34** (1995) 5550

Umezawa H., Taniuchi H., Arima T., Tachiki M., Tsugawa K., Yamanaka S., Takeuchi D., Okushi H. and Kawarada H.,

Japanese Journal of Applied Physics, **39** (2000) L908

Williams O.A., Whitfield M.D., Jackman R.B., Foord J.F., Butler J.E., Nebel C.E.,

Diamond and Related Materials, **10** (2001) 423

Chapter 9

Polished Polycrystalline CVD Diamond

Contents

Section 9.1 Introduction

If the "Achilles Heel" of diamond is the resulting polycrystalline nature of heteroepitaxial diamond films, then polishing could be a promising solution. Flat films are vital for the utilisation of photolithography during device fabrication and hence the only valid substrate for micron and smaller scale devices.

However polishing diamond is something of a "black art" and little is known about the possible negative effects on device characteristics due to surface damage. Conventional mechanical polishing is performed using diamond powder of various grain sizes, starting with a large grit for high speed, and reducing to finer powder for a smoother surface [Malshe 1999]. However, there is a limit on the minimum roughness achieved by this technique due to micro cavities formed by the polycrystalline growth mechanism of diamond. These micro cavities appear as pits on the surface as the diamond is polished, and a planarisation technique must be used to fill in these surface pits [Malshe 1994].

As with previous work, this chapter utilises the hydrogen surface conductivity layer and hence plasma exposure could etch damage effects from the surface.

Section 9.2 Experimental Aims

The aim of work outlined in this chapter is to assess the use of polished polycrystalline diamond for device applications using the hydrogen surface conductivity layer.

Section 9.3 Experimental Methods

The diamond used in this chapter was a commercially available polished white polycrystalline diamond. RAMAN spectra were taken with a RENISHAW 2000 system with red (He-Ne) laser excitation.. Prior-to hydrogenation all samples were immersed in a boiling ammonium persulphate / sulphuric acid mixture which is known to result in a contaminant free oxidised surface [Baral 1996]. Hydrogenation was performed using pure atomic hydrogen plasma generated within a purpose built

MWPECVD chamber (sample temperature 500°C, 800W, 40torr, 5 minutes). Au contacts were thermally evaporated in the Van Der Pauw configuration for conformal mapping using an Edwards A306 evaporator with a base pressure better than 4×10^{-7} mbar. Hall effect measurements were carried out in a vacuum better than 6×10^{-6} mbar (10-300K, 0.3-1.8 T magnetic field strength). Al was deposited with an Edwards A306 evaporator with a base pressure better than 4×10^{-7} mbar to a thickness of 300nm. The structure of the schottky conacts were defined with photolithography as a 200μm dot using etching. The lift off technique was used to define the Au ohmic. I / V Testing was performed with a Hewlett Packard HP4145B Semiconductor Parameter Analyser.

Section 9.4 Experimental Results

Section 9.4.1 Raman

Figure 9.1 displays a typical RAMAN spectra of a polished polycrystalline white diamond.
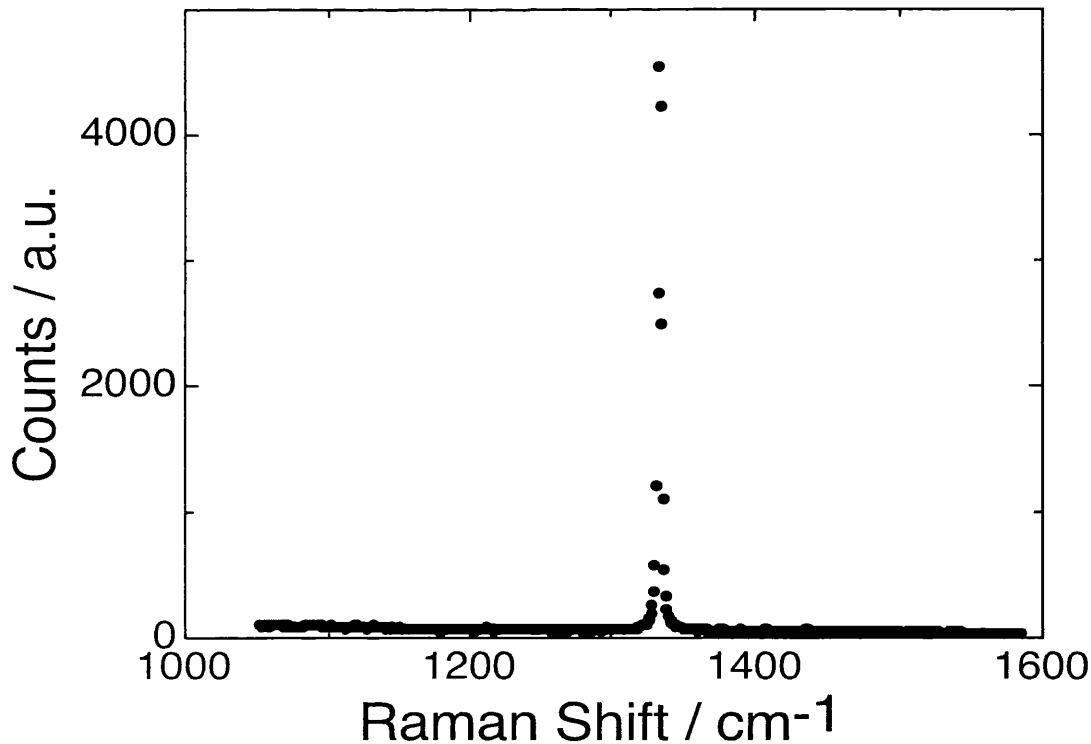
Figure 9.1 Raman spectra of polished diamond film

An intense 1332cm^{-1} is clearly evident with no indications of the G and D bands in the spectra. This is typical of all white diamond films studied.

Section 9.4.2 Hall Data

Figure 9.2 shows the variation of sheet resistivity with temperature of the polished polycrystalline diamond film. It can be seen that this film is very conductive, at room temperature its sheet resistivity is 9KΩ / $\square$ which is the lowest measured by the author. The variation is also rather slight, reaching less than 20KΩ at 20K. Again as with unpolished films there is no single activation energy evident over this temperature range.
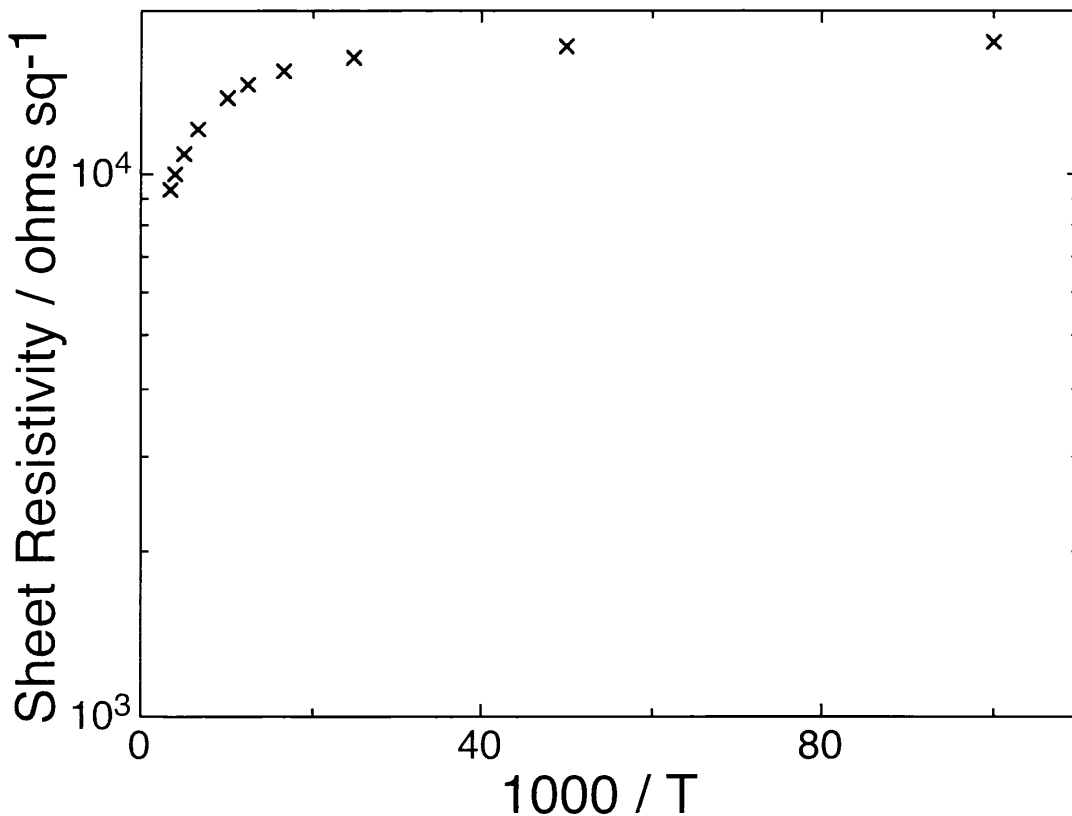
Figure 9.2 Sheet Resistivity Against Reciprocal Temperature

The variation of sheet carrier concentration with temperature is shown in figure 9.3. Again there is the characteristic increase in sheet carrier concentration with reducing temperature observed on unpolished films. The change is again very slight, varying between 3 and 4×10^{13} cm^{-2} over the entire 300K temperature range. This indicates that the mobility is the driving force of the sheet resistivity variations which is shown in figure 9.4. Mobility values half from 20 – 10 cm2 V^{-1} s^{-1} over the 300K range, which is slight as the variation in sheet resistivity. The mobility at room temperature compares well with unpolished films.
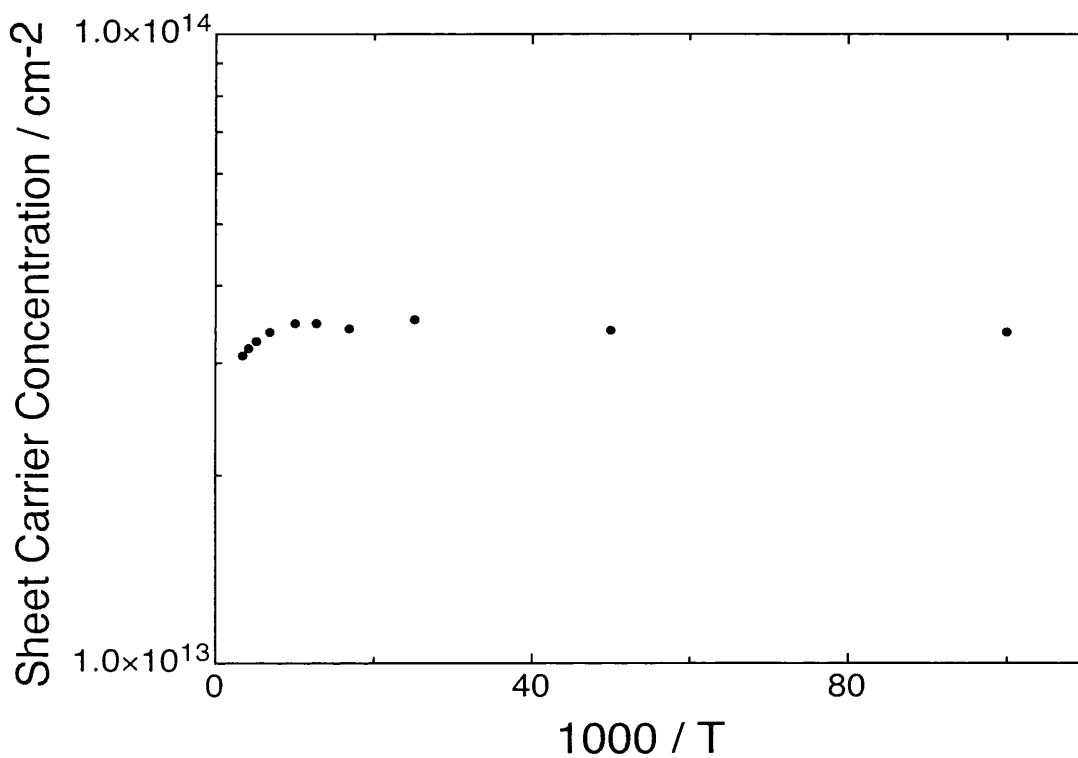
Figure 9.3 Sheet Carrier Concentration Against Reciprocal Temperature
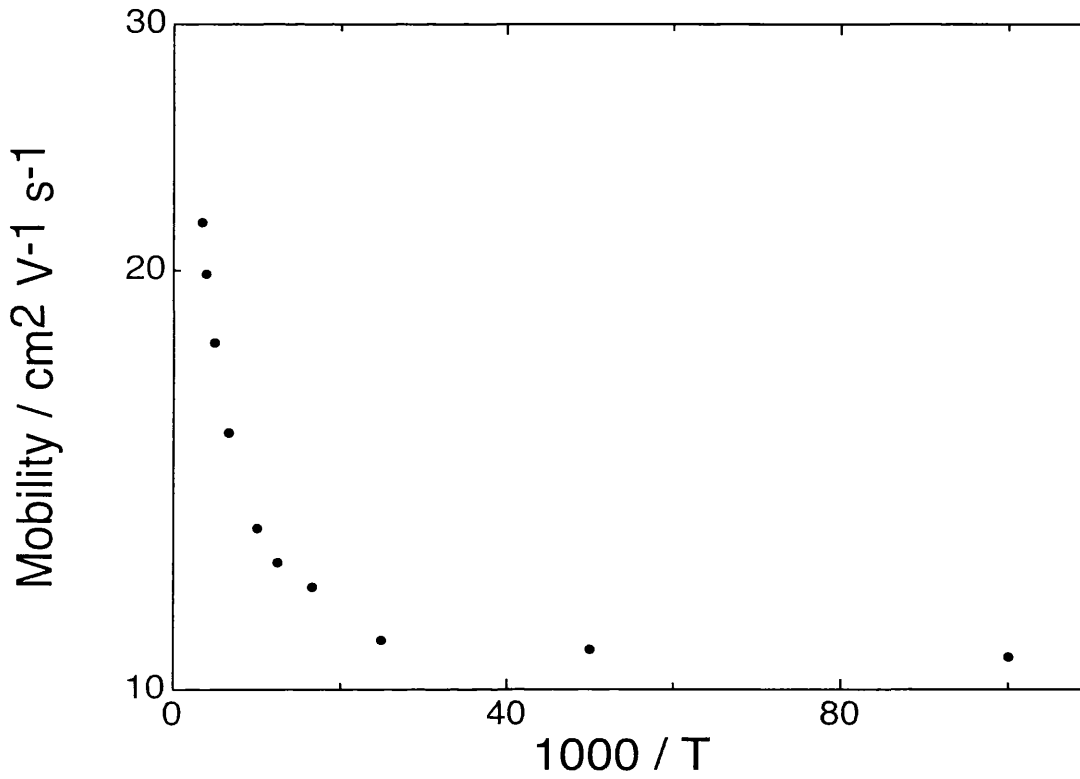
Figure 9.4 Mobility Against Reciprocal Temperature

Section 9.4.3 Device Characteristics

I / V measurements of the schottky diode formed by depositing Al contacts are shown in figure 9.5
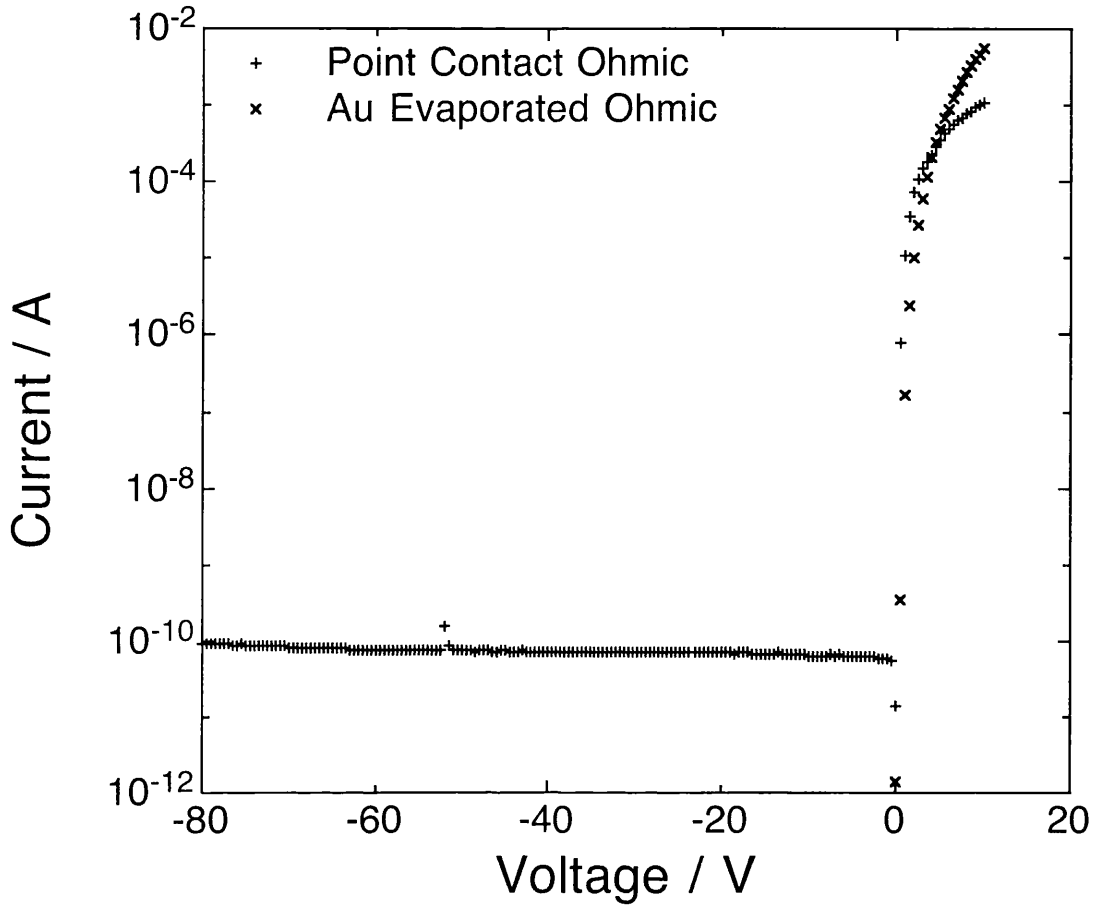
Figure 9.5 Al Schottky Diode on Polished Diamond

The Schottky contact is very near to ideal (n~1) and demonstrates over 8 orders of magnitude rectification ratio. The reverse bias leakage is very low ($<10^{-10}$ A) and breakdown is not evident below 100V. In fact the diode broke down at 600V which was surface arcing due to the breakdown of air. The forward current is also appreciable (mA @ 10V) and there is little sign of linearization at these voltages except with the point contact ohmic. The schottky barrier height is around 0.7 eV.

Section 9.5 Discussion

There is little study of the performance of hydrogenated polished polycrystalline diamond films available in the literature [Kitatani 1999, Williams 2001]. The work shown here clearly shows that the material compares with the best single crystal as far as device performance is concerned.

Due to the nature of diamond growth, competing crystals form micro - cavities that are exposed on polishing the diamond which puts a natural limit on the average surface roughness that can be achieved [Malshe 1999]. Polishing and planarising this film may have adverse effects of the surface of this diamond, but the data shown here yields no evidence of this

Figure 9.1 shows that polishing has little effect on the RAMAN spectra of the diamond film. This is not surprising as polishing is a surface effect which is unlikely to have any serious effect on the bulk properties of the film. Even if a small amount of graphitisation occurred during the process, it will most likely be removed by the acid treatment and the hydrogen plasma step, and this would not be detectible by RAMAN spectroscopy.

The resistivity after hydrogenation is among the lowest reported and clearly shows that these films can be hydrogenated. This is shown in figure 9.2 and the variation of this temperature regime is slight.

The sheet carrier concentration (figure 9.3) of the polished film increases with decreasing temperature as with unpolished films in previous chapters and in the literature [Sauerer 2001, Williams 2001]. This effect has been explained in chapter 6. This value also proves that the surface of the film is not damaged beyond the point at which it can be successfully hydrogenated.

Figure 9.4 shows again that the mobility is the driving force of the reduction in conductivity in this sample and this phenomenon is also discussed in detail in chapter 6. The value at room temperature is around 22 cm^2 V^{-1} s^{-1} which is comparable with

the values on single crystal reported in the literature [Jiang 1999]. Thus, polishing diamond films does not really have any major negative effect on carrier transport within the near surface. This is particularly exciting as polishing is essential for the commercial realisation of diamond devices on polycrystalline diamond films.

Figure 9.5 shows a "state of the art" diode on this film. This diode equals and exceeds any schottky contact on single crystal reported in the literature [Mori 1991, Kiyota 1995, Gluche 1997]. The highest reported reverse breakdown voltage on diamond is around 200V [Gluche 1997] and is exceeded by 600V on this structure. This value was also the breakdown of the air so the actual device breakdown is not known. The forward current is very high, reaching almost 10mA at 10V which is also an exceptional value.

There is some controversy in the explanation of the method of operation behind schottky diodes from on hydrogen termination diamond. In chapter 8 the correlation between schottky barrier height and metal electronegativity was discussed, and was explained as a consequence on the hydrogen termination reducing Fermi level pinning at the interface [Kawarada 1996]. Chapter 7 described the origin of the free carriers as being due to surface adsorbates [Sung Gi 1995], and so this poses the question of how these adsorbates can be present under a metal layer, especially when it has been thermally evaporated. If one imagines a copolanar surface contact, it is very possible that the current can in fact flow out of the side of the contact, and hence there need not be any carriers beneath it. This would still result in a metal- semiconductor interface, and hence one could still get a schottky or ohmic contact depending on the metal work function. If this were the case then the capacitance of the schottky diode would actually be proportional to the periphery of the contact and not the area. This has actually been confirmed by CV measurements [Garrido 2002].

An alternative non – conventional explanation for the behaviour of schottky contacts on hydrogen terminated diamond has been proposed by the Walter Schottky Institute [Nebel 2002]. This work showed that the surface potentials measured by Kelvin Probe techniques for hydrogen terminated diamond and gold were the same, but aluminium

differed from gold by 0.6 V. By considering the respective work functions, it is possible to construct a band diagram which is shown in figure 9.6.
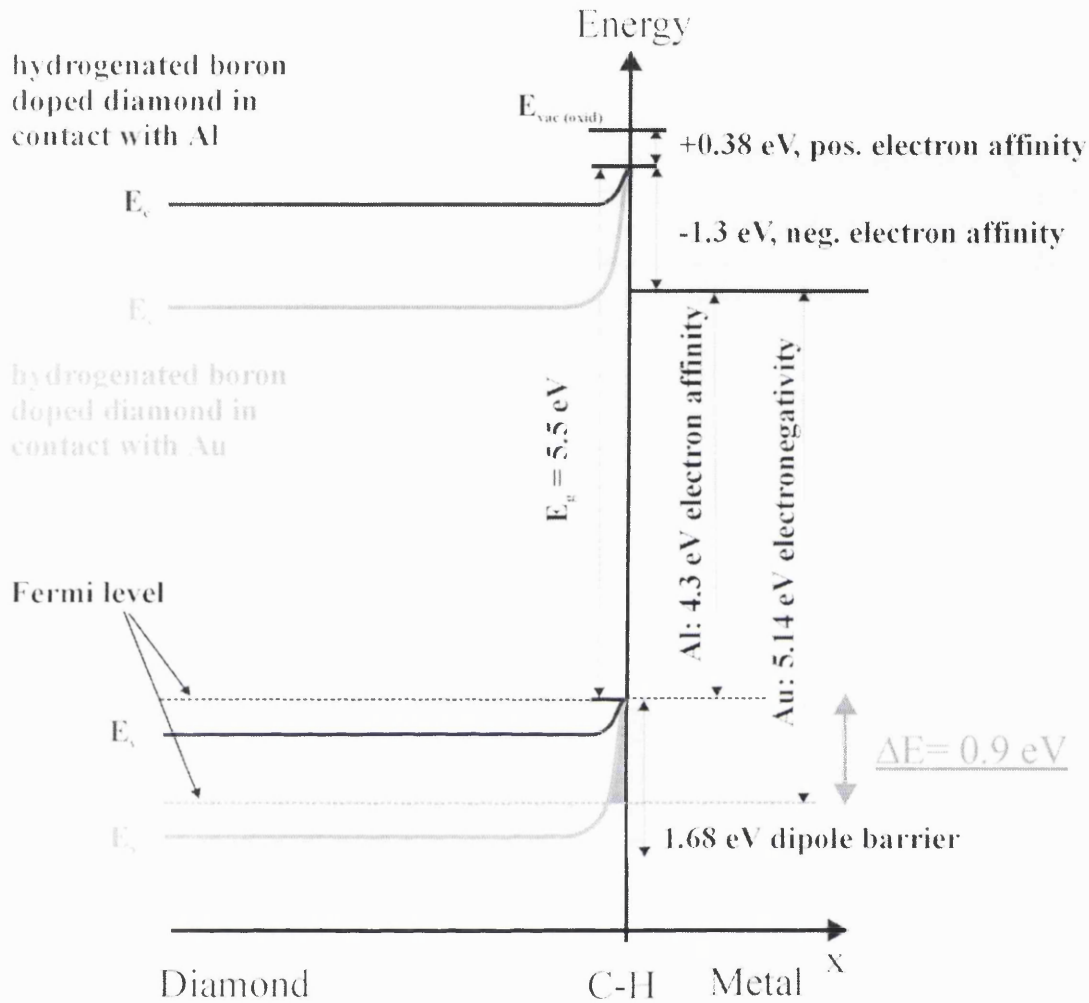
Figure 9.6 Proposed Band Diagram [Nebel 2002]

It can be seen from figure 9.6 that when considering the negative electron affinity of the hydrogen terminated diamond surface and the work function of gold, the Fermi level under this metal will be pushed into the valence band, hence hole accumulation will take place as electrons out diffuse into the metal. This will cause the valence band to bend up at the surface, the metal however is unaffected by the relatively few extra electrons. This situation is very similar to having an adsorbate such as an oxonium ion on the surface, as in the Sung Gi model, and hence is an extension of this model [Sung Gi 1995].

The case for aluminium is rather different due to the substantially lower work function. It can be seen from figure 9.6 that the work function of aluminium is not sufficient to drive the Fermi level into the valence band, this means that one must apply a bias to overcome the potential barrier, and hence the contact is blocking like a schottky contact. This model also allows the variation of schottky barrier height with work function and yields a schottky - like behaviour.

It is obvious to see from figure 9.6 that if the surface is oxygen terminated, as there is now a positive electron affinity, the metal work function of even gold is not sufficient to drive the Fermi level into the valence band and hence there is no hole accumulation. It can be seen again that the negative electron affinity of diamond along with its bandgap are the key reasons that this phenomenon is witnessed on this material and only this material.

It should be noted however, that Kelvin Probe measurements can be very controversial and those here were not performed under UHV conditions, thus the work functions of the metals could be substantially different to those quoted in the literature. However, similar results have been reported [Shirafuji 1996], and these measurements were also repeated and confirmed by Ristein et al [Ristein 2002]. Perhaps the most significant problem with this model is the use of boron doped diamond. This has been used in the model as it had a well characterised Fermi level position which is required to construct this band diagram. Obviously, if the material is intrinsic, much more substantial valence band up bending is required to reach the Fermi level. In fact, from this diagram (figure 9.6), the 0.9 eV increase in the valence band maximun would result in it being positioned well below the Fermi level. This is not the case that has been observed experimentally [Ristein 2001], and hence an alternative explanation is required.

It should also be noted that the above explanation is not entirely necessary if one addresses the structure as a coplanar metal – semiconductor contact, where there need not be any carriers underneath the contact and they just flow out of the side of the contact into the adsorbate covered (and hence hole accumulated) diamond surface.

The mechanism of operation for the metal hydrogen terminated diamond is still not fully understood, and further confusion has arisen from the lack of tunnelling in forward bias with such a high density holes [Denisenko 2000]. This has been tentatively explained by the inclusion of a thin insulating layer between the metal and the diamond. However, this layer has been calculated to be 30 – 50 nm with a dielectric constant of 50, and can therefore not be diamond [Denisenko 2000]. There is no experimental evidence for this and this model would contradict the above Kelvin Probe measurements and the correlation of schottky barrier height with metal work function. In fact, where such a layer would arise from is also not clear.

Section 9.6 Summary

A polished diamond film with extreme properties has been characterised and a high performance device fabricated on it. These results show that this material class is excellent for electronic devices, and this is particularly exciting due to the low cost of the material in comparison to single crystal diamond. It is surprising that hydrogen surface conductivity is not adversely effected by polishing, especially due to the near surface transport mechanism.

Device characteristics have been discussed in detail with reference to the literature, and various models addressed. To date, there is no clear all encompassing model, however the models proposed by Sung Gi / Ristein / Nebel are perhaps the most promising.

References

Baral B., Chan S.S.M. and Jackman R.B.,
Journal of Vacuum Science and Technology **14** (1996) 2303

Garrido J.A., Nebel C.E., Stutzmann M., Snidero E., and Bergonzo P.,
Applied Physics Letters, **81** (2002) 637

Gluche P., Aleksov A., Vescan A., Ebert W. and Kohn E.,
IEEE Electron Device Letters **19** (1997) 547

Jiang N. and Ito T.,
Journal of Applied Physics **85**(1999) 8267

Kawarada H.,
Surface Science Reports, **26** (1996) 205

Kitatani K., Umezawa H., Tsugawa K., Ueyama K., Ishikura T., Yamashita S. and
Kawarada H.,
Diamond and Related Materials **8** (1999) 1831

Kiyota H., Matsushima E., Sato K., Okushi H., Ando T., Kamo M., Sato Y. and Iida
M,
Applied Physics Letters, **67** (1995) 3596

Malshe A.P., Brown W.D., Naseem H.A. and Schaper L.W.,
US Patent 5472370 (1994)

Malshe A.P., Park B.S., Brown W.D. and Naseem H.A.,
Diamond and Related Materials **8** (1999) 1198

Mori Y., Kawarada H. and Hiraki A.,
Applied Physics Letters, **58** (1991) 940

Nebel C.E., Ertl F., Sauerer C., Stutzmann M., Graeff C.F.O., Bergonzo P., Williams O.A. and Jackman R.B.,

Diamond and Related Materials, **11** (2002) 351

Ristein J., Maier F., Riedel M., Stammer M. and Ley L.,

Diamond and Related Materials **10** (2001) 416

Ristein J., Ley L.,

Diamond Films 2002, Granada, Spain, oral presentation

Sauerer C., Ertl F., Nebel C.E., Stutzmann M., Bergonzo P., Williams O.A. and Jackman R.B.,

Physica Status Solidi **186**(2001) 241

Shirafuji J. and Sugino T.,

Diamond and Related Materials, **5** (1996) 706

Sung Gi R., Mizumasa T., Akiba Y., Hirose Y., Kurosu T. and Iida M.,

Japanese Journal of Applied Physics, **34** (1995) 5550

Williams O.A., Whitfield M.D., Jackman R.B., Foord J.F., Butler J.E., Nebel C.E.,Diamond and Related Materials, **10** (2001) 423

Chapter 10

Homoepitaxy

Contents

Section 10.1 Introduction

Work within this thesis so far has been based primarily on CVD diamond grown on silicon wafers, which were subsequently sacrificially etched. This material can yield very impressive results, especially for large areas. The growth of large area wafers takes at least 100 hours for high quality white free standing material. However, homoepitaxial growth on single crystal substrates can result high quality single crystal material which should give higher mobilities and increased reproducibility. Single crystal material also has a much lower roughness than polycrystalline material.

Another common misconception that is dissolved earlier within this thesis is the myth that only high quality diamond can yield high mobilities. Black diamond has been shown to yield similar properties to white diamond with the exception of HFCVD grown material. Therefore, the growth of a thin layer of high quality diamond on this poor quality material is investigated.

Section 10.2 Experimental Aims

This chapter evolves the earlier ideas by using both high and low quality substrates with a high quality growth regime to produce homoepitaxial layers. Substrates very from the cheapest HFCVD black diamond to the highest quality HPHT single crystal available. Comparisons are made between the performance of "high" and "low" quality substrates from hall measurements and I / V device characteristics.

Section 10.3 Experimental Methods

All of the substrates used in this chapter were free standing diamond films grown by either HFCVD or Type 1b HPHT synthesis techniques. The substrates were placed within an Astex PDS-18 Plasma Deposition System and diamond layers were grown on top using standard Astex conditions (478 sccm hydrogen, 20 sccm methane, 2 sccm oxygen, 2.5 KW, 800°C, 120 torr, 1 hour). After diamond growth the microwave power was shut off immediately and the diamonds were allowed to cool in vacuum ambient. As grown films demonstrate p –type conductivity so no hydrogenation was required after growth.

Au contacts were thermally evaporated under a base pressure better than 4×10^{-7} mbar in the Van der Pauw configuration for conformal mapping. Hall measurements were carried within the 10 – 300K regime under a field of ±1 Tesla using a Lakeshore 7504 hall measurement system, a hall signal tracking procedure was used as detailed in chapter 6. Al contacts were also thermally evaporated using simple shadow masking as 500 µm dots under similar pressures. I / V Characterisation was performed using a Hewlett Packard HP4145B Semiconductor Parameter Analyser and Signatone probe station. STM measurements were made in air using a Nanosurf Easyscan STM system with a Pt / Ir tips.

Section 10.4 Experimental Results

Section 10.4.1 STM

Figure 10.1 shows plan view topographical STM views and line scales (underneath). It can be seen that this film is still extremely flat after homoepitaxy, although atomic resolution could not be achieved with this simple apparatus.
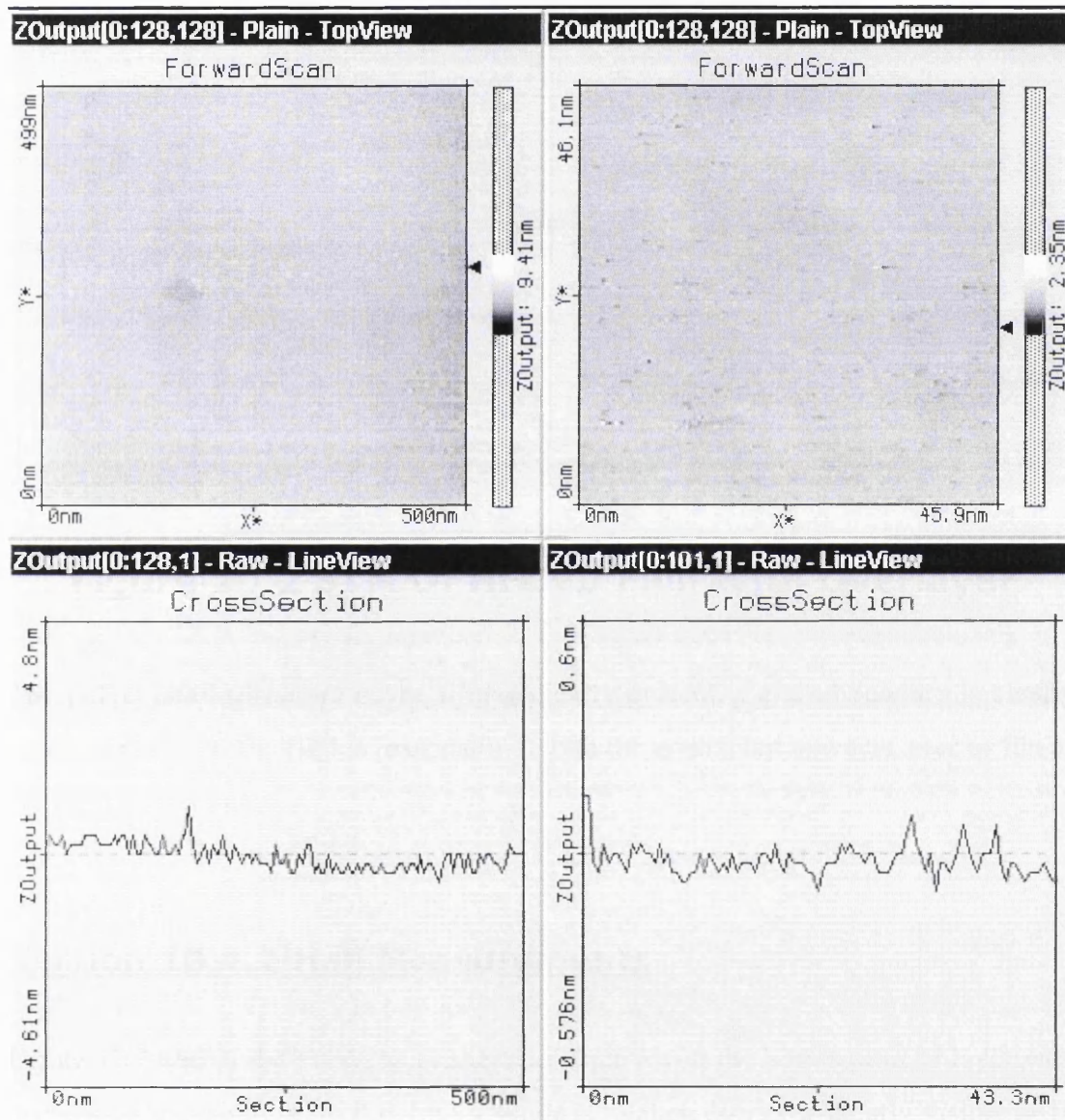

Figure 10.1 STM Of Type 1b Diamond With Overlayer

It was impossible to obtain STM images on either HFCVD or HPHT material before overgrowth due to the high resistivity of the film – attempts resulted in tip crashing. It is also rather controversial to attempt such resolution in air, as 0.1 °C temperature variation can result in several nm drift in the apparatus. Figure 10.2 shows STM images of a HFCVD film with a thin layer of high quality diamond grown on top.
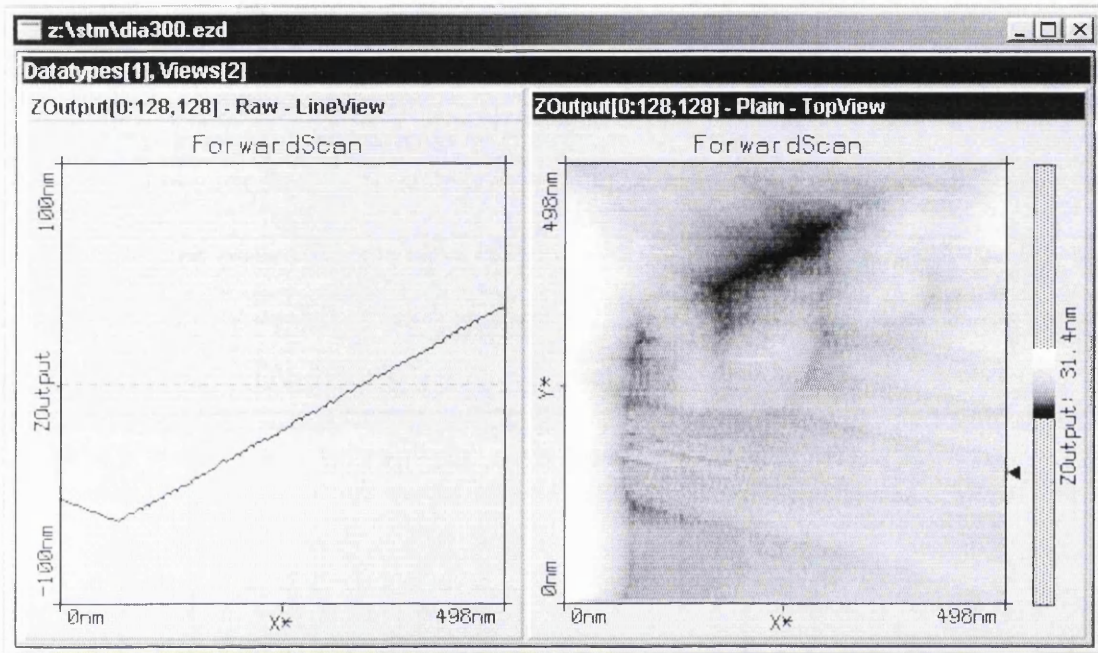
Figure 10.2 STM Of HFCVD Film With Overlayer

The polycrystalline nature of the film is clearly evident, a grain boundary is clearly visible. However, the film is reasonably flat on the grains, but nowhere near as flat as the HPHT substrate.

Section 10.4.2 Hall Measurements

Figure 10.3 shows the variation of sheet conductivity of the homoepitaxial layer with decreasing temperature, in this case a single activation energy is clearly visible at 16 meV. Figure 10.4 shows the variation of sheet carrier concentration with reducing temperature.
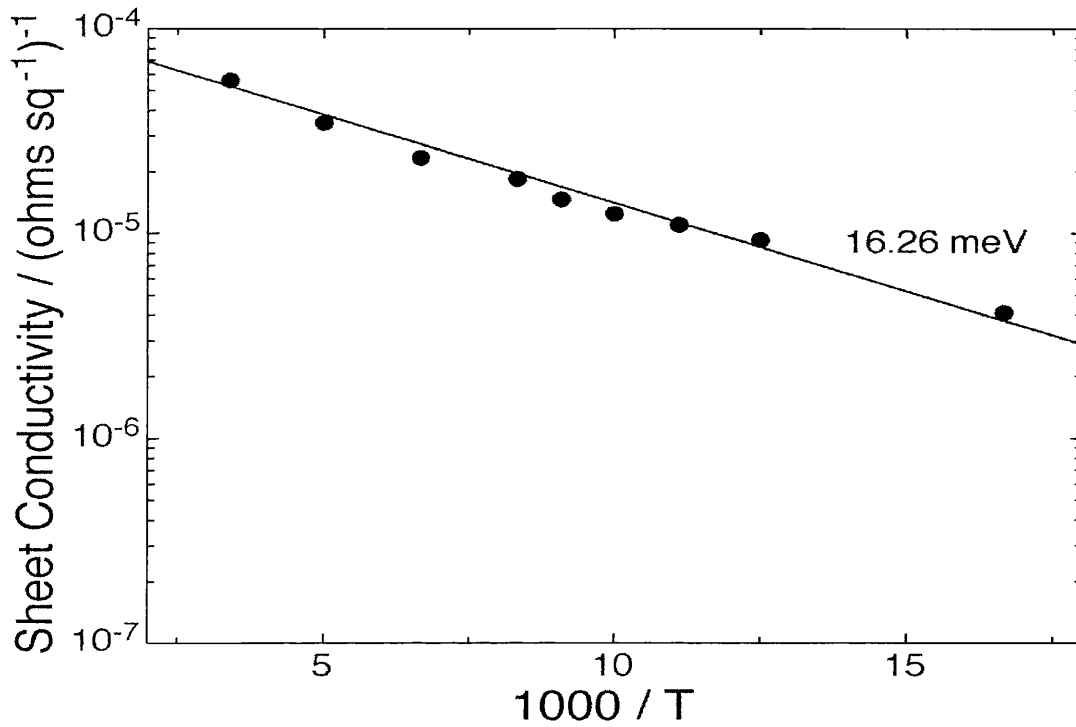
Figure 10.3 Sheet Conductivity Against Temperature For Single Crystal Homo - layer.
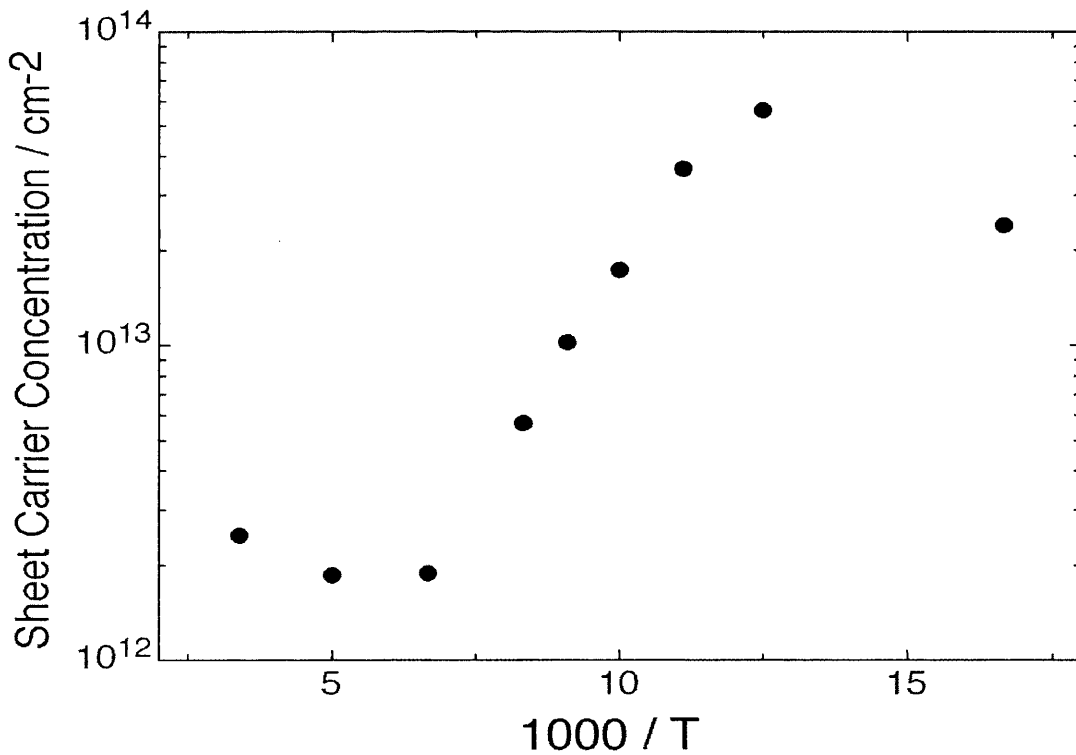
Figure 10.4 Sheet Carrier Concentration Against Temperature For Homo – Layer

The variation of the mobility of this single crystal diamond is shown in figure 10.5.
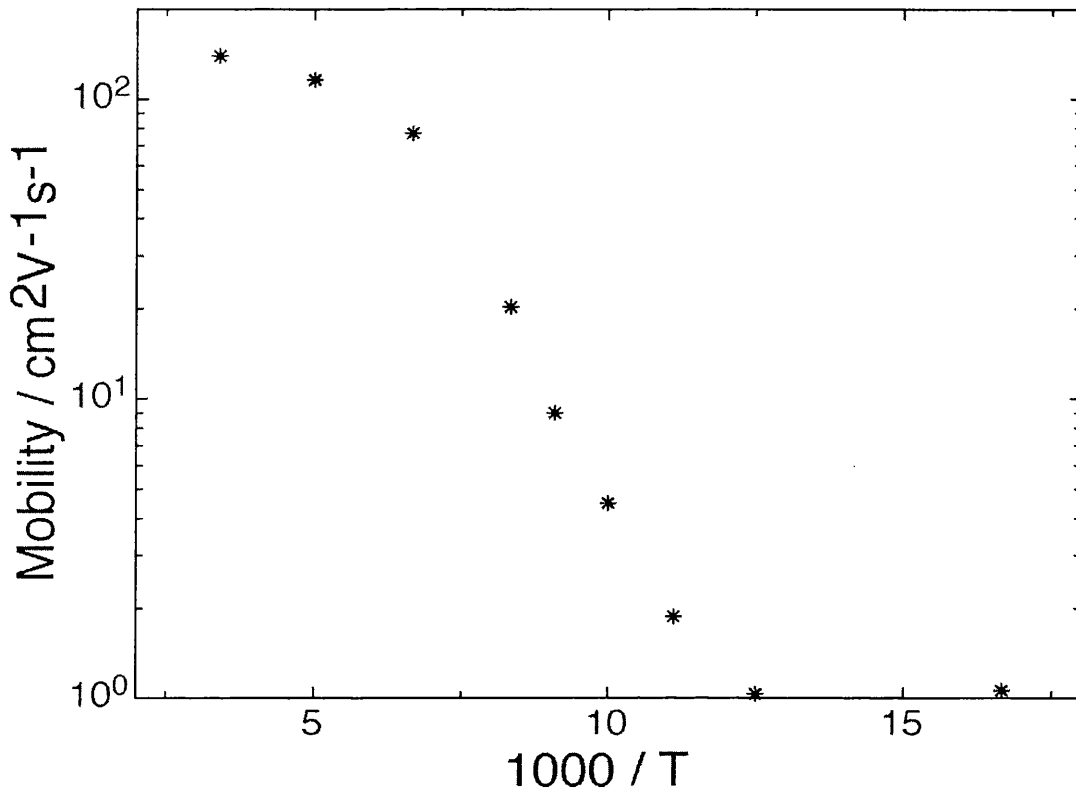
Figure 10.5 Mobility Against Temperature For Single Crystal Homo – Layer

The sheet carrier concentration can be seen to rise monotonically with decreasing temperature. The values at 150K and 200K were taken the next day, hence the slight difference. The value at 60K has a low mobility and should be treated with caution. The mobility is again the driving force behind the reduction in conductivity with temperature.

Figure 10.6 shows the variation of sheet conductivity with decreasing temperature for the HFCVD substrate with diamond over - layer. The sheet conductivity can be seen to drop as expected but this time there is no indication of any single activation energy.
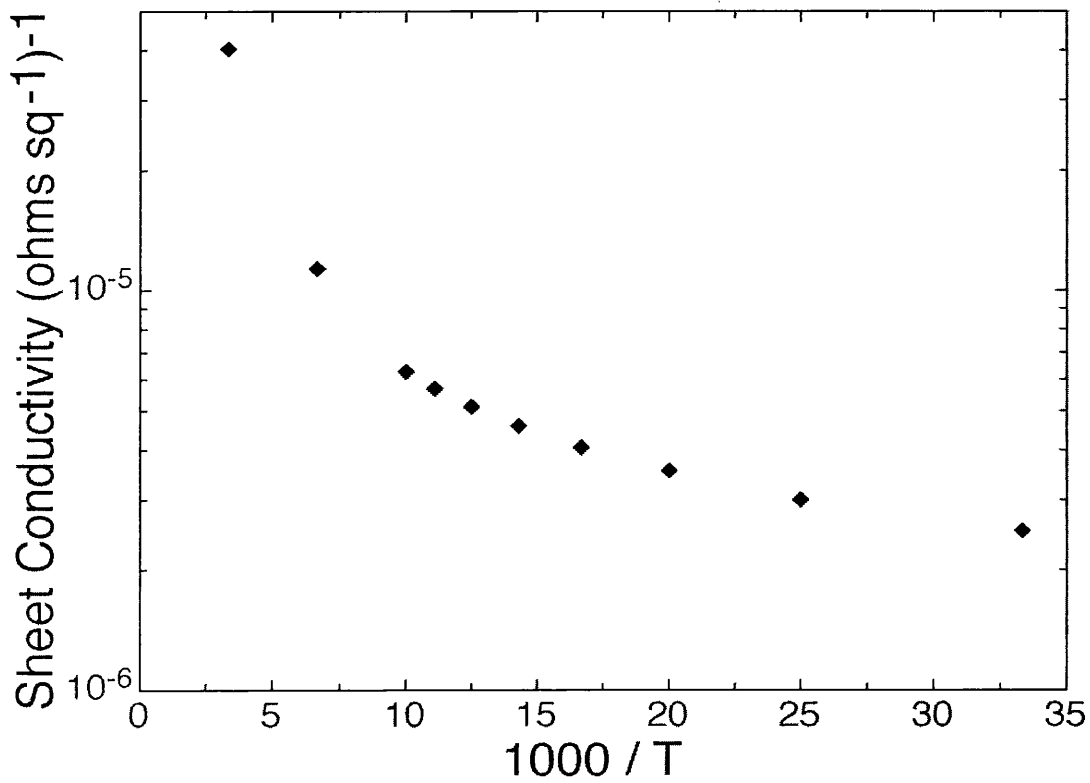
Figure 10.6 Sheet Conductivity Against Temperature For HFCVD Film With Over - Layer
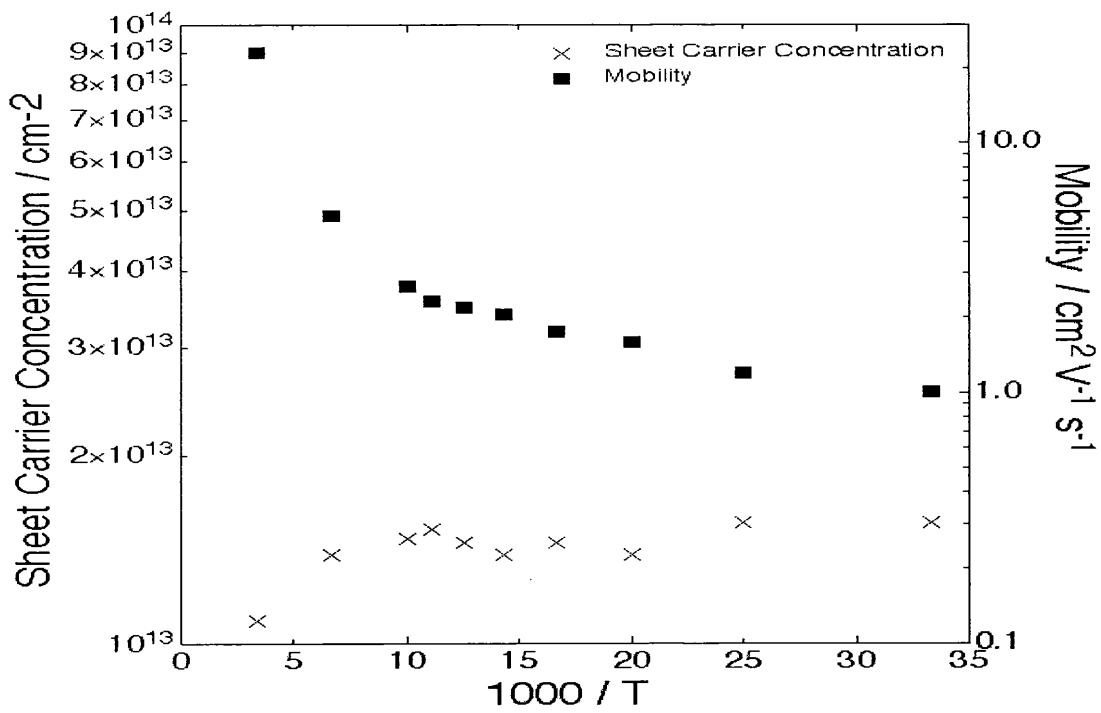
Figure 10.7 Hall Data For HFCVD Film With Over – Layer

The increase in sheet carrier concentration with decreasing temperature is slight as in earlier chapters, however, here for the first time it was possible to measure HFCVD material at low temperatures. The mobility value at room temperature was 23 $cm^2V^{-1}s^{-1}$, which is an order of magnitude higher than rehydrogenated HFCVD material without a homo − layer. Again, the mobility is the controlling variable of the reduction in sheet conductivity with reducing temperature.

Section 10.4.2 Device Characteristics

Figure 10.8 shows a comparison between diodes formed on HFCVD with those on HFCVD / homo − layer material.
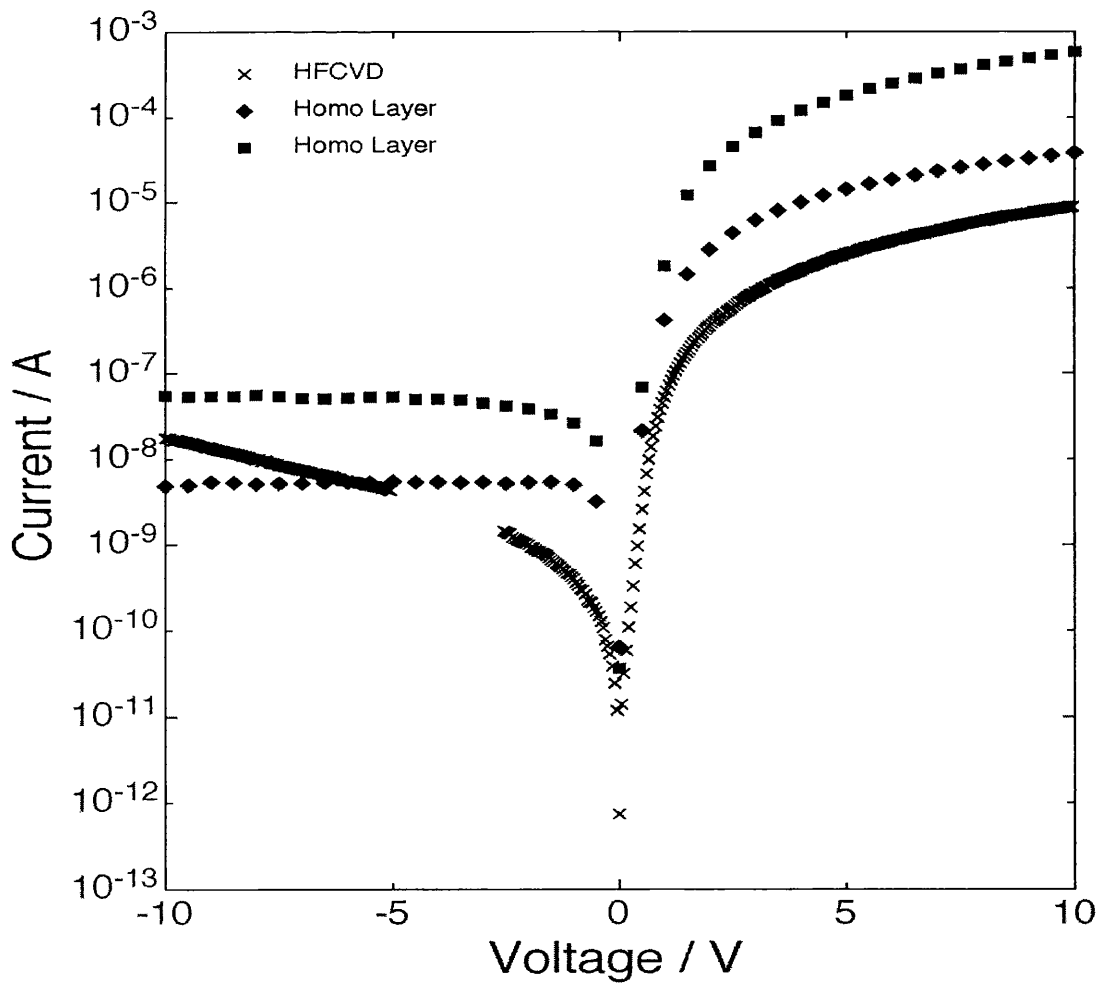
Figure 10.8 Diodes On HFCVD / HFCVD + Homo − Layer Diamond

There is a marked improvement between diodes fabricated on pure HFCVD with those on HFCVD plus homo – layer. It can be seen that the forward current on the HFCVD is two orders of magnitude lower than that on the HFCVD with a homo layer. Leakage currents are also substantially improved by the homo layer, and there was no evidence of breakdown up to 40 V in reverse bias, whereas leakage currents constantly increased with applied reverse bias on the HFCVD film.

Section 10.5 Discussion

The growth of diamond on single crystal diamond is known to produce single crystal material [Okushi 2001] Figure 10.1 shows the high quality of the diamond layer grown on a HPHT substrate, The conductivity is also rather uniform, however, it can be difficult to deconvolute the conductivity of a sample from it's surface roughness with STM.

Figure 10.2 shows STM data of a HFCVD substrate with a homo layer. It can be seen that although these diamond films are polycrystalline and hence macroscopically rough, the actual grain faces are reasonably smooth and hence we can expect the carrier transport across the grain to be unhindered by these effects. The conductivity can also be seen to be rather uniform across the diamond grain, and somewhat lower at the grain boundary. Atomic resolution was not achievable on either film, but these measurements were made in air, and UHV is preferred for these resolutions [Stallcup 1995].

The sheet conductivity decreases with decreasing temperature as with previous chapters and in the literature [Sauerer 2001, Williams 2001]. The single crystal diamond shows evidence of an activation energy of 16 meV which is comparable to the values in the literature and in chapter six [Sauerer 2001]. However, this value should be treated with caution, as shown in earlier chapters and in the literature this value varies substantially with the environment. In fact, this figure is the only evidence the author has ever seen of a single activation energy. The HFCVD film with over – layer shows no evidence of a single activation energy, as with all other polycrystalline films that have been measured, Thus, the evidence of the activation is

not due to the helium atmosphere promoting stability of the hydrogen surface conductivity layer. (i.e. buffering desorption of adsorbates).

The sheet carrier concentration of both samples rises with decreasing temperature, but the effect is much more pronounced on the single crystal sample, presumably due to lower room temperature value. This phenomenon has been explained in chapter six and will not be explained in detail here. Briefly, the carriers are more attracted to the surface by the surface dipole at lower temperatures, leading to a slight increase in the overall carrier concentration as measured by the hall effect. The dipole is also partly responsible for the reduction in mobility at lower temperatures along with the increased surface scattering.

HPHT Ib material does not exhibit high conductivity without a homo – layer due to the high concentration of nitrogen compensation [Ristein 2001], however, with a homo layer this diamond has extremely good hall characteristics. The mobility value is higher than any value reported in the literature [Jiang 1999]. It could be speculated that hydrogenation etches the surface and thus this can have a negative effect on mobility values. However, growth should circumvent this problem and thus one could expect better performance from as - grown material. This result is also better than hydrogenated type IIa material. This is also probably due to the etching effect, but the damage due to polishing cannot be ruled out. In previous chapters polished material has been shown to demonstrate good p – type characteristics, but mobility values like the above have never been recorded on this material.

A similar result is evident on the HFCVD material, however, in this case the substrate is probably highly contaminated with filament material. The mobility here reaches 23 $cm^2V^{-1}s^{-1}$ which is comparable with the best polycrystalline white diamond measured in earlier chapters and the literature [Williams 2001, Looi 1998, Sauerer 2001]. The extremely thin active region (<20nm) [Hayashi 1997] of the hydrogen surface conductivity can explain how such a thin layer of diamond can have such a drastic improvement in performance. The growth procedure used here grows around 1μm in the 1 hour duration.

The improvement in device characteristics can also be explained by this thin high quality diamond layer. Highly contaminated material cannot be expected to produce good devices, but with this high quality layer, the diamond performs very much like white polycrystalline material. The rectificication ratio is improved to over four orders which is far from that capable on white diamond, but this material is of large grain size and the structure is fundamentally compromised by this. Although the device is far from ideal it is encouraging that it demonstrates such rectification and improvements may be possible.

Section 10.6 Summary

This chapter has demonstrated the growth of high quality diamond layers on lower quality diamond substrates. This procedure has been demonstrated to improve electrical characteristics substantially, with extremely high mobilities on single crystal diamond ($>140 \text{cm}^2 \text{V}^{-1} \text{s}^{-1}$). HFCVD material has also been used and modest devices realised. The improvements shown are largely due to the thin layer isolating the active region from contaminated or compensated substrates.

The performance of as – grown material has been shown to be superior to that of rehydrogenated material. It is not clear why this is so, but the idea that etching of the surface due to hydrogen plasma has been proposed. The stability of these layers also seem to surpass that of rehydrogenated diamond, and again it is not clear why this is the case.

References

Hayashi K., Yamanaka S., Watanabe H., Sekiguchi T., Okushi H. and Kajimura K.,
Journal of Applied Physics **81**(1997) 744

Jiang N. and Ito T.,
Journal of Applied Physics **85**(1999) 8267

Looi H.J., Jackman R.B. and Foord J.S.,
Applied Physics Letters **72**(1998) 353

Looi H.J., Pang L.Y.S., Molloy A.B., Jones F., Foord J.S. and Jackman R.B.,
Diamond and Related Materials **7**(1998) 550

Okushi H.,
Diamond and Related Materials, **10** (2001) 281

Ristein J., Riedel M., Maier F., Mantel B.F., Stammler M. and Ley L.,
Physica Status Solidi, **186** (2001) 249

Sauerer C., Ertl F., Nebel C.E., Stutzmann M., Bergonzo P., Williams O.A. and Jackman R.B.,
Physica Status Solidi **186**(2001) 241

Stallcup R.E., Aviles A.F. and Perez J.M.,
Applied Physics Letters **66**(1995) 2331

Williams O.A., Whitfield M.D., Jackman R.B., Foord J.F., Butler J.E., Nebel C.E.,
Diamond and Related Materials, **10** (2001) 423

Chapter 11

Conclusions

Diamond has many problems that will have to be addressed before it can be realised as the high performance device material it was always promised to be. Both the polycrystalline nature of heteroepitaxially deposited films and the lack of dopants with low activation energies have crippled the use of this extreme material, and the progress on either of these milestones to date is not encouraging.

The initial discovery of hydrogen surface conductivity and the encouraging performance of devices fabricated on it led to much excitation and speculation about the utilisation of diamond in high performance electronics. However, although some impressive devices have been fabricated to date, such as a single hole transistor, MESFETs and logic gates, the extreme instability of the layer with atmosphere is likely to hinder any commercialisation of these devices. It is also scarcely mentioned that all of the advantages of diamond that are so frequently quoted, are lost on the utilisation of the hydrogen surface conductivity layer. These include high temperature capabilities (annealing removes conductivity), Inertness (surface sensitive to environment), and high performance (highest mobility recorded on hydrogen terminated diamond is 140 $cm^2V^{-1}s^{-1}$). In fact, the concept of fabricating a device based on surface properties is abhorrent to most device engineers, a common quote being "If God invented the bulk, then the devil invented the surface"

The work in this thesis has focused on the origin and transport mechanism behind hydrogen surface conductivity in diamond. Hydrogen surface conductivity is a curious phenomenon and it is obvious from the data presented in this thesis, along with that in the literature, that it is inappropriate to consider it in terms of conventional doping. Hall effect measurements have been used to quantify the layer, and conductivity measurements to demonstrate the instability. Devices with good

characteristics have been demonstrated and low grade diamond activated electrically. Extensive low temperature characterisation has been carried out for the first time on this layer and this has revealed highly unusual behaviour.

Despite the lack of an obvious application, hydrogen surface conductivity is interesting, as hydrogen does not have such an extreme effect on any other material. The studying of such a surface phenomenon has shed more light on unusual transport behaviour and the stability of such surface conduction within various environments.

Homoepitaxy is a promising direction for the improvement of surface conductive devices. Further development in this field should produce cheap, high performance, reproducible material which could help towards the realisation of diamond electronics. Conditions need to be optimised to obtain this goal and this needs to be investigated systematically.

Perhaps the most promising area for diamond is as a biomaterial. The combination of the hydrogen terminated surface and its associated semiconductivity, the chemical inertness and transparency of this material could revolutionise this field. Further work on hydrogen terminated diamond should focus on Ion Sensitive Field Effect Transistors (ISFETs) as a means of achieving this goal. Hydrogen terminated diamond is also and ideal starting point for biological functionisation.

It is not clear when or even if diamond electronics will become a reality, but research in this field is still of academic value and can certainly enhance our understanding of other materials. It should also be noted that all wide bandgap semiconductors have problems with doping, and growth problems plague almost all materials excluding the irritating wonderful silicon. Diamond is successful in many other areas such as UV light detection, extreme optics and thermal management. It is hoped that the information here can assist these or other field in some way.

Related Publications

Formation of shallow acceptor states in the surface region of thin film diamond
OA Williams, MD Whitfield, JS Foord, CE Nebel, JE Butler and RB Jackman.
Applied Physics Letters, **78** (2001), 3460

Carrier Generation within the surface region of hydrogenated thin film polycrystalline diamond
OA Williams, MD Whitfield, JS Foord, JE Butler, CE Nebel and RB Jackman
Diamond and related materials, **10** (2001), 423

Low temperature conductivity of hydrogenated diamond
C Saurer, F Ertl, CE Nebel, M Stutzman, P Bergonzo, OA Williams and RB Jackman
Physica Status Solidi, **186** (2001), 241-247

Low Temperature properties of the p-type surface conductivity of diamond
CE Nebel, F Ertl, C Sauerer, M Stutzmann, CFO Graeff, P Bergonzo, OA Williams and RB Jackman
Diamond and Related Materials, **11** (2002) 351

Hydrogen – induced transport properties of holes in diamond surface layers
CE Nebel, C. Sauerer, F Ertl, M Stutzmann, CFO Graeff, P Bergonzo, OA Williams and RB Jackman
Applied Physics Letters, **79** (2001) 4541

Black Diamond: A new material for active electronics devices
OA Williams, RB Jackman, CE Nebel and JS Foord
Diamond and related materials, Accepted (September 2001)

The influence of hydrogen on the electrical properties of diamond
OA Williams and RB Jackman
Semiconductor Science and technology, invited review paper, submitted October 2001

High carrier mobilities in black diamond
OA Williams, JS Foord, CE Nebel and RB Jackman
Semiconductor Science and Technology, invited review paper, accepted Januarry 2002

Hydrogenated Black Diamond: An Electrical Study
OA Williams, CE Nebel and RB Jackman
Physica Status Solidi, Accepted (August 2002)

Influence of postplasma process conditions on the surface conductivity of hydrogenated diamond surfaces
E Snidero, D Tromson, C Mer, P Bergonzo, JS Foord, C Nebel, OA Williams, RB Jackman
Journal of Applied Physics, **93** (2003) 2700

The Formation of Insulating Layers on Hydrogenated Diamond
S Curat, OA Williams and RB Jackman
Diamond and Related Materials, Accepted (September 2002)

In – Plane Transistors in H – Terminated Diamond
JA Garrido, B. Rezek, CE Nebel, M Stutzmann, R. Todt, G. Rosel, MC. Amann, E Snidero, P Bergonzo, OA Williams and RB Jackman,
Diamond and Related Materials, Accepted (September 2002)